

Aus dem Institut für Medizinische Mikrobiologie und Krankenhaushygiene

Geschäftsführender Direktor: Prof. Dr. Michael Lohoff

des Fachbereichs Medizin der Philipps-Universität Marburg

**Identifizierung funktioneller Untereinheiten des
Transkriptionsfaktors *interferon regulatory factor 4***

Kumulative Dissertation zur Erlangung des Doktorgrades der
Naturwissenschaften (Dr. rer. nat.)

Vorgelegt dem Fachbereich Medizin der Philipps-Universität Marburg von

Daniel Staudenraus

aus Saarbrücken

Marburg, 2022

Angenommen vom Fachbereich Medizin der Philipps-Universität Marburg am: 17.01.2023

Gedruckt mit der Genehmigung des Fachbereichs Medizin.

Dekanin: Prof. Dr. Denise Hilfiker-Kleiner

Referent: Prof. Dr. Michael Lohoff

Korreferent/in: Prof. Dr. Markus Schnare

“It is the struggle itself that is most important. We must strive to be more than we are. It does not matter that we will not reach our ultimate goal.

The effort yields its own rewards.”

Gene Roddenberry

Contents

Abstract	III
Zusammenfassung	IV
List of Figures	V
List of Abbreviations	VI
1 Introduction	1
1.1 Adaptive immunity	1
1.2 Helper T cells	2
1.2.1 Th1 and Th2 cells	3
1.2.2 Th17 cells	4
1.2.3 Th9 cells	5
1.3 Interferon regulatory factor 4	6
1.3.1 Structure, domains and binding motifs	6
1.3.2 IRF4 in T helper cells	7
1.3.3 IRF4 in B cells	8
1.3.4 Point mutations in IRF4	9
1.4 Aim of the study	11
2 Results	12
2.1 A hyperactive mutant of interferon regulatory factor 4	12
2.2 Impact of point mutations in IRF4 on Th2, Th9 and Th17 cell differentiation	14
2.2.1 Defects in IRF4 functionality in mutants in the DBD and at the IAD/AD transition	14
2.2.2 Point mutations in the 399-401 region show graded impairment of IRF4 function	15
2.2.3 Of eight point mutations with previously postulated effects only E406P abrogates IRF4 function	17
2.2.4 Amino acid residue D117 is vital for IRF4 function	19

2.3	Point mutation L116R in interferon regulatory factor 4 differentially impacts key cytokine production in Th2, Th9, and Th17 cells	21
2.4	IRF4 deficiency vulnerates B-cell progeny for leukemogenesis via somatically acquired <i>Jak3</i> mutations conferring IL-7 hypersensitivity	23
3	Discussion	25
3.1	Deletion of dAD increases effect strength in Th9 and Th17, but not Th2.....	25
3.2	Th2 differentiated cells are more robust than Th9 and Th17 cells	26
3.3	Many reported Mutations based on structural analysis and binding assays lack relevance during T cell differentiation <i>in vitro</i>	27
3.4	DBD and IAD/AD transition mutants lead to severe disruption in IRF4 function	28
3.5	Development of a mouse model for the human disease Ph-like B-ALL	31
4	Literature	33
5	Appendix	38
5.1	Curriculum vitae	38
5.2	Verzeichnis akademischer Lehrer.....	39
5.3	Danksagung	40
5.4	Vollständiges Veröffentlichungsverzeichnis	41
5.5	Ehrenwörtliche Erklärung.....	Fehler! Textmarke nicht definiert.
6	Publications	42

Abstract

Interferon regulatory factor 4 is a crucial factor in adaptive immunity in both T and B cell mediated processes. Knockout mice lacking IRF4 show severe defects in developing functional T cell subsets, including Th2, Th9 and Th17, as well as B cells arrested in early development stages, which leads to absence of IgM in the serum. In T cells, IRF4 serves as an initiation factor conveying TCR signals, priming cells for proliferation and inducing master transcriptional regulators such as GATA3, T-bet and ROR γ t. To fulfil this central role, interaction with several partners is required, among them BATF and PU.1. We hypothesize that through precise alterations in IRF4, its functionality can be altered to achieve selective modification of its immunoregulatory effects. Based on literature results from binding assays, structural analysis and recurring mutations in cancer patients, we tested many point mutations in IRF4 for their functionality in Th2, Th9 and Th17 differentiation. Several mutations show immunomodulatory potential. Most prominent among them is L116R, which induces Th9 differentiation and IL-9 production in Th2 cells, while at the same time reducing Th2 and Th17 differentiation. Further, we could show that autoinhibition of IRF4 is differentially affecting helper T cell subtypes, acting much stronger on Th9 and Th17 cells compared to Th2 differentiated cells. In addition, tumors emerging in old IRF4 knockout mice allowed us to further study leukemogenesis and B cell development in the context of IRF4 deficiency, leading to a disease similar to human Ph-like B-ALL. Treatment of this disease with the JAK inhibitor Ruxolitinib increased survival by reducing blast infiltration in the central nervous system and solid organs.

Here we show that immunomodulation via point mutations is possible and that IRF4 has subdomains that differentially affect helper T cell subtypes, further scrutinize the effects of autoinhibition in IRF4 and establish a potential mouse model for human Ph-like B-ALL.

Zusammenfassung

Interferon regulatory factor 4 ist ein entscheidender Transkriptionsfaktor in der adaptiven Immunantwort, sowohl bei T- als auch bei B-Zell vermittelten Prozessen. Ein IRF4 Knockout bedingt in Mäusen, schwere Defekte bei der Entwicklung funktioneller T-Zell-Untergruppen, einschließlich Th2, Th9 und Th17, sowie bei B-Zellen, die in frühen Entwicklungsstadien verhaftet sind, was zu einem Mangel an IgM im Serum führt. In T-Zellen dient IRF4 als Initiationsfaktor, der TCR-Signale übermitteln, die Zellen zur Proliferation anregt und Haupttranskriptionsregulatoren wie GATA3, T-bet und ROR γ t induziert. Um diese zentrale Rolle zu erfüllen, ist die Interaktion mit mehreren Partnern erforderlich, darunter BATF und PU.1. Wir stellen die Hypothese auf, dass eine gezielte Mutation von IRF4 dessen Funktion verändert und damit seine immunregulatorische Wirkung selektiv modifiziert werden kann. Auf Grundlage von Literaturergebnissen aus Bindungsversuchen, Strukturanalysen und wiederkehrenden Mutationen bei Krebspatienten testeten wir mehrere Punktmutationen in IRF4 auf ihre Funktionalität bei der Th2-, Th9- und Th17-Differenzierung. Einige Mutationen weisen ein immunomodulatorisches Potenzial auf. Insbesondere zeigt dies die Mutation L116R, welche die Th9-Differenzierung und die IL-9-Produktion in Th2-Zellen induziert, während sie gleichzeitig die Th2- und Th17-Differenzierung reduziert. Darüber hinaus konnten wir zeigen, dass die Selbstinhibition von IRF4 die Subtypen der T-Helferzellen unterschiedlich beeinflusst und auf Th9- und Th17-Zellen viel stärker wirkt als auf Th2-differenzierte Zellen. Zusätzlich konnten wir anhand von Tumoren, die in alten IRF4 Knockout-Mäusen auftreten, die Leukämogenese und die Entwicklung von B-Zellen im Zusammenhang mit IRF4 Defizienz weiter untersuchen, was zu einem Krankheitsbild führte, die der im Menschen auftretenden Ph-like B-ALL ähnelt. Die Behandlung dieser Krankheit mit dem JAK-Inhibitor Ruxolitinib führte zu einer erhöhten Überlebensrate, da die Infiltration von Blasten im zentralen Nervensystem und in soliden Organen reduziert wurde.

Hier zeigen wir, dass eine Immunmodulation durch Einführen von Punktmutationen möglich ist und dass IRF4 Untereinheiten besitzt, die unterschiedlich auf distinkte Subtypen der Helfer-T-Zellen wirken. Wir untersuchen weiterhin die Auswirkungen der Autoinhibition von IRF4 und etablieren ein potenzielles Mausmodell für die humane Ph-like B-ALL.

List of Figures

Figure 1: Mutations R411P+Q412P and R98A+C99A in Th2, Th9 and Th17 differentiated cells	14
Figure 2: Mutants in K399, L400, I401 and double mutants in Th2, Th9 and Th17 cells.	16
Figure 3: Mutants E406P, E305K, F391W, R328K, K349R, S344A, S344P and T384F in Th2, Th9 and Th17 cells	18
Figure 4: Mutants D117K, D117W, D117A, D117H, D117N, L116A+D117A, V111A+L116A+D117A, K59R and K59A in Th2, Th9 and Th17 differentiated cells.....	20

List of Abbreviations

AP-1	activator protein 1
aa	amino acid
AD	autoinhibitory domain
APC	antigen presenting cells
AICE	AP-1–IRF4 composite elements
BATF	basic leucine zipper transcription factor ATF-like
DAMP	damage associated molecular pattern
DBD	DNA binding domain
EICE	ETS-IRF composite elements
GATA3	GATA Binding Protein 3
ISRE	interferon-stimulated response element
ITAM	immunoreceptor tyrosine-based activation motif
IAD	interferon association domain
ISG	interferon-stimulated genes
IRF	interferon regulatory factor
JAK	janus kinase
LPS	lipopolysaccharide
LCK	lymphocyte-specific protein tyrosine kinase
LSIRF	lymphoid-specific IRF
MHC	major histocompatibility complex
NFAT	nuclear factor of activated T cells
PAMP	pathogen associated molecular patterns
PRR	pattern recognition receptors
ICSAT	interferon consensus sequence binding for activated T cells
Pip	PU.1 interacting protein
RORγt	receptor-related orphan receptors gamma
Treg	regulatory T cell
SLO	secondary lymphoid organs
STAT	signal transducers and activators of transcription
TCR	T cell receptor
Tfh	T follicular helper
Th	T helper
T-bet	T-box expressed in T cells
ZAP-70	zeta-chain-associated protein kinase 70
ZICE	Zinc finger–IRF composite element

1 Introduction

1.1 Adaptive immunity

To protect the body from danger, both from without as well as within, the immune system is based on two distinct responses that differ greatly. Innate immune responses rely on sensing of conserved structures by pattern recognition receptors (PRR), either provided by pathogens themselves (pathogen associated molecular patterns (PAMPs)) or tissue damaged during infection (damage associated molecular pattern (DAMPs)). Identification of such patterns leads to inflammation, activation of the complement system and, eventually and indirectly, to the activation of the adaptive immune system.

Uptake, processing and presentation of antigens by antigen presenting cells (APCs) is a vital process for activation of humoral and cellular adaptive immunity. Self- and foreign- antigens are presented in different ways. While all cells present antigens found in their cytosol via major histocompatibility complex (MHC) class I, foreign antigens, acquired by phagocytosis, are presented by professional APCs such as macrophages, dendritic cells and B cells via MHC class II.

The humoral part of the adaptive immune system is mediated by B cells, which rest in secondary lymphoid organs (SLO) and bind antigens provided by the flow of lymph fluid on their B cell receptor. Their presentation of antigen leads to activation of T follicular helper cells, which in return provide activation signals to the B cell, both as soluble mediators, i.e. cytokines (IL-4, IL-21) and through direct contact (CD40 ligand). Activated B cells then proliferate into either plasma blasts, plasma cells or memory B-cells. Plasma blasts are short-lived and provide a fast but low-affinity antibody reaction, whereas B cells that undergo affinity maturation in germinal centers and provide longer-lived and highly specific antibodies are termed plasma cells. Memory B cells remain in circulation in a quiescent state to provide immunity in case a reinfection occurs.

Specific responses to intracellular pathogens in the adaptive immune system are organized by T cells. Those are subdivided into either CD4⁺ helper T cells or CD8⁺ cytotoxic T cells, depending which co-receptors of the T cell receptor they express. Cytotoxic T cells monitor antigens presented by MHC class I for foreign peptides, thus identifying and killing cells infected with intracellular pathogens. Depending on the type of APC, the activation of the T cell leads to different results. If the antigen is presented by a professional APC (e.g. a dendritic cell), the APC usually is not attacked. Any other cell presenting foreign antigens

will be identified as infected and, through the release of granzymes and perforins from the cytotoxic T cell, destroyed. Usually T cells first encounter their antigen in SLOs, where they then proliferate, similar to B cells, into large quantities of reactive cytotoxic cells and a smaller T cell memory subset. To activate and support these processes, the second type of T cell is essential. CD4⁺ helper T cells interact with professional APCs through MHC class II and license them to strongly induce CD8⁺ T cell activity. They also secrete IL-2 and IFN γ , which both provide activation/proliferation signals to the cytotoxic T cell in SLOs and infected tissues.

1.2 Helper T cells

The importance of CD4⁺ helper T cells for the immune system cannot be overstated. Without their orchestration of immunological processes, the human body is prone to severe infections by seemingly harmless microbes, as witnessed in patients afflicted with AIDS and similar immunodeficiency diseases, where CD4⁺ helper T cells are severely disturbed. Both the humoral and cellular arms of the adaptive immune system rely heavily on CD4⁺ T cells to function properly: Th cells play vital roles in activation of macrophages and B cells, thus enabling phagocytosis of microbes and a robust humoral immunity, respectively. Furthermore, they stimulate cytotoxic CD8⁺ T cells to kill infected target cells and license professional APCs to unleash their full potential. These activating processes are intricately balanced by their ability to suppress immune activity, when needed, to prevent auto-reactivity and thus autoimmune diseases.

To achieve this plethora of functions, T helper cells are divided in several subtypes that achieve their function through cytokine secretion and/or direct cell-cell contact. The cytokine milieu at the time of their activation determines the fate of a naïve T helper cell (Saravia, Chapman and Chi, 2019).

Upon interaction with a peptide-laden MHC class II, found on antigen-presenting cells, and their own T cell receptor (TCR) which specifically recognizes this peptide/MHC complex, the activation is initiated. The co-receptors CD3 and CD4 relay the activation signal inside the cell: CD4 activates lymphocyte-specific protein tyrosine kinase (Lck) which phosphorylates immunoreceptor tyrosine-based activation motif (ITAMs) on CD3's γ, δ, ϵ and ζ chain, leading to the binding of zeta-chain-associated protein kinase 70 (ZAP-70) and its phosphorylation. Thus, a signalling cascade is started, which eventually forwards the activation signal to the nucleus and initiates an activated state of the T cell. One important step of this cascade is the dephosphorylation of the transcription factor nuclear factor of

activated T cells (NFAT), which then relocates to the nucleus. In order to properly activate the T cell, NFAT needs activator protein 1 (AP-1) to form heterodimeric transcription complexes, which is provided only in T cells that underwent co-stimulation. Co-stimulatory molecules (CD80/CD86, ICOS) are presented by APCs and interact with CD28 on T cells, providing a vital verification that a foreign antigen is triggering the activation process. When lacking AP-1, NFAT forms homodimers inducing anergy in the cell (Soto-Nieves *et al.*, 2009). If both TCR/CD3 signalling and co-stimulation through CD28 are successful, the T cell upregulates both IL-2 and its receptor which leads to autocrine proliferation/differentiation signals. Depending on the cytokines present during these activation processes, helper T cells express distinct cytokines under the control of key transcription factors and are thus divided into subtypes such as Th1, Th2, Th9, and Th17 (further discussed below) as well as T follicular helper cells (Tfh) and regulatory T helper cells (Tregs). However, their fate is not fully determined after initial differentiation. Helper T cells are able to repolarize and adapt to changing cytokine environments; a process known as T cell plasticity (Dupage and Bluestone, 2016). Several master regulator genes in differentiated CD4⁺ T cells maintain a bivalent histone modification, keeping them in a state ready to switch expression patterns (Wei *et al.*, 2009) This means that a helper T cell can, during its lifetime, acquire the capabilities of several subtypes and even transitory states between them.

1.2.1 Th1 and Th2 cells

The Th1 and Th2 subtypes of CD4⁺ T cells were the first described in 1986 (Mosmann *et al.*, 1986), and were for a long time thought to be the only two available fates for a helper T cell. Th1 cells produce IFN γ , IL-2 and TNF α , leading to an increased macrophage and cytotoxic T cell activity. This bolsters the defence against intracellular pathogens and protozoa, but can also lead to pathologies like type 1 diabetes if autoantigens are the cause for activation. Strengthening the defence against extracellular pathogens such as helminths is the main effect of Th2 cells. They secrete mainly IL-4, -5 and -13 and lead to IgE production from B cells and thus mast cell stimulation, as well as activation of eosinophils. Pathologies associated with over-activated Th2 cells are mainly allergies like asthma, rhinitis and atopic dermatitis.

Sensing the relevant cytokines in the micro-milieu, through their respective receptors (IL-12R and IFN γ R for Th1 or IL-4R for Th2), signalling cascades are initiated that lead to expression of master transcription factors, which control subtype-specific cytokine

expression. For Th1 cells, IL-12 and IFN γ signalling leads to the phosphorylation of signal transducers and activators of transcription (STAT) 4 and STAT1 by janus kinases (Jak). Phosphorylated STATs homodimerize and enter the nucleus to induce transcription. STAT4 signalling further enhances IFN γ production while STAT1 leads to the transcription of Th1 master transcription factor T-bet, which again furthers IFN γ expression. IL-4R signalling leads to the phosphorylation of STAT6 which in turn induces the transcription of Th2's master regulator GATA Binding Protein 3 (GATA3), promoting further IL-4 production. Thus, although the initial differentiation of CD4⁺ T cells to both Th1 and Th2 is triggered by cytokines released from innate cells reacting to pathogens or allergens, both subtypes thereafter promote a positive feedback loop through either IFN γ /T-bet or IL-4/GATA3 signalling. As they enable further differentiation of their respective subtype while suppressing the other, Th1 and Th2 differentiation states are considered mutually exclusive.

1.2.2 Th17 cells

The discovery of immunosuppressive regulatory T cells in 1995 was the first step to expanding the model of dichotomous Th1/2 helper T cells (Sakaguchi *et al.*, 1995). Regulatory T cells add another layer of complexity, but do not contradict the general idea of split responsibilities for the defence against intra- and extracellular pathogens. With the description of IL-17 producing cells in 2005 however, a new ambiguous subtype was uncovered (Harrington *et al.*, 2005; Park *et al.*, 2005). Named after their key cytokine, Th17 cells secrete both IL-17A and IL-17F, as well as IL-21 and IL-22. These cytokines are associated with mucosal host defence against extracellular pathogens, orchestrated by increased neutrophil production and recruitment to the site of infection (Weaver *et al.*, 2013). In addition to their pro-inflammatory function, it has been shown that Th17 are able to secrete IL-10 and thus also play a regulatory role (Esplugues *et al.*, 2011). Dysregulated Th17 cells, which are a key mediator of autoimmune diseases such as multiple sclerosis and psoriasis, can acquire a pathogenic phenotype, co-expressing T-bet and IFN γ together with IL-17 (Zambrano-Zaragoza *et al.*, 2014).

The differentiation of Th17 cells is guided by IL-6 and TGF- β , cytokines released by professional APCs, inducing STAT3 and SMAD signalling through their respective receptors (IL-6R and TGF- β R). Similar to other helper T cells, this induces a master transcription factor, in this case retinoic acid receptor-related orphan receptors gamma (ROR γ t); furthermore, IL-21 is produced, which leads to a positive feedback loop by further inducing STAT3 and thus ROR γ t expression. In addition, strong STAT3 signalling leads to

the expression of the IL-23 receptor, whose signalling has been shown to further stabilize Th17 differentiation. ROR γ t then controls the expression of IL-17A, IL-17F and IL-22 (Ivanov *et al.*, 2006).

1.2.3 Th9 cells

The last and latest helper T cell subset covered in this work was characterised as a distinct subtype in 2008, after two decades of research elucidating the role of IL-9 (Dardalhon *et al.*, 2008; Veldhoen *et al.*, 2008a). Besides their secretion of IL-9, immunoregulatory IL-10 is the key cytokine produced by Th9 cells. Functionally the Th9 subset is, similar to Th17 cells, ambiguous. While IL-10 is an anti-inflammatory cytokine, IL-9 is important for clearing parasitic infections, through mast cell activation (Veldhoen *et al.*, 2008b). In a similar fashion, Th9 cells reduce melanoma size in a mast cell dependant manner (Purwar *et al.*, 2012). On the other hand, Th9 cells are involved in exacerbating airway inflammation and experimental autoimmune encephalomyelitis (EAE), by bolstering Th2 responses and IgE levels in the lung (Kaplan, Hufford and Olson, 2015) and attracting Th17 cells to the central nervous system via CC-chemokine ligand 20 (Zhou *et al.*, 2011).

Polarization of Th9 cells requires IL-2, IL-4 and TGF β . In contrast to other subtypes described earlier, there is no known master transcription factor for specific Th9 cells. There is however an intricate complex of transcription factors at work either binding the *IL9* locus directly or forming complexes with other TFs that anchor there (extensively reviewed in (Kaplan, 2017)). Some of the key TFs binding the *IL9* locus are STAT5 and STAT6, PU.1 and BATF. TGF β signalling leads to trimerization of SMADs, which directly bind the *IL9* locus, as well as to expression of PU.1 (H. C. Chang *et al.*, 2010). Signalling through its receptor, IL-2 induces STAT5 dimerization, which then upregulates IL-4R expression (Liao *et al.*, 2008). In a similar fashion IL-4 induces STAT6 signalling (Goswami *et al.*, 2012). STAT6 induces BATF expression, which forms another part of the TF complex at the *IL9* locus and regulates several genes associated with the Th9 phenotype (Jabeen *et al.*, 2013a). A plethora of studies is trying to elucidate the exact working of the transcription complex formed at the IL-9 locus, but to date it is not fully understood. Knockout and blocking antibody experiments show that losing any of the above described signals heavily impairs Th9 function.

1.3 Interferon regulatory factor 4

A crucial factor for many processes occurring in our immune system in both health and disease, that has not been discussed so far, is interferon regulatory factor (IRF) 4. Reflecting its variety of functions, IRF4 was described in several contexts under different names. As PU.1 interacting protein (Pip) in B cells, where it was recruited to an enhancing composite element of the MHC class I promotor by PU.1 (Eisenbeis, Singh and Storb, 1995), lymphoid-specific IRF (LSIRF) found in IL-4 stimulated murine splenocytes (Matsuyama *et al.*, 1995) and IFN consensus sequence-binding protein in adult T cell leukaemia (ICSAT) (Yamagata *et al.*, 1996). With the IRF4 knockout mouse described in 1997, nomenclature was unified and the importance of IRF4 for the immune system could be investigated further (Mittrücker *et al.*, 1997).

1.3.1 Structure, domains and binding motifs

IRF4 is part of the interferon regulatory factor family, which comprises 10 members in total and shares several structural features common in this family. Among them are a n-terminal 139 amino acid (aa) DNA binding-domain (DBD), forming a helix-turn-helix motif with 5 tryptophan residues conserved at 10-18 amino acid intervals at its core. The DBD is flexibly linked (aa 139 to 238) to a c-terminal regulatory domain containing an interferon association domain (IAD; aa 238 to 420), which allows for homo- and heterodimerization of IRF4, as well as an autoinhibitory domain (AD; aa 420-450) for blocking DNA binding of IRF4 in its monomeric form (Huber and Lohoff, 2014).

IRF4 either signals as a homodimer that recognizes the canonical IFN-stimulated response element (ISRE), which leads to the activation of interferon-stimulated genes (ISGs). However, IRF4 homodimers have a low binding affinity for ISREs and thus signalling in T and B cells often occurs via heterodimeric or -trimeric complexes on composite elements. In B cells, IRF4 is mainly, but not exclusively, recruited by PU.1 or SPI-B, which are abundantly expressed, to ETS-IRF composite elements (EICE) (Brass, Zhu and Singh, 1999; Escalante *et al.*, 2002). T cells however show less PU.1 expression and IRF4 thus forms complexes with activator protein 1 (AP-1) family member JUN and basic leucine zipper transcription factor ATF-like (BATF) on AP-1-IRF4 composite elements (AICE) (Glasmacher *et al.*, 2012; Li *et al.*, 2012; Tussiwand *et al.*, 2012). In contrast to IRF4 homodimers on ISRE, where no direct protein-protein interaction is observed, both complexes on EICE and AICE show direct protein contact of PU.1/IRF4 and

BATF/JUN/IRF4, respectively. These direct interactions strongly contribute to the binding strength and partly explain the low affinity of IRF4 at ISREs (Sundararaj *et al.*, 2021). More recently, an additional binding motif has been discovered that shows IRF4 binding in concert with Ikaros, a regulator of development in both B and CD4⁺ T cells, to a Zinc finger–IRF composite element (ZICE). These ZICEs can envelop an ISRE, so that direct competition between IRF4 homodimers and IRF4/Ikaros dimers occurs, or include an EICE motif, which leads to Ikaros/PU.1/IRF4 complex formation and binding (Ochiai *et al.*, 2018).

Although of similar structure compared to other members of the interferon regulatory factor family, IRF4 is not upregulated by type 1 interferons. Instead, stimuli like lipopolysaccharide, IL-4, CD40 and, most importantly, TCR stimulation induce IRF4 (Gupta *et al.*, 1999; Honma *et al.*, 2005; El Chartouni, Schwarzfischer and Rehli, 2010; Man *et al.*, 2013). IRF4 expression is also dependant on several signalling pathways, such as NFAT, C-Rel and mTOR, major TFs regulating cell survival, proliferation and differentiation (Matsuyama *et al.*, 1995; Grumont and Gerondakis, 2000; Yao *et al.*, 2013).

1.3.2 IRF4 in T helper cells

As IRF4 is upregulated upon T cell activation, it is unsurprisingly important for differentiation processes in T helper cells. For Th1 cells, the role of IRF4 is still under discussion, as contradictory data has been reported. *In vitro* cultured IRF4 knockout cells have been reported as severely compromised (Lohoff *et al.*, 2002) or showing normal levels of Th1 differentiation (Tominaga *et al.*, 2003). In Th2 cells IRF4 directly binds the IL-4 promotor in complex with NFAT, regulating the key transcription factor GATA3 in both mice and humans (Hu *et al.*, 2002; Rengarajan *et al.*, 2002). Interactions of IRF4 and BATF are likely important for Th2 differentiation too, as BATF has been shown to be required for Th2 differentiation (Betz *et al.*, 2010) and AICE motifs are found in key genes regulating the Th2 programming (Glasmacher *et al.*, 2012). *In vivo* studies in IRF4 knockout mice describe a lack of both Th1 as well as Th2 differentiation. In *Leishmania major* experiments, the mice cannot clear the infection and show eventually a complete loss of cellularity in the draining lymph nodes after initial increase of lymph node size (Sacks and Noben-Trauth, 2002; Lohoff *et al.*, 2004). Similarly, transfer of IRF4^{-/-} cells to *Listeria monocytogenes* -infected mice showed very little Th1 differentiation, with cells expressing only minimal T-bet and IFN γ (Mahnke *et al.*, 2016).

For the regulation of Th17 driven diseases, experiments with IRF4^{-/-} mice showed remarkable results. These mice are resistant to several T cell mediated colitis models

(Mudter *et al.*, 2008) and lack of IRF4 also conveys complete resistance to EAE, a mouse model for multiple sclerosis. Resistance was proven to be T cell intrinsic by restoring the disease through adoptive transfer of IRF4^{+/+} CD4⁺ T cells (Brüstle *et al.*, 2007). Conversely, increase in IRF4 activity led to rheumatoid-arthritis-like diseases with increased levels of IL-17 and IL-21. This was achieved by blocking IRF4 binding protein and thus increased phosphorylation of ROCK2, leading to increased IRF4 activity at the IL-17 and IL-21 promoters (Biswas *et al.*, 2010). Similar to the Th2 program, several key genes of Th17 cells show AICE motifs (*il17*, *il21*, *il23r* and *rorc*) (Ciofani *et al.*, 2012; Glasmacher *et al.*, 2012; Li *et al.*, 2012; Tussiwand *et al.*, 2012) and mice lacking BATF show reduced Th17 differentiation (Schraml *et al.*, 2009). Adding another layer of control is the direct interaction of IRF4 and ROR γ t (Ouyang *et al.*, 2011), the key Th17 TF, as well as STAT3 mediated upregulation of IRF4 upon IL-6 signalling (Durant *et al.*, 2010).

Th9 as well are affected by lack of IRF4. Knockout cells did not display Th9 differentiation and accordingly, siRNA knockdown of IRF4 in IRF4 sufficient cells blocked IL-9 production. In a model of allergic airway disease it was shown, that IRF4 deficient mice are resistant and do not develop symptoms (Staudt *et al.*, 2010).

On a molecular level, AICE motifs have been reported in regulatory elements of the *il9* and *il10* genes (Glasmacher *et al.*, 2012) and BATF was shown to cooperate with IRF4 to induce IL-9 (Jabeen *et al.*, 2013). STAT6 signalling in Th9 differentiation induces BATF and IRF4, which also both directly interact at the IL-9 locus and are necessary for proper Th9 function and promotion of allergic airway inflammation (Übel *et al.*, 2014). Linking both cytokine signals needed for Th9 differentiation (IL-4 and TGF β), IRF4 function is also heavily dependent on SMAD expression. Smad2/Smad3 and IRF4 cooperatively bind IL-9 regulatory elements and Smad3 cannot induce IL-9 in IRF4 deficient cells nor can IRF4 induce IL-9 in smad2/3 deficient cells (Tamiya *et al.*, 2013).

PU.1, more prominently known for its role in B cells, was shown to be necessary for Th9 differentiation in T helper cells. Apart from signalling through EICE motifs together, IRF4 and PU.1 as a dimer are both found in the intricate transcription complex formed on the IL-9 locus (H.-C. Chang *et al.*, 2010).

1.3.3 IRF4 in B cells

IRF4 plays a vital role in B cell development as well as in differentiating between plasma cell and germinal center programming. IRF4 knockout mice show high amounts of B cells, however lack both germinal centers as well as serum immunoglobulins produced by plasma

cells (Mittrücker et al., 1997). It was later discovered that mice lacking both IRF4 and IRF8 show a complete arrest of B cell development at the pre-B cell stage, proving some redundancies between IRF4 and IRF8 during early development (Lu *et al.*, 2003). The transition from pre-B cells to a mature state is achieved by IRF4 and IRF8 leading to the expression of Ikaros, which in turn downregulates the pre-BCR (Ma *et al.*, 2008).

In later stages, the abundance of IRF4 determines B cell fate (Ochiai *et al.*, 2013). In B cells that express high amounts, IRF4 engages ISRE motifs, which upregulates Blimp-1, a transcription factor that leads to plasma cell differentiation (Shaffer *et al.*, 2002). At the same time ZICE motifs are engaged by Ikaros/IRF4, which leads to downregulation of Ebf1 and other genes driving germinal center reactions (Ochiai *et al.*, 2018). If IRF4 levels are lower, their respective IRF4 complexes engage both AICE and EICE motifs. This leads to upregulation of activation-induced cytidine deaminase (AID), an enzyme essential for both class switching recombination and somatic hypermutation, and Bcl6, a key regulator for germinal center formation and maintenance (Willis *et al.*, 2014).

1.3.4 Point mutations in IRF4

In early years of IRF4 research, many different point mutations have been reported to affect its function. These reports are mainly based on binding assays trying to identify domains critical for IRF4's function. In 1996 Brass et al. could prove that IRF4 contains an activation domain they assumed to be located in either the proline rich area (ranging from aa151-237) or the carboxyterminal region (aa 354-419). In addition, they identified an autoinhibitory domain in the c-terminal end of IRF4 (Brass *et al.*, 1996). They furthered their work later by providing several point mutations that showed impaired interaction between PU.1 and IRF4 at the intersection of the IAD and AD (aa 400-420) and mapped the border between the two regions to aa 401-404. Most prominently the lysine 399 to alanine exchange (K399A) as well as a glutamate to proline substitution at residue 406 (E406P) showed next to no interaction with PU.1, with the mutations L400A and K399R showing less prominent effects (Brass, Zhu and Singh, 1999). In a similar study it was shown that substitution of arginine 328 with lysine (R328K) reduced PU.1/DNA/IRF4 interaction by 50% in gel retardation assays and curiously, glutamate 305 to lysine (E305K) did not show reduction in interaction but greatly reduced activity in an luciferase assay (Ortiz *et al.*, 1999).

Advances in techniques allowed for resolution of the DNA/PU.1/IRF4 complex's crystal structure, revealing several key amino acids for PU.1/IRF4 interaction (V111, L116, D117) and confirming older data stating the importance of residues R98, C99 and N102 for IRF4's

DNA binding capability (Escalante *et al.*, 2002). More recently, full-length structure analyses using small angle x-ray scattering and crystallization clarified the tertiary structure of IRF4. It could be shown that the autoinhibitory domain is flexible and reveals the DNA binding domain upon dimerization of IRF4. In addition the linker between the DBD and IAD of IRF4 is not extended straight but folded into a domain, keeping the DBD and IAD closer together than expected (Remesh, Santosh and Escalante, 2015). This report also validated data acquired by Brass *et al.* in 1999 confirming L400 and K399 to be important residues for PU.1/IRF4 interaction, as well as introducing residues in close proximity as potentially important (e.g. F391 and T384), albeit of lesser extent. SUMOylation, a posttranslational protein modification, of K349 was also reported to regulate IRF4 stability and function (Ding *et al.*, 2016).

Several human centered trials identified point mutations of IRF4 present in leukemia patients. K59R is a mutation found in adult T cell leukemia/lymphoma patients, which has been reported to lead to higher IRF4 expression and increased localisation in the nucleus of affected T cells (Cherian *et al.*, 2018). Following further studies, a crystal structure of K59R mutated IRF4 was shown to allow R59 to interact with the DNA phosphate backbone, strengthening DNA binding compared to WT IRF4, whereas the K59A mutation lowered the DNA binding 3-fold (Sundararaj *et al.*, 2022).

A study in chronic lymphatic leukemia (CLL) patients first described the L116R mutation, leading to increased levels of IRF4 mRNA in *in vitro* transfected cells (Havelange *et al.*, 2011). L116R is mentioned in several other studies looking at genetic risk factors in CLL patients, being prominent in relapsed patients and patients associated with a shorter time to first treatment (Puente *et al.*, 2015; Kadri *et al.*, 2017; Vaisitti *et al.*, 2018). One study attributed a proliferative advantage to IRF4 L116R mutated CLL cells in patients (Benatti *et al.*, 2021). On a molecular level, Sundararaj and colleagues could show a 2-4-fold increase in DNA binding affinity by L116R mutated IRF4 on ISRE, AICE and EICE motifs. This, similar to the K59R mutation, they explain by increased interaction with the DNA phosphate backbone facilitated by the lysine residue (Sundararaj *et al.*, 2021).

1.4 Aim of the study

IRF4 is an essential factor for both B and T cell function. In T cells, it serves as an initiation factor conveying TCR signals, priming cells for proliferation and inducing master transcriptional regulators such as GATA3, T-bet and ROR γ t. Elucidating IRF4's role in health and disease opens several avenues for future treatment. Dysregulated helper T cell responses are the cause for rheumatoid arthritis, asthma and multiple sclerosis/EAE and several B cell malignancies have been linked to IRF4.

The aim of this study is to explore the role of point mutations of IRF4 in the differentiation of T helper cell subsets. We hypothesize that IRF4's interaction site with its binding partners is different from partner to partner, allowing for fine-tuning of immune responses by blocking subdomains. Here we employ viral particles genetically conveying *Irf4* with point mutations to naïve CD4⁺ T cells of IRF4^{-/-} mice to identify the effects of these mutations on Th2, Th9 and Th17 differentiation. In addition, we further investigate the effects of IRF4 deficiency in leukemogenesis

2 Results

2.1 A hyperactive mutant of interferon regulatory factor 4

Kang, Chol Ho, Enno Hartmann, Lisa Menke, Daniel Staudenraus, El Fadil Abass, Hartmann Raifer, Alekya Porapu, Bärbel Camara, Anne Brüstle, Olaf Pinkenburg, Maria Bieringer, Michael Lohoff. "A Hyperactive Mutant of Interferon-Regulatory Factor 4." *European Journal of Immunology* 49, no. 5 (May 1, 2019): 812–15.

In theory, the activity of IRF4 can be regulated in two different ways, by either altering IRF4 quantity or the quality of IRF4 signal. Depending on the strength of TCR signalling, IRF4 quantities are increased accordingly (Man *et al.*, 2013). As for quality, DNA binding capabilities of IRF4 have been shown to be hindered by its autoinhibitory domain, which is released upon dimerization (Brass *et al.*, 1996). This AD is flexible (Remesh, Santosh and Escalante, 2015), thus it is possible that DNA binding is affected gradually instead of regulating strict on/off states. This study aimed at elucidating the effect of the autoinhibitory domain of IRF4 at the differentiation of Th2, Th9 and Th17 cells. For this, two mutants were designed. The first contained a deletion of the AD (amino acids 421-450), while in the second, the deletion extended into the α -helical structure at the junction of IAD and AD (amino acids 411-450), previously shown to be important for IRF4 function (Brass, Zhu and Singh, 1999).

CD4⁺ T cells from IRF4^{-/-} mice were transfected with viral particles carrying plasmids containing either wildtype IRF4, the d421-450 (deletion of autoinhibitory domain(dAD)) or the d411-450 mutant. All vectors used contain an IRES followed by the *Gfp* gene, to identify transfected cells by fluorescence. A GFP only vector served as a negative control. Transfected cells were differentiated to either Th2, Th9 or Th17 and their function assessed. Intercellular cytokine staining of IL-13, IL-9 and IL-17, respectively, showed strong increases in the amount of IL-17 positive cells compared to wildtype IRF4, while IL-9 producing cells were only slightly affected and IL-13 did not show any significant change (Fig. 1A and B). Supernatants from cultured cells were then analysed for their cytokine content using ELISAs. While Th2 cells did not show increased IL-13 in d421-450 transfected cells, amounts of both IL-4 and IL-5 were increased. The effects on Th9 and Th17 differentiated cells carrying d421-50 could be reproduced in a similar way by ELISA. IL-9 was slightly increased in Th9 cells, while IL-17A, IL-17F and IL-21 were greatly induced in Th17 cells (Fig. 1 C). To further analyse the effect of d421-450, cells were also analysed for two non-cytokine markers of Th17 differentiation, namely CC chemokine receptor 6 (CCR6), a surface molecule important for Th17 migration and *Rorc*, the gene

encoding for the Th17 master transcription factor ROR γ t. Both proteins are markedly increased in cells carrying the d421-450 mutated IRF4 (Fig. 1 D and SFig 3 A and B). In order to confirm that the GFP signal measured by flow cytometry actually translates to protein amounts of IRF4, his-tagged IRF4 and d421-450 transfected cells were used for western blotting. Supernatants that generated similar frequencies of GFP positive cells also showed similar protein levels of IRF4 or its mutation. This finding also shows that the above described effects of the mutants seen in ICS and ELISA measurements are not due to increased protein amount of the mutant, but due to functional differences (SFig. 4 A and B). Repetition of the ICS and ELISA experiments in CD8⁺ T effector cells resulted also in significant increases in IL-17 production in d421-450-transfected cells compared to control cells transfected with wildtype IRF4. Here, IL-13 production was slightly increased, while IL-9 was not altered. In general, cytokine levels were lower than in CD4⁺ T cells. CCR6 again was increased in comparable amounts as in CD4⁺ T cells (Fig. 2). The d411-450 mutation was functionally inactive in all experiments (ICS, ELISA and CCR6 staining) in both CD4⁺ and CD8⁺ T cells, achieving only results comparable to the GFP control vector (Fig. 1 and Fig. 2).

In summary, these results show how the autoinhibitory domain of IRF4 affects T helper cell subtypes in distinct ways, an effect reproducible to some extent in CD8⁺ T cells primed in similar conditions. It seems that autoinhibition plays a more critical role in Th17 cells compared to Th9 and Th2 cells.

For this work I contributed in planning and carrying out the experiments leading to the supplementary figures 2, 3 and 4. I helped in redacting and revising the manuscript (text and figures) and created the graphical abstract.

2.2 Impact of point mutations in IRF4 on Th2, Th9 and Th17 cell differentiation

2.2.1 Defects in IRF4 functionality in mutants in the DBD and at the IAD/AD transition

As deletion of d411-450 showed complete lack of function, another mutant in the transitory helix between IAD and AD was created. Double proline mutations at aa R411 and Q412 were generated in both IRF4 and dAD background, as side by side proline residues induce a helix break. Strong reduction in cytokine production was measured in all subtypes and both backgrounds. IL-9 production was affected the least with a reduction of 60%, increasing to 70% reduction in IL-13 and 86% in IL-17. While there was no difference between IRF4 and dAD background in Th2 cells, both Th9 and Th17 cells carrying the R411P+Q412P showed a greater reduction on the dAD background (88% and 96%, respectively). To test whether any IRF4 function is retained upon loss of DNA binding capacity, the R998A+C99A mutants located in the DBD, were created, which showed almost complete lack of function, however retaining 20% of IL-13 producing cells compared to control (Figure 1).

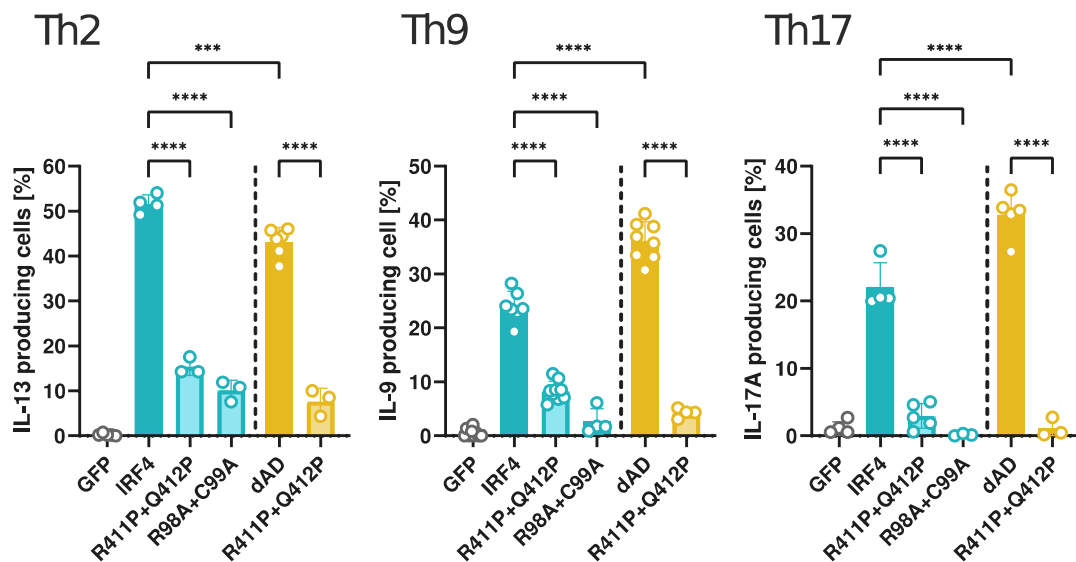
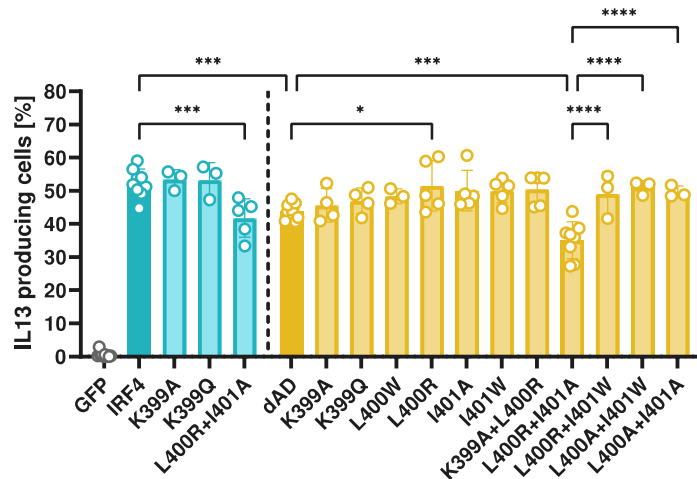


Figure 1: Mutations R411P+Q412P and R98A+C99A in Th2, Th9 and Th17 differentiated cells. Naïve IRF4^{-/-} CD4⁺ T cells were transduced with viral supernatants, containing the respective mutant, and differentiated into Th2, Th9 and Th17 cells. The cells were then restimulated, stained for cytokines intracellularly and analysed by flow cytometry. Backgrounds of vectors are denoted in colour: Teal for IRF4, orange for dAD. All biological replicates shown were acquired in independent experiments. *p<0.05; **p<0.01; ***P<0.001; ****P<0.0001. p-values were calculated using two-way ANOVA with Tukey post-hoc test.

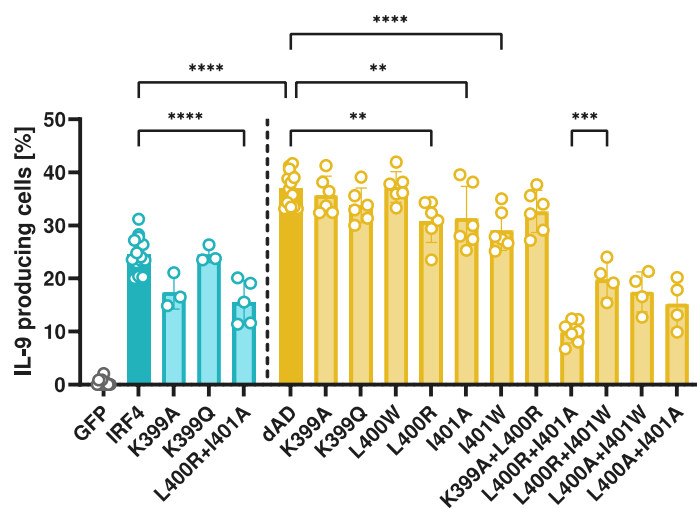
2.2.2 Point mutations in the 399-401 region show graded impairment of IRF4 function

Brass et al. showed greatly reduced binding of PU.1 and IRF4 to a DNA template mutated in K399 (Brass, Zhu and Singh, 1999). When tested in our experimental setup however, no significant effects on cytokine production were observed in K399A and K399Q mutants in any T helper subtype in both IRF4 and dAD backgrounds (Figure 2). Mutations in the neighbouring residues L400 and I401 showed minor effects. Here we introduced a positive charge with an arginine residue or altered the size of residue through replacement by the large tryptophan or the small alanine residue. L400R increased the amount of IL-13 producing cells slightly, while reducing Th9 and Th17 differentiated cells, also only by a small amount. Replacing L400 with a tryptophan (L400W) showed no significant changes. For aa 401, an alanine and a tryptophan mutant (I401A and I401W) was generated. Both showed no effects in Th2, however led to reduced numbers of IL-9 producing cells. In Th17, a similar trend was visible although not significant. All effects in K399, L400 and I401 were surprisingly small, contrary to the literature. Thus, double mutations of the most promising mutants were generated, first on the dAD background, combining L400R with K399A and L400R with I401W (and additionally several mutations containing alanine instead of arginine and tryptophan). K399A+L400R did not show the effects seen in L400R alone, but returned to levels of the control in all subsets. Of the combination mutants, only L400R+I401A reduced the amount of IL-13 producing cells. In Th9 and Th17 cells, all combination mutants (L400R+I400W, L400A+I401W, L400R+I401A and L400A+I401A) reduced cytokine production. L400R+I401A showed the strongest effect, while the other 3 were similar. Markedly, the effect strength in Th9 was lower than in Th17. It seems that there is a gradual decrease in cytokine production most prominently seen in L400R+I401A, as Th2 cells are affected the least (75% of control), Th9 show a stronger reduction (30%) and Th17 are reduced to 20% of control. L400R+I401A was then also tested in wildtype IRF4. Here the effect on Th2 cells was the same as in dAD, however in Th9 effect strength was diminished to roughly half of that in the dAD mutant (70% of control) and Th17 cell showed only a slight non-significant reduction.

Th2



Th9



Th17

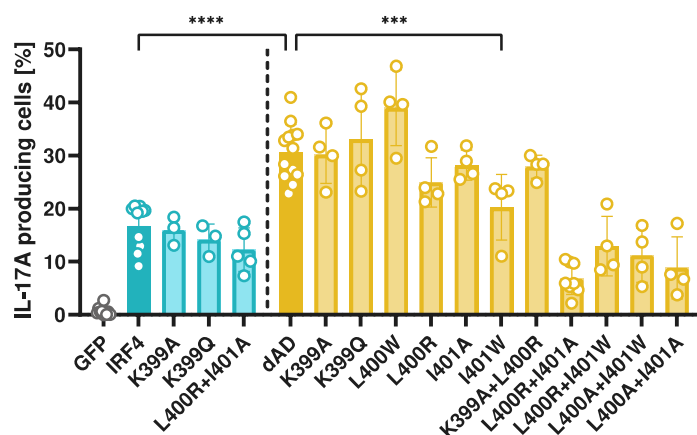
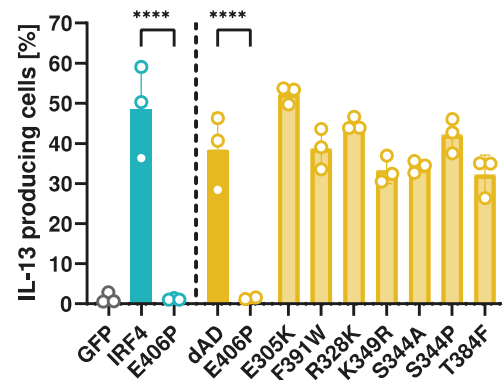


Figure 2: Mutants in K399, L400, I401 and double mutants in Th2, Th9 and Th17 cells. Naïve IRF4^{-/-} CD4⁺ T cells were transduced with viral supernatants, containing the respective mutant, and differentiated into Th2, Th9 and Th17 cells. The cells were then restimulated, stained for cytokines intracellularly and analysed by flow cytometry. Backgrounds of vectors are denoted in colour: Teal for IRF4, orange for dAD. L400 and I401 double mutants show all significantly reduced efficacy compared to dAD in Th9 and Th17. All biological replicates shown were acquired in independent experiments. *p<0.05; **p<0.01; ***P<0.001; ****P<0.0001. p-values were calculated using two-way ANOVA with Tukey post-hoc test.

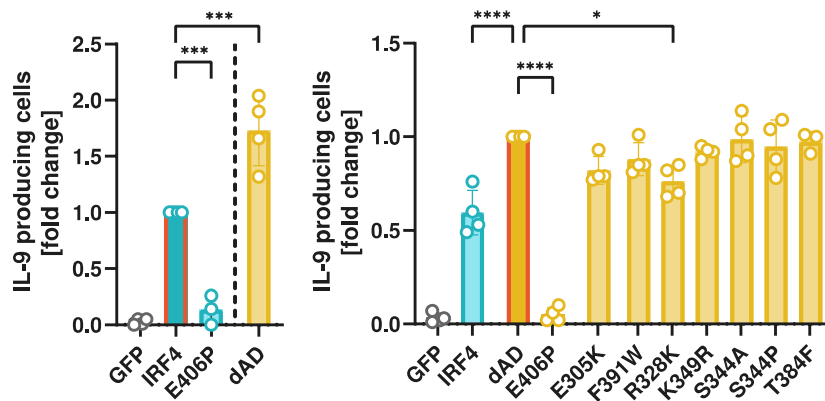
2.2.3 Of eight point mutations with previously postulated effects only E406P abrogates IRF4 function

There are several point mutations mentioned in the literature either postulated to be of importance for IRF4 function based on crystal structures or tested in gel shift binding assays. Both R328K and E305K were described by Ortiz *et al.* to inhibit ternary complex formation (Ortiz *et al.*, 1999). A report validating K399 mutants described by Brass *et al.* also identified less functionally relevant aa F391 and T384 (Remesh, Santosh and Escalante, 2015). Finally a phosphorylation and a SUMOylation site were targeted, both potentially affecting IRF4 function (Ding *et al.*, 2016). When tested in our system only E406P revealed strong effects (Figure 3). In both backgrounds, this mutation provoked complete loss of function in Th2, Th9 and Th17 cells, stressing the importance of E406P for IRF4. Of the other 7 mutants (E305K, F391W, R328K, K349R, S344A, S344P and T384F), R428K reduced IL-9 producing cells by a small amount, while E305K seemed to increase IL-13 producing cells slightly, however this effect was non-significant. All other measurements barely varied from controls.

Th2



Th9



Th17

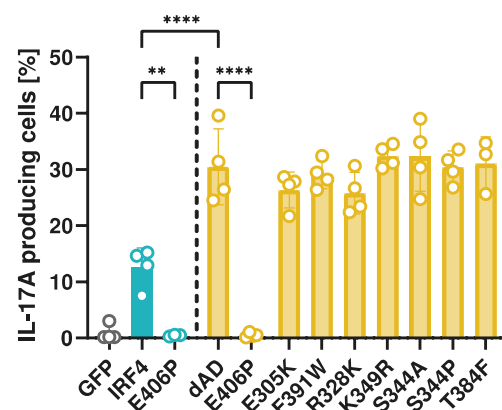


Figure 3: Mutants E406P, E305K, F391W, R328K, K349R, S344A, S344P and T384F in Th2, Th9 and Th17 cells. Naïve IRF4^{-/-} CD4⁺ T cells were transduced with viral supernatants, containing the respective mutant, and differentiated into Th2, Th9 and Th17 cells. The cells were then restimulated, stained for cytokines intracellularly and analysed by flow cytometry. Backgrounds of vectors are denoted in colour: Teal for IRF4, orange for dAD. Due to high variance in Th9 differentiation, results are shown as fold change to control (marked in red) and are thus displayed in two graphs according to proper control. All biological replicates shown were acquired in independent experiments. *p<0.05; **p<0.01; ***p<0.001; ****p<0.0001. p-values were calculated using two-way ANOVA with Tukey post-hoc test.

2.2.4 Amino acid residue D117 is vital for IRF4 function

The crystal structure of the ternary complex formed by DNA, PU.1 and IRF4 stressed the importance of aa V111, L116 and D117 for the interaction of IRF4 with PU.1 (Remesh, Santosh and Escalante, 2015). We tested the D117K mutant in both IRF4 and dAD backgrounds and detected complete loss of function in Th2 cells, while in Th9 and Th17 minor cytokine production remained (Figure 4). In contrast, the double and triple mutations L116A+D117A and V111A+L116A+D117A showed only minimal effects in Th2 and Th17 cells and none in Th9. To further elucidate the effect of D117W, the mutants D117A, D117H and D117N were generated and tested. While W, H and N mutants of D117 were very similar to D117K with strong reduction in all three subtypes, D117A showed effects similar to those observed with the L400 and I401 mutants (Figure 2): No effect was observed in Th2 while a 50% and 70% reduction in cytokine producing cells was observed in Th9 and Th17 cells, respectively. We then decided to further look into aa L116 mutants (described in 2.3, see below), not only because it was neighbouring D117, this aa exchange was also described in several papers studying mutations in human leukemia patients. Another mutation found in leukemic patients is K59R, which was described as inducing IRF4 and Myc levels in the nucleus (Cherian *et al.*, 2018). When we tested the R and A mutation at aa 59, conflicting results were revealed (Figure 4). K59R led to less cytokine producing cells in all subtypes, with moderate effects in Th2 and Th9 and strong reduction in Th17. The alanine mutation did not show an effect in Th2, but further reduced Th9 cells compare to the R mutant. In Th17, there was no significant difference between K59R and K59A, however all measurements showed slightly more Th17 producing cells in K59A transfected cells.

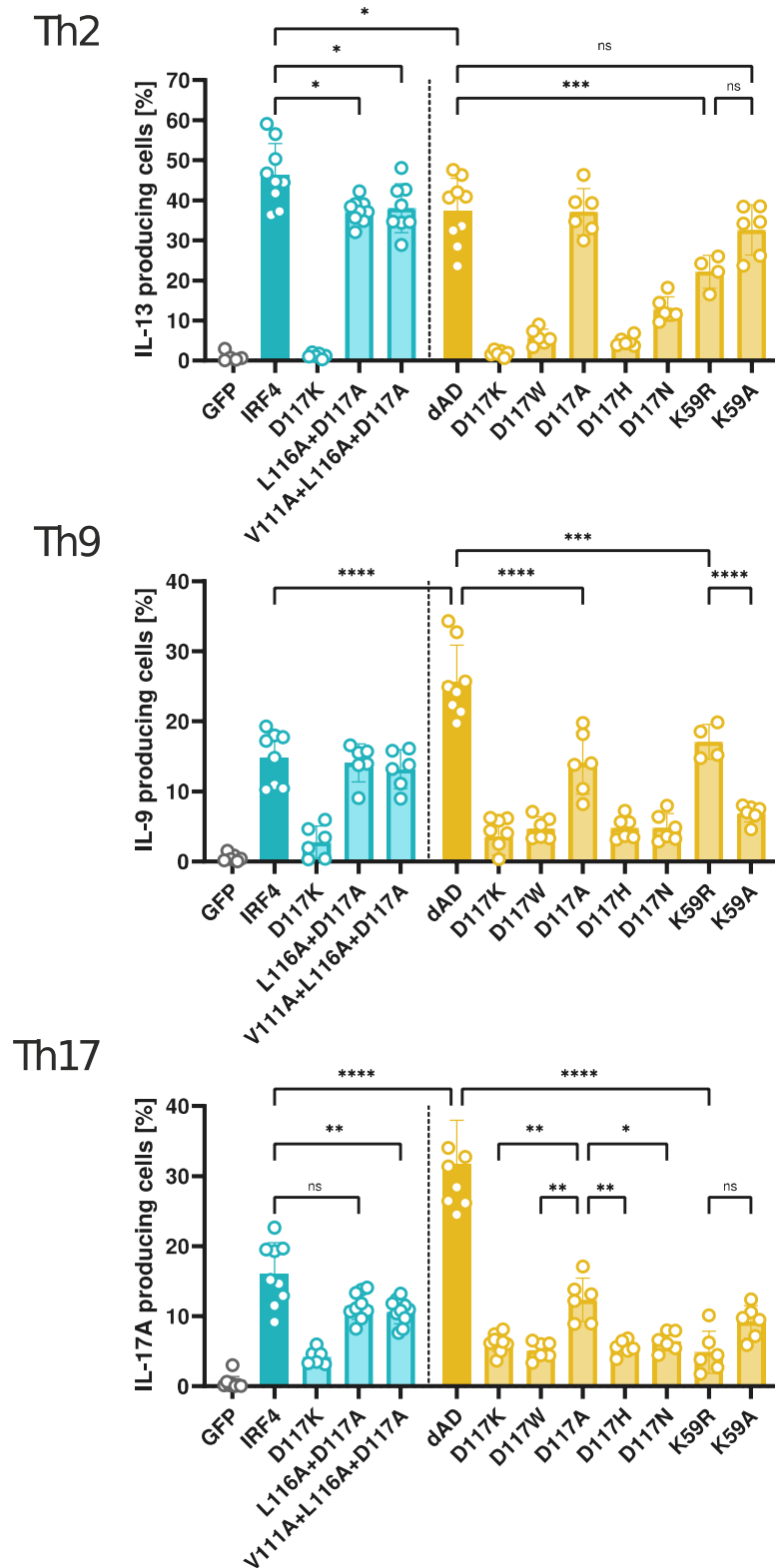


Figure 4: D117K, D117W, D117A, D117H, D117N, L116A+D117A, V111A+L116A+D117A, K59R and K59A in Th2, Th9 and Th17 differentiated cells. Naïve IRF4^{-/-} CD4⁺ T cells were transduced with viral supernatants, containing the respective mutant, and differentiated into Th2, Th9 and Th17 cells. The cells were then restimulated, stained for cytokines intracellularly and analysed by flow cytometry. Backgrounds of vectors are denoted in colour: Teal for IRF4, orange for dAD. Several indicators for significance are not shown to reduce visual clutter (e.g. all D117 mutants except for D117A in Th2 are highly significant compared to dAD). All biological replicates shown were acquired in independent experiments. *p<0.05; **p<0.01; ***P<0.001; ****P<0.0001. p-values were calculated using two-way ANOVA with Tukey post-hoc test.

2.3 Point mutation L116R in interferon regulatory factor 4 differentially impacts key cytokine production in Th2, Th9, and Th17 cells

Daniel Staudenraus, Alekhya Porapu, Hanna Leister, Dennis Das Gupta, Michael Lohoff. “Point Mutation L116R in Interferon-Regulatory Factor 4 Differentially Impacts Key Cytokine Production in Th2, Th9, and Th17 Cells.” *European Journal of Immunology*, September 2022.

The study of point mutations in IRF4 yielded several interesting mutants (see 2.2). Based on results acquired in our lab (see 2.2.4), as well as studies published by others, we argued that leucine 116 is a suitable target for mutation. Structural studies showed the importance of L116 (as well as V111 and D117) for the complex formation of DNA, PU.1 and IRF4 (Escalante *et al.*, 2002). Furthermore, L116R is a recurring mutation found in leukemia patients (Havelange *et al.*, 2011) and has been shown to increase IRF4 binding to ISRE, AICE and EICE motifs (Sundararaj *et al.*, 2021).

As in our aforementioned experiments, we employed site directed mutagenesis and viral transduction to introduce mutated IRF4 into IRF4^{-/-} naïve CD4⁺ T cells. Here we generated the mutation L116R into full length IRF4 as well as L116R combined with the deletion of the autoinhibitory domain (dAD), a mutant shown to have differential enhancing effects on T helper subtypes (see 2.1; dAD and d421-450 describe the same mutant). As in the above-explained experiments, vectors carrying only GFP, wildtype IRF4 or the dAD mutant served as controls. Further control flow cytometry experiments concluded that IRF4^{-/-} cells transfected with the wildtype IRF4 vector and wildtype cells transfected with the GFP control vector showed similar levels of IRF4 protein in transcription factor stainings (sFig. 1). This result is important, because it establishes that the technology employed by us results in physiological levels of IRF4 protein.

We first used a bead based multiplex assay to assess a broader spectrum of cytokines (IL-2, IL-6, IL-10, IL-13, IL-17A, IL-17F, IFN γ , IL-5 and IL-22) in cells differentiated under Th2 and Th9 conditions. We observed an increase in IL-9 in L116R mutations (L116R_{wt} and L116R_{dAD}) over their respective controls under Th2 conditions, but not under Th9 conditions. Nevertheless, IL-9 levels in L116R mutated Th2 cells were still lower than IL-9 quantities under Th9 conditions, as they showed 30-40% of IL-9 in IRF4 transduced Th9 cells (Fig. 1 B). Later experiments done in Th17 differentiated cells showed abrogated IL-17A and IL-17F production in L116R_{wt} and L116R_{dAD}, while confirming the IL-17 enhancing effect of dAD over wildtype IRF4 (sFig. 2 A). The enhancing effect of L116R in IL-9 was not seen in other cytokines under Th2 conditions. IL-2 and IL-6 even showed a

reduction in L116R mutated cells. A slight suppressive effect of L116R was also observed when looking at IL-13 under Th9 skewing conditions (Fig. 1 C).

As the most promising effects occurred in IL-9 versus IL-13 production, we repeated those measurements with single cytokine ELISAs, using supernatants either directly after differentiation (48h-72h, see methods) or after restimulation with ionomycin/brefeldin for 8h. In general, IL-13 levels were higher in Th2 and IL-9 levels in Th9 skewed cells (not shown). L116R on both backgrounds and both conditions induced IL-9 secretion roughly 2-fold (Fig. 2 A). IL-13 on the other hand was reduced, slightly in Th2 skewed cells (80-90% of control) and more robustly in Th9 skewed cells (50-70% of control) (Fig. 2 A).

Intracellular cytokine staining could confirm the results of the ELISA measurements. L116R_{wt} and L116R_{dAD} increased the amount of IL-9 producing cells. Effect strength was similar (1.5-fold) in Th9 L116R_{wt}, Th9 L116R_{dAD} and Th2 L116R_{dAD} and especially prominent in Th2 L116R_{wt} (2.75-fold). For IL-13 producing cells, a reduction to 0.6-fold was measured for Th2 L116R_{dAD}, Th9 L116R_{wt} and Th9 L116R_{dAD}. Here L116R_{wt} showed only a slight non-significant reduction. When looking at Th17 differentiated cells, we saw a reduction of IL-17 producing cells similar in magnitude to that of IL-13 in Th2 cells in both backgrounds of L116R.

Taken together we here show that a single point mutation can differentially affect cytokine production in Th2, Th9 and Th17 cells. i.e. Increasing IL-9 production in Th9 and Th2 skewed cells, leading to IL-9 secretion in Th2 cells in the same order of magnitude to that of wildtype Th9 cells, while at the same time decreasing IL-13 in Th2 and IL-17 in Th17 subtypes.

For this work I planned, executed and analysed all experiments, with kind help of the colleagues mentioned. I prepared the manuscript and figures and conducted experiments for the major revision, under the supervision of Michael Lohoff.

2.4 IRF4 deficiency vulnerates B-cell progeny for leukemogenesis via somatically acquired *Jak3* mutations conferring IL-7 hypersensitivity

Gupta, Dennis Das, Christoph Paul, Nadine Samel, Maria Bieringer, Daniel Staudenraus, Federico Marini, Hartmann Raifer, et al. “IRF4 Deficiency Vulnerates B-Cell Progeny for Leukemogenesis via Somatically Acquired *Jak3* Mutations Conferring IL-7 Hypersensitivity.” *Cell Death & Differentiation* 2022, April 22, 2022, 1–14.

During B cell lymphopoiesis pro-B cells adhere to the bone marrow stromal cells' CXCL12 by expression of CXCR4, while relying on IL-7 production by stromal cells to proliferate. The next step in B cell maturation is the formation of the pre-BCR composed of I μ and the surrogate light chain. The cells are now considered pre-B cells. When pre-BCR signalling occurs on pre-B cells, IRF4 is expressed, which then halts cell cycling and facilitates further maturation. In IRF4^{-/-} animals there are still mature B cells found, however in lower numbers (Mittrücker et al., 1997). This is in part due to a redundant function of IRF8, as IRF4^{-/-}/IRF8^{-/-} B cells completely arrest at the pre-B cell stage (Lu *et al.*, 2003).

Old IRF4^{-/-} mice develop spontaneous tumors in lymph nodes, accompanied by splenomegaly and lymphadenopathy. These tumors were identified to be arrested at the fraction C pre-B cell stage (according to the Hardy classification (Hardy *et al.*, 1991)), resembling a human disease known as B cell progenitor acute lymphoblastic leukemia (BCP-ALL) (Fig. 1).

The enlarged pre-B cell compartment was already found in healthy IRF4^{-/-} mice, where it could be induced by IL-7 to undergo unchecked proliferation and remain in an undifferentiated state, compared to wt cells. Inhibition of IL7R downstream signalling by JAK3 and JAK1 (through inhibitors NIBR3049 and Ruxolitinib) showed abrogation of the hyper proliferative behaviour (Fig. 2 A to G).

Spleens of IRF4^{-/-} mice showed increased numbers of early B cell progenitors, accumulating with age, hinting at premature bone marrow evasion (Fig. 2 H). Further analysis revealed greater distance between IL-7 producing stromal bone marrow cells and B cell progenitors in IRF4^{-/-} mice, when looking at femur cryosections (Fig. 2 J to M), probably due to reduced expression of CXCR4 on the progenitors (Fig. 2 N). In accordance with a functional relevance of reduced CXCR4 expression, chemokine migration assays showed reduced migration to CXCL12 by IRF4^{-/-} pre/pro B cells (Fig. 2 O).

This preleukemic state present in all IRF4^{-/-} mice probably required a second alteration to induce leukemia, as the incidence rate is only 17.5%. Whole exome sequencing and RNA sequencing of several tumors revealed among others, a recurring mutation of *Jak3*, which is

associated with IL-7 signalling, in all tumors tested (Fig. 3 A to D). Retrovirally induced active mutants of JAK3 (R653H and T844M) into IRF4^{-/-} cells greatly reduced their dependency on IL-7 to proliferate, (Fig. 3 E to G).

Re-expression of IRF4 in tumor cells retrovirally, gradually led to apoptosis over 96h (Fig. 5 A). Transcriptomic analyses of IRF4 transduced cells after 24h revealed induction of gene ontologies associated with apoptotic processes. At the same time, gene sets of B cell differentiation were upregulated, while B cell progenitor genes showed downregulation (Fig. 5 B to H). Thus, the malignant phenotype of the tumor cells was still dependent on IRF4 deficiency.

As the JAK3 inhibitor Ruxolitinib showed promising cytotoxic effects *in vitro* on IRF4^{-/-} leukemia cells (sFig. 6) it was employed in an *in vivo* study of established B-ALL. For this, wildtype mice were transferred with cells from one of the tumors studied and treated with Dexamethasone after the leukemic state was established (Fig. 6 A). Dexamethasone reduced leukemic cells in peripheral blood, but did not fully abolish the disease (Fig. 6 B). Maintenance therapy with Ruxolitinib followed for 12 days via oral gavage, controlled by a group receiving only a vehicle control. Ruxolitinib treatment could not prevent reoccurrence of leukemic cells in peripheral blood (Fig. 6 C). However, there was a clear survival benefit upon Ruxolitinib treatment (Fig. 6 D). In addition, an unexpected neurological symptom appeared during the study, ranging from limpness of the tail to hind leg paresis upon oral gavage. These symptoms were significantly reduced in Ruxolitinib treated mice, while being stronger in the control group (Fig. 6 E). Ultrasound imaging and histology revealed a mass of blasts in the spinal canal and spinal nerve roots resulting in leukemic meningeosis, which triggered paraparesis by the rise of intra-abdominal pressure during gavage. This was relieved upon Ruxolitinib treatment, as mice showed less perimyelon infiltration compared to the control group (Fig. 6 F to J). Liver infiltration was also markedly reduced in Ruxolitinib treated mice (Fig. 6 K and L).

The data shown in this work concedes insights into conditions promoting leukemogenesis in IRF4^{-/-} mice, functionally supported by a second-hit event in *Jak3*, and introduces Ruxolitinib as a potential treatment for JAK-driven BCP-ALL in humans.

For this work I helped in planning and execution of the animal experiments (applying oral gavages) and devised the scoring system upon the manifestation of paraparesis. In addition I helped collating data, created figures for the animal experiment and discussed results for the work in general.

3 Discussion

IRF4 is under scrutiny for almost four decades now, but many of its functions are still poorly understood. Its vital role for T helper cell differentiation for example is almost comically complicated, with a plethora of signalling molecules inducing second messengers and transcription factors, forming a multi-layered network featuring forward inducing loops, intricate crosstalk and poised gene sets that even allow for plasticity of fully differentiated helper cells. To shine a light on some parts of this network, we introduced mutations in IRF4 and tried to identify their effects on helper T subsets Th2, Th9 and Th17. It is a work that only glimpses at a part of a bigger picture, as many regulating factors such as professional APCs, tissue specific cytokine milieu or Tregs are not regarded. However, it allows for direct observation of how mostly minute changes in IRF4 structure heavily influence T helper subsets in distinct ways.

3.1 Deletion of dAD increases effect strength in Th9 and Th17, but not Th2

The deletion of the autoinhibitory domain (d421-450, dAD) was the first indicator for functional subdomains of IRF4, as uninhibited IRF4 differentially affected T helper subsets, slightly reducing Th2, while increasing Th9 and Th17 in a moderate or strong way, respectively (Kang *et al.*, 2019, Fig. 1 (see 2.1) and controls in Figure 1 to 4 (see 2.2)). The AD is a flexible part of IRF4, that folds away upon dimerization of IRF4 (Remesh, Santosh and Escalante, 2015). Our data suggests that this is not regulated in an on/off state, but depends on the partner IRF4 dimerizes with, as Th2 differentiation is much less affected than Th9 and Th17.

The major factor for dimerization of IRF4 on AICE motifs is BATF, which has been shown to be of importance in both Th2 (Betz *et al.*, 2010) and Th17 cells (Schraml *et al.*, 2009), while PU.1 in Th9 cells is binding EICE motifs (H.-C. Chang *et al.*, 2010). Also IL-9 was first described as a Th2 cytokine, before later experiments could show distinct differences between the subsets, eventually leading to definition of Th9 cells (Dardalhon *et al.*, 2008; Veldhoen *et al.*, 2008). Thus we expected similar effects in either Th2 and Th9 or Th2 and Th17, while actual data suggests a closer link between Th9 and Th17.

Our study implies another level of regulation in addition to dimer formation acting on response elements, as there is a clear separation between Th2 and Th9/Th17 cells when comparing dAD mutated IRF4 and wildtype IRF4 as well as mutations added to either of

them. In this regard, point mutants show subset-specific differences depending on their background (IRF4 or dAD). R411P+Q412P (Figure 1) shows the same effect strength in Th2 cells (IRF4 to R411P+Q412P_{wt} equals dAD to R411P+Q412P_{dAD}), while Th9 and Th17 both show increased effect strength in dAD (dAD shows more cytokine production than IRF4 but R411P+Q412P_{dAD} less than R411P+Q412P_{wt}). The same applies to the L400R+I401A mutant, where Th2 cells show the same effect on IRF4 and dAD background, while in Th9 cells the reduction in IL-9 is less on IRF4 than on dAD. Th17 cells do show an effect of the L400R+I401A mutant only on the dAD background, but not when it is present in wt IRF4. The effects of R411P+Q412P and L400R+I401A and all other distinct mutants is discussed in further detail below (3.4), of interest here is mainly the difference introduced by the autoinhibitory domain. Why exactly autoinhibition is less impactful in Th2 cells and what factors separate Th2 from Th9/Th17 differentiation in this regard, needs to be scrutinized further.

3.2 Th2 differentiated cells are more robust than Th9 and Th17 cells

Another curious effect seen in several mutants is that Th2 differentiated cells seem to be less affected than Th9 not only by lack of AD, but also by point mutations, while Th17 are affected the most. This appears to occur independent of the dAD/IRF4 background effect discussed above, yet both appear alongside each other and interplay cannot be ruled out. In the L400 and I401 double mutants, only L401R+I401A negatively affected Th2, while all reduced Th9 cells moderately and Th17 cells even stronger (Figure 2). The effect is mirrored by D117A (Figure 4) and similar in R98P+C99P (Figure 1). However, R98P+C99P showed strong effects in Th2 already, which gradually increased further to Th9, then Th17 cells. A special case here is D117K, which is the only mutant with a complete loss of IL-13 production, while Th9 and Th17 cells retained minimal function, stressing the importance of that residue for the Th2 program in particular (further discussed below in 3.4). What leads to these graded effects and difference in robustness to mutations remains unknown. It could be that the IRF4/BATF interaction is generally stronger in Th2 cells, as they are also less affected by the autoinhibitory domain (see. 3.1) and thus less prone to the mutations. However, the strong effects in Th17, where BATF/IRF4 is also important, implies additional explanations. Accessor proteins specific for Th2 or lack of repressing factors come to mind, but ultimately no explanation is directly deducible from the data gathered here. Probably competition with other transcription factors and the methylation dependant accessibility of

lineage specific target genes addresses the differences seen between subsets, where the same heterodimers are involved.

3.3 Many reported mutations based on structural analysis and binding assays lack relevance during T cell differentiation *in vitro*

Several studies published, thoroughly scrutinized IRF4 and identified domains and single mutants important for its function based on protein-protein interaction experiments and crystal structure analyses. Many of the published ideas hold true in our experiments, as shown by several mutants that displayed functional alterations. In this regard, mutating aa R98 and C99 strongly reduced differentiation in any subset (Figure 1), probably due to the postulated importance for DNA binding, deleting 420-450 leads to increased IRF4 activity (Kang *et al.*, 2019) and the transition between IAD/AD around aa 411 is extremely important for IRF4 function (Figure 1), which will be discussed in 3.4.

However, many of the mutants tested in our experimental setup did not match the literature. Mutating K399 and L400 did not reduce IRF4 activity the way reported by Brass *et al.* (Brass, Zhu and Singh, 1999), where ternary complex formation was completely abolished. Both mutants employed, one replacing the positive charge (K399Q) and the other greatly decreasing the size of the residue (K399A), did not show any significant effect, albeit K399A showed a slight reduction in Th9 differentiation. Increasing the size (L400W) and introducing a charge (L400R) only led to minor effects in inducing Th2 and reducing Th9 differentiation, which we deemed too small for biological relevance compared to the effects postulated (Figure 2). As mutation I401W led to reduced Th17 and Th9 differentiation, we decided to test several double mutations of L400 and I401, as well as K399A+L400R. The mutation of K399A+L400R curiously lacked the effect of L400R alone. Nonetheless, combination mutants of L400 and I401 at last showed robust effects. While L400R+I401W, L400A+I401W and L400A+I401A did not show reduction in Th2 differentiation, they negatively affected Th9 and Th17. Prominently, L400R+I401A further enhanced reduction of Th9 and Th17 and also showed an effect in reducing Th2 differentiation. Apparently, the long flexible arginine residue is able to place its charged end only in a disruptive position, when the sterical hindrance of isoleucine 401 is also removed by the substitution with the smaller alanine. It might be of interest to further look into this region of IRF4, as downregulation of both Th9 and Th17 without affecting Th2 differentiation potentially allows for treatment of Th9/Th17 mediated diseases. This however needs to be further tested in animal studies to be stated as a fact.

Still there were many other mutants mentioned in the literature about IRF4: R328K was proposed to reduce IRF4/PU.1 interaction drastically, while E305K showed reduced effectiveness in IRF4/PU.1 luciferase assays (Brass, Zhu and Singh, 1999; Ortiz *et al.*, 1999). Remesh *et al.* showed aa F391 and T384 as being important for PU.1/IRF4 binding due to their close proximity to K399 and L400 (Remesh, Santosh and Escalante, 2015). Finally phosphorylation site S344 and SUMOylation site K349 have been studied (Ding *et al.*, 2016). Of those mutants, only R328K showed a slight reduction in Th9 differentiation, whereas all others did not vary from the control levels (Figure 3). Again, the discrepancy between the literature and our data indicates other factors, apart from direct interaction between IRF4 and a binding partner, at play in our *ex vivo* model. It is possible that redundancies in biological processes, which are not present during biochemical assays and structural analysis, can attenuate impaired IRF4 function induced by point mutations.

3.4 DBD and IAD/AD transition mutants lead to severe disruption in IRF4 function

Even though not all IRF4 mutants gave results according to the literature, four demonstrated a strong reduction in all subtypes. Deletion of the transitory α -helix in the d411-450 mutant led to a lack of function in IRF4 (Kang *et al.*, 2019). Two mutants that introduce two side-by-side prolines (known to break α -helical secondary structures) were tested in addition. E406P neighbours P407 and led to a complete loss of Th2, Th9 and Th17 differentiation (Figure 3) as postulated by Brass *et al.* (Brass, Zhu and Singh, 1999). R411P+Q412P shows reduction in all three subtypes, however only in a graded manner (as described in 3.2), even though it is part of the same α -helix as E406/P407. Taken together with the experiments in K399, L400 and I401 (discussed in 3.3), it seems that the central part of the helix is most important for function, as L400R+I401A and R411P+Q412P retain some cytokine production, compared to E406P.

Another target tested to validate reported structural data was R98P+C99P, located in the DBD and supposedly of great importance for the formation of the ternary complex with PU.1 and DNA (Escalante *et al.*, 2002). Again, introduction of a helix break led to impaired function. Curiously, Th2 differentiation still yielded 10% activity, while Th9 (3%) and Th17 (0%) were almost totally inhibited. In close proximity, mutation D117K completely abrogated IL-13 production, while still retaining, albeit minimal, Th9 and Th17 differentiation, a major difference compared to the usually less affected Th2 function in all other mutants. This effect is even more prominent in preliminary data acquired in IRF4/IRF1

double knockout mice (data not shown). Due to the lack of IRF1, which antagonizes IRF4 in Th2 differentiation, these mice show Th2 differentiated cells even in GFP controls. Introduction of D117K led to similar results as presented here in Th9 and Th17 cells. However, D117K acts in a dominant negative role for Th2 differentiation, as cells lacking IRF4 completely showed more IL-13 production compared to D117K transduced cells. This was not seen in other D117 mutants, which reduced function, but never below levels of untransduced cells.

As the D117K mutant validated supposed effects described in the literature, we focused on aa 111, 116 and 117 for further research. This work was also stimulated by a report on L116R as a risk factor for CLL (Havelange *et al.*, 2011). After initial promising results with L116R, we also included K59R (and K59A as a control) in our experiments, as it too was implicated in T cell leukemia and described as increasing DNA binding (Cherian *et al.*, 2018; Sundararaj *et al.*, 2021). The D117 mutations to tryptophan, histidine and asparagine did not show differences to D117K in Th9 and Th17 differentiated cells. 20% and 15% of cytokine producing cells remained, respectively. In Th2 differentiation, the aa change at D117 has greater impact. Here all three (D117W, D117H and D117N) restored some activity and did not show a dominant negative effect in IRF4^{-/-}/IRF1^{-/-} cells (Figure 4 and data not shown). The last point mutation of D117 tested, namely D117A, revealed the most prominent immunomodulatory potential. In contrast to the other mutants at D117, it revealed no reduction in Th2 differentiation, but reduced Th9 by 40% and Th17 by 60%, showing robustness of Th2 and gradual reduction in Th9/Th17 as described in 3.2. Obviously, presence of aspartic acid and thus a negative charge is only needed in Th9 and Th17 but not in Th2. That also explains why W, H and N mutations do not differentially affect Th9 and Th17, because they all abolish the negative charge. More complicated processes are at work during Th2 differentiation, as the missing negative charge has no effect on its own. Apparently, disruption of activity in Th2 is dependent on the introduction of the flexible positive charge in the lysine, as the similarly charged but inflexible histidine and the two large but uncharged residues tryptophan and asparagine did significantly reduce activity, but still showed cytokine production of 10-20% compared to controls.

Combination mutants of V111A+L116A and V111A+L116A+D117A showed small effects compared to D117 or L116 point mutations. Th2 differentiation was slightly reduced in both, while Th9 did not show significant reduction in either. Differentiation of Th17 was only slightly impaired in the triple mutant, while the double mutant showed a similar yet

insignificant trend. This is surprising insofar as the D117A did not affect Th2 at all but produced strong effects in Th9 and Th17 differentiation.

Mutation of K59 to R and A again showed differing results compared to studies published that describe this exchange as activating, with increased IRF4 and Myc protein levels in the nucleus and stronger DNA binding in K59R, while K59A displayed reduced DNA binding capacity (Cherian *et al.*, 2018). Significant changes were observed, but affected the differentiation of all subtypes in a negative manner. K59R reduced Th2 and Th9 in similar ways (by 40% and 32%, respectively) and Th17 by 90%. The alanine mutation at the same site did not show any effect on Th2 cells but reduced Th9 and Th17 both by 72%. Thus as in D117, both site and amino acid are important for effect strength and specificity. The effects of the alanine mutation correlate to some extent to the literature, as reduced activity can be attributed to lesser DNA binding capacity. Nonetheless, as K59R does not show any inducing effects it is questionable if the results of said study apply to the *ex vivo/in vitro* environment of our experiments.

So far we identified mutations that reduce IRF4 function in several subtypes to different extents. This could be used to target specific diseases driven by a certain subtype. D117K for example completely abolishes Th2 differentiation, while keeping low levels of Th9 and Th17. On the other hand, D117A and R59A do not affect Th2 differentiation while robustly reducing Th9/Th17 with R59K further reducing Th17 without abolishing Th2 or Th9.

One mutant is singled out from all others tested, as it had both an enhancing and reducing effect. L116R boosts Th9 differentiation in both IRF4 and dAD background, while at the same time reducing Th2 and Th17 differentiation (Staudenraus *et al.*, 2022 (see 2.3)). This IL-9 enhancing effect could also be observed when looking for IL-9 in Th2 differentiated cells, which led to IL-9 levels in Th2 cells in the same order of magnitude as in Th9 differentiated cells. It has been reported, that L116R causes increased binding strength of IRF4, due to direct interaction of the positively charged arginine with the DNA phosphate backbone (Sundararaj *et al.*, 2021). The increase in binding potential of IRF4 to its response elements was 4-fold to EICE and ISRE motifs, while binding to AICE was also increased but showed a lower affinity in general. This could justify the increase in IL-9 production, but does not explain why Th17 and Th2 cells are so markedly reduced. The effect on Th17 and Th2 remains astonishing and cannot be attributed to improved DNA binding. Similar to the effects discussed in 3.1 and 3.2, there have to be other mechanisms involved, unique to the respective subtype that are yet to be understood.

In conclusion, it is possible to modulate helper T cell responses by altering IRF4's structure in distinct locations, either by abolishing a subtype known to cause disease or by boosting another helpful one. The exact extent of each mutant has to be further elucidated *in vivo* to assess its respective therapeutic potential and there are possibly more mutants, not yet identified, that will further help in modulating T helper cell subtypes in health and disease. One method for identification of such mutants is close scrutiny of mutations found in cancer patients, as both L116R and K59R have been identified by case reports of leukemia cohorts.

3.5 Development of a mouse model for the human disease Ph-like B-ALL

The spontaneous development of BCP-ALL in old IRF4 mice allowed us to gain insights in the leukemogenesis of pre-B cell arrested cells and identify a second hit needed to fully form leukemia (Das Gupta *et al.*, 2022 (see 2.4)).

After identifying the cells as fraction C pre-B cells in tumors, we could find an enlarged pre-B cell population in still healthy mice, that were susceptible for IL-7 induced unchecked proliferation on the one hand and prevented differentiation on the other. Displaying reduced CXCR4 and less migration to CXCL12, IRF4^{-/-} pre-B cells prematurely evade the bone marrow and accumulate in the periphery. Here a lack of IL-7 and contact with PAMP/DAMP could possibly induce AID, a DNA-editing enzyme usually active during somatic hypermutation (Swaminathan *et al.*, 2015). Mutations in *Jak3*, found in all tumors tested and possibly generated by AID, could represent a bottle-neck and explain why full blown leukemia is only present in 17.5% of IRF4 KO mice, as activating JAK3 mutants reduce the dependency of the enlarged pre-B cell compartment in IRF4^{-/-} mice on IL-7. Reestablishment of IRF4 with viral supernatants reprogram IRF4^{-/-} pre-B cells for apoptosis, as they try to enter a normal maturation program but lack proper signals from their usual bone marrow niche.

While in our model JAK3 was affected, in human Ph-like ALL JAK2 is often mutated. We established structural and functional similarities between murine JAK3 and human JAK2 by comparison via the alpha-fold algorithm (Jumper *et al.*, 2021). A JAK3 mutation found in IRF4^{-/-} tumors is R653, which corresponds to R683 in human JAK2, which is commonly mutated in Ph like ALL patients. This implies that our model might be relevant to assess possible treatments for human Ph-like ALL by targeting JAK2 by substances such as Ruxolitinib.

We tested the Ruxolitinib treatment in mice with established B-ALL and could show increased survival over the sham controls. However, leukemic B cells in the peripheral blood

were not reduced by Ruxolitinib. Instead the effect seemed to be solid organ specific, as blast infiltration into the central nervous system and the liver was markedly reduced. This is probably due to the dose dependant decrease of CD29 (integrin β 1) upon Ruxolitinib treatment in tumor cells, which is involved in tissue homing of B cells.

We thus show how IRF4^{-/-} pre-B cells acquire a second hit and develop leukemia and can connect this murine disease through JAK2/JAK3 similarities with Ph-like human ALL. Ruxolitinib proved to be effective in increasing survival in B-ALL, due to reduced CNS and tissue infiltration. As current CNS treatments of ALL are toxic, Ruxolitinib is a potential treatment in human disease.

4 Literature

- Benatti, S. *et al.* (2021) 'IRF4 L116R mutation promotes proliferation of chronic lymphocytic leukemia B cells inducing MYC', *Hematological oncology*, 39(5), pp. 707–711. Available at: <https://doi.org/10.1002/HON.2915>.
- Betz, B.C. *et al.* (2010) 'Batf coordinates multiple aspects of B and T cell function required for normal antibody responses', *The Journal of experimental medicine*, 207(5), pp. 933–942. Available at: <https://doi.org/10.1084/JEM.20091548>.
- Biswas, P.S. *et al.* (2010) 'Phosphorylation of IRF4 by ROCK2 regulates IL-17 and IL-21 production and the development of autoimmunity in mice', *The Journal of clinical investigation*, 120(9), pp. 3280–3295. Available at: <https://doi.org/10.1172/JCI42856>.
- Brass, A.L. *et al.* (1996) 'Pip, a lymphoid-restricted IRF, contains a regulatory domain that is important for autoinhibition and ternary complex formation with the Ets factor PU.1', *Genes and Development*, 10(18), pp. 2335–2347. Available at: <https://doi.org/10.1101/GAD.10.18.2335>.
- Brass, A.L., Zhu, A.Q. and Singh, H. (1999) 'Assembly requirements of PU.1-Pip (IRF-4) activator complexes: inhibiting function in vivo using fused dimers', *The EMBO Journal*, 18(4), pp. 977–991.
- Brüstle, A. *et al.* (2007) 'The development of inflammatory T(H)-17 cells requires interferon-regulatory factor 4', *Nature immunology*, 8(9), pp. 958–966. Available at: <https://doi.org/10.1038/NI1500>.
- Chang, H.-C. *et al.* (2010) 'The transcription factor PU.1 is required for the development of IL-9-producing T cells and allergic inflammation', *Nature Immunology*, 11(6), pp. 527–534. Available at: <https://doi.org/10.1038/ni.1867>.
- El Chartouni, C., Schwarzfischer, L. and Rehli, M. (2010) 'Interleukin-4 induced interferon regulatory factor (Irf) 4 participates in the regulation of alternative macrophage priming', *Immunobiology*, 215(9–10), pp. 821–825. Available at: <https://doi.org/10.1016/J.IMBIO.2010.05.031>.
- Cherian, M.A. *et al.* (2018) 'An activating mutation of interferon regulatory factor 4 (IRF4) in adult T-cell leukemia', *The Journal of biological chemistry*, 293(18), pp. 6844–6858. Available at: <https://doi.org/10.1074/JBC.RA117.000164>.
- Ciofani, M. *et al.* (2012) 'A validated regulatory network for Th17 cell specification', *Cell*, 151(2), pp. 289–303. Available at: <https://doi.org/10.1016/J.CELL.2012.09.016>.
- Dardalhon, V. *et al.* (2008) 'IL-4 inhibits TGF- β -induced Foxp3⁺ T cells and, together with TGF- β , generates IL-9⁺ IL-10⁺ Foxp3⁻ effector T cells', *Nature Immunology*, 9(12), pp. 1347–1355. Available at: <https://doi.org/10.1038/ni.1677>.
- Ding, X. *et al.* (2016) 'Protein SUMOylation Is Required for Regulatory T Cell Expansion and Function', *Cell Reports*, 16(4), pp. 1055–1066. Available at: <https://doi.org/10.1016/J.CELREP.2016.06.056>.
- Dupage, M. and Bluestone, J.A. (2016) 'Harnessing the plasticity of CD4⁺ T cells to treat immune-mediated disease', *Nature Reviews Immunology* 2016 16:3, 16(3), pp. 149–163. Available at: <https://doi.org/10.1038/nri.2015.18>.
- Durant, L. *et al.* (2010) 'Diverse Targets of the Transcription Factor STAT3 Contribute to T Cell Pathogenicity and Homeostasis', *Immunity*, 32(5), p. 605. Available at: <https://doi.org/10.1016/J.IMMUNI.2010.05.003>.
- Eisenbeis, C.F., Singh, H. and Storb, U. (1995) 'Pip, a novel IRF family member, is a lymphoid-specific, PU.1-dependent transcriptional activator.', *Genes & Development*, 9(11), pp. 1377–1387. Available at: <https://doi.org/10.1101/GAD.9.11.1377>.
- Escalante, C.R. *et al.* (2002) 'Crystal Structure of PU.1/IRF-4/DNA Ternary Complex', *Molecular Cell*, 10(5), pp. 1097–1105. Available at: [https://doi.org/10.1016/S1097-2765\(02\)00703-7](https://doi.org/10.1016/S1097-2765(02)00703-7).

- Esplugues, E. *et al.* (2011) 'Control of TH17 cells occurs in the Small Intestine', *Nature*, 475(7357), p. 514. Available at: <https://doi.org/10.1038/NATURE10228>.
- Glasmacher, E. *et al.* (2012) 'A genomic regulatory element that directs assembly and function of immune-specific AP-1-IRF complexes', *Science (New York, N.Y.)*, 338(6109), pp. 975–980. Available at: <https://doi.org/10.1126/SCIENCE.1228309>.
- Goswami, R. *et al.* (2012) 'STAT6-Dependent Regulation of Th9 Development', *The Journal of Immunology*, 188(3), pp. 968–975. Available at: <https://doi.org/10.4049/jimmunol.1102840>.
- Grumont, R.J. and Gerondakis, S. (2000) 'Rel Induces Interferon Regulatory Factor 4 (IRF-4) Expression in Lymphocytes: Modulation of Interferon-Regulated Gene Expression by Rel/Nuclear Factor κ B', *The Journal of Experimental Medicine*, 191(8), p. 1281. Available at: <https://doi.org/10.1084/JEM.191.8.1281>.
- Das Gupta, D. *et al.* (2022) 'IRF4 deficiency vulnerates B-cell progeny for leukemogenesis via somatically acquired Jak3 mutations conferring IL-7 hypersensitivity', *Cell Death & Differentiation* 2022, pp. 1–14. Available at: <https://doi.org/10.1038/s41418-022-01005-z>.
- Gupta, S. *et al.* (1999) 'Lineage-Specific Modulation of Interleukin 4 Signaling by Interferon Regulatory Factor 4', *The Journal of Experimental Medicine*, 190(12), p. 1837. Available at: <https://doi.org/10.1084/JEM.190.12.1837>.
- Hardy, R.R. *et al.* (1991) 'Resolution and characterization of pro-B and pre-pro-B cell stages in normal mouse bone marrow.', *Journal of Experimental Medicine*, 173(5), pp. 1213–1225. Available at: <https://doi.org/10.1084/JEM.173.5.1213>.
- Harrington, L.E. *et al.* (2005) 'Interleukin 17-producing CD4⁺ effector T cells develop via a lineage distinct from the T helper type 1 and 2 lineages', *Nature Immunology*, 6(11), pp. 1123–1132. Available at: <https://doi.org/10.1038/ni1254>.
- Havelange, V. *et al.* (2011) 'IRF4 mutations in chronic lymphocytic leukemia', *Blood*, 118(10), p. 2827. Available at: <https://doi.org/10.1182/BLOOD-2011-04-350579>.
- Honma, K. *et al.* (2005) 'Interferon regulatory factor 4 negatively regulates the production of proinflammatory cytokines by macrophages in response to LPS', *Proceedings of the National Academy of Sciences of the United States of America*, 102(44), pp. 16001–16006. Available at: <https://doi.org/10.1073/PNAS.0504226102>.
- Hu, C.M. *et al.* (2002) 'Modulation of T cell cytokine production by interferon regulatory factor-4', *The Journal of biological chemistry*, 277(51), pp. 49238–49246. Available at: <https://doi.org/10.1074/JBC.M205895200>.
- Huber, M. and Lohoff, M. (2014) 'IRF4 at the crossroads of effector T-cell fate decision', *European Journal of Immunology*, 44(7), pp. 1886–1895. Available at: <https://doi.org/10.1002/eji.201344279>.
- Ivanov, I.I. *et al.* (2006) 'The Orphan Nuclear Receptor ROR γ t Directs the Differentiation Program of Proinflammatory IL-17⁺ T Helper Cells', *Cell*, 126(6), pp. 1121–1133. Available at: <https://doi.org/10.1016/J.CELL.2006.07.035>.
- Jabeen, R. *et al.* (2013a) 'Th9 cell development requires a BATF-regulated transcriptional network', *The Journal of Clinical Investigation*, 123(11), p. 4641. Available at: <https://doi.org/10.1172/JCI69489>.
- Jumper, J. *et al.* (2021) 'Highly accurate protein structure prediction with AlphaFold', *Nature*, 596(7873), pp. 583–589. Available at: <https://doi.org/10.1038/S41586-021-03819-2>.
- Kadri, S. *et al.* (2017) 'Clonal evolution underlying leukemia progression and Richter transformation in patients with ibrutinib-relapsed CLL', *Blood advances*, 1(12), pp. 715–727. Available at: <https://doi.org/10.1182/BLOODADVANCES.2016003632>.

- Kang, C.H. *et al.* (2019) 'A hyperactive mutant of interferon-regulatory factor 4', *European Journal of Immunology*, 49(5), pp. 812–815. Available at: <https://doi.org/10.1002/EJI.201847530>.
- Kaplan, M.H. (2017) 'The Transcription factor network in Th9 cells', *Seminars in immunopathology*, 39(1), p. 11. Available at: <https://doi.org/10.1007/S00281-016-0600-2>.
- Kaplan, M.H., Hufford, M.M. and Olson, M.R. (2015) 'The Development and in vivo function of TH9 cells', *Nature reviews. Immunology*, 15(5), p. 295. Available at: <https://doi.org/10.1038/NRI3824>.
- Li, P. *et al.* (2012) 'BATF-JUN is critical for IRF4-mediated transcription in T cells', *Nature*, 490(7421), pp. 543–546. Available at: <https://doi.org/10.1038/NATURE11530>.
- Liao, W. *et al.* (2008) 'Priming for T helper type 2 differentiation by interleukin 2-mediated induction of IL-4 receptor α chain expression', *Nature immunology*, 9(11), p. 1288. Available at: <https://doi.org/10.1038/NI.1656>.
- Lohoff, M. *et al.* (2002) 'Dysregulated T helper cell differentiation in the absence of interferon regulatory factor 4', *Proceedings of the National Academy of Sciences of the United States of America*, 99(18), pp. 11808–11812. Available at: <https://doi.org/10.1073/PNAS.182425099>.
- Lohoff, M. *et al.* (2004) 'Enhanced TCR-induced apoptosis in interferon regulatory factor 4-deficient CD4(+) Th cells', *The Journal of experimental medicine*, 200(2), pp. 247–253. Available at: <https://doi.org/10.1084/JEM.20040182>.
- Lu, R. *et al.* (2003) 'IRF-4,8 orchestrate the pre-B-to-B transition in lymphocyte development', *Genes & development*, 17(14), pp. 1703–1708. Available at: <https://doi.org/10.1101/GAD.1104803>.
- Ma, S. *et al.* (2008) 'Interferon regulatory factors 4 and 8 induce the expression of Ikaros and Aiolos to down-regulate pre-B-cell receptor and promote cell-cycle withdrawal in pre-B-cell development', *Blood*, 111(3), p. 1396. Available at: <https://doi.org/10.1182/BLOOD-2007-08-110106>.
- Mahnke, J. *et al.* (2016) 'Interferon Regulatory Factor 4 controls TH1 cell effector function and metabolism', *Scientific Reports 2016 6:1*, 6(1), pp. 1–12. Available at: <https://doi.org/10.1038/srep35521>.
- Man, K. *et al.* (2013) 'The transcription factor IRF4 is essential for TCR affinity-mediated metabolic programming and clonal expansion of T cells', *Nature immunology*, 14(11), pp. 1155–1165. Available at: <https://doi.org/10.1038/NI.2710>.
- Matsuyama, T. *et al.* (1995) 'Molecular cloning of LSIRF, a lymphoid-specific member of the interferon regulatory factor family that binds the interferon-stimulated response element (ISRE)', *Nucleic acids research*, 23(12), pp. 2127–2136. Available at: <https://doi.org/10.1093/NAR/23.12.2127>.
- Mittrücker, H.W. *et al.* (2017) 'Requirement for the transcription factor LSIRF/IRF4 for mature B and T lymphocyte function', *Journal of Immunology*, 199(11), pp. 3717–3720. Available at: <https://doi.org/10.1126/science.275.5299.540>.
- Mosmann, T.R. *et al.* (1986) 'Two types of murine helper T cell clone. I. Definition according to profiles of lymphokine activities and secreted proteins.', *The Journal of Immunology*, 136(7).
- Mudter, J. *et al.* (2008) 'The transcription factor IFN regulatory factor-4 controls experimental colitis in mice via T cell-derived IL-6', *The Journal of clinical investigation*, 118(7). Available at: <https://doi.org/10.1172/JCI33227>.
- Ochiai, K. *et al.* (2013) 'Transcriptional regulation of germinal center B and plasma cell fates by dynamical control of IRF4', *Immunity*, 38(5), pp. 918–929. Available at: <https://doi.org/10.1016/J.IMMUNI.2013.04.009>.
- Ochiai, K. *et al.* (2018) 'Zinc finger-IRF composite elements bound by Ikaros/IRF4 complexes function as gene repression in plasma cell', *Blood advances*, 2(8), pp. 883–894. Available at: <https://doi.org/10.1182/BLOODADVANCES.2017010413>.

- Ortiz, M.A. *et al.* (1999) 'Mutation analysis of the pip interaction domain reveals critical residues for protein-protein interactions', *Proceedings of the National Academy of Sciences of the United States of America*, 96(6), pp. 2740–2745. Available at: <https://doi.org/10.1073/PNAS.96.6.2740/ASSET/34BAFB2A-2E63-4197-8837-741C7064AB68/ASSETS/GRAPHIC/PQ0690162004.JPEG>.
- Ouyang, X. *et al.* (2011) 'Transcription factor IRF8 directs a silencing programme for TH17 cell differentiation', *Nature Communications*, 2(1), p. 314. Available at: <https://doi.org/10.1038/NCOMMS1311>.
- Park, H. *et al.* (2005) 'A distinct lineage of CD4 T cells regulates tissue inflammation by producing interleukin 17', *Nature Immunology*, 6(11), pp. 1133–1141. Available at: <https://doi.org/10.1038/ni1261>.
- Puente, X.S. *et al.* (2015) 'Non-coding recurrent mutations in chronic lymphocytic leukaemia', *Nature*, 526(7574), pp. 519–524. Available at: <https://doi.org/10.1038/NATURE14666>.
- Purwar, R. *et al.* (2012) 'Robust tumor immunity to melanoma mediated by interleukin-9-producing T cells', *Nature Medicine* 2012 18:8, 18(8), pp. 1248–1253. Available at: <https://doi.org/10.1038/nm.2856>.
- Remesh, S.G., Santosh, V. and Escalante, C.R. (2015) 'Structural Studies of IRF4 Reveal a Flexible Autoinhibitory Region and a Compact Linker Domain', *The Journal of Biological Chemistry*, 290(46), p. 27779. Available at: <https://doi.org/10.1074/JBC.M115.678789>.
- Rengarajan, J. *et al.* (2002) 'Interferon regulatory factor 4 (IRF4) interacts with NFATc2 to modulate interleukin 4 gene expression', *The Journal of experimental medicine*, 195(8), pp. 1003–1012. Available at: <https://doi.org/10.1084/JEM.20011128>.
- Sacks, D. and Noben-Trauth, N. (2002) 'The immunology of susceptibility and resistance to *Leishmania major* in mice', *Nature reviews. Immunology*, 2(11), pp. 845–858. Available at: <https://doi.org/10.1038/NRI933>.
- Sakaguchi, S. *et al.* (1995) 'Immunologic self-tolerance maintained by activated T cells expressing IL-2 receptor alpha-chains (CD25). Breakdown of a single mechanism of self-tolerance causes various autoimmune diseases.', *The Journal of Immunology*, 155(3).
- Saravia, J., Chapman, N.M. and Chi, H. (2019) 'Helper T cell differentiation', *Cellular and Molecular Immunology*, 16(7), pp. 634–643. Available at: <https://doi.org/10.1038/s41423-019-0220-6>.
- Schraml, B.U. *et al.* (2009) 'The AP-1 transcription factor Batf controls T(H)17 differentiation', *Nature*, 460(7253), pp. 405–409. Available at: <https://doi.org/10.1038/NATURE08114>.
- Shaffer, A.L. *et al.* (2002) 'Blimp-1 orchestrates plasma cell differentiation by extinguishing the mature B cell gene expression program', *Immunity*, 17(1), pp. 51–62. Available at: [https://doi.org/10.1016/S1074-7613\(02\)00335-7](https://doi.org/10.1016/S1074-7613(02)00335-7).
- Soto-Nieves, N. *et al.* (2009) 'Transcriptional complexes formed by NFAT dimers regulate the induction of T cell tolerance', *Journal of Experimental Medicine*, 206(4), pp. 867–876. Available at: <https://doi.org/10.1084/JEM.20082731>.
- Staudenraus, D. *et al.* (2022) 'Point mutation L116R in interferon-regulatory factor 4 differentially impacts key cytokine production in Th2, Th9, and Th17 cells', *European Journal of Immunology* [Preprint]. Available at: <https://doi.org/10.1002/EJI.202249869>.
- Staudt, V. *et al.* (2010) 'Interferon-Regulatory Factor 4 Is Essential for the Developmental Program of T Helper 9 Cells', *Immunity*, 33(2), pp. 192–202. Available at: <https://doi.org/10.1016/J.IMMUNI.2010.07.014>.
- Sundararaj, S. *et al.* (2021) 'Structural determinants of the IRF4/DNA homodimeric complex', *Nucleic Acids Research*, 49(4), pp. 2255–2265. Available at: <https://doi.org/10.1093/NAR/GKAA1287>.

- Sundararaj, S. *et al.* (2022) 'The molecular basis for the development of adult T-cell leukemia/lymphoma in patients with an IRF4 K59R mutation', *Protein science: a publication of the Protein Society*, 31(4), pp. 787–796. Available at: <https://doi.org/10.1002/PRO.4260>.
- Swaminathan, S. *et al.* (2015) 'Mechanisms of clonal evolution in childhood acute lymphoblastic leukemia', *Nature immunology*, 16(7), pp. 766–774. Available at: <https://doi.org/10.1038/NI.3160>.
- Tamiya, T. *et al.* (2013) 'Smad2/3 and IRF4 play a cooperative role in IL-9-producing T cell induction', *Journal of immunology (Baltimore, Md. : 1950)*, 191(5), pp. 2360–2371. Available at: <https://doi.org/10.4049/JIMMUNOL.1301276>.
- Tominaga, N. *et al.* (2003). 'Development of Th1 and not Th2 immune responses in mice lacking IFN-regulatory factor-4', *International Immunology*, 15(1), 1–10. <https://doi.org/10.1093/INTIMM/DXG001>
- Tussiwand, R. *et al.* (2012) 'Compensatory dendritic cell development mediated by BATF-IRF interactions', *Nature*, 490(7421), p. 502. Available at: <https://doi.org/10.1038/NATURE11531>.
- Übel, C. *et al.* (2014) 'The activating protein 1 transcription factor basic leucine zipper transcription factor, ATF-like (BATF), regulates lymphocyte- and mast cell-driven immune responses in the setting of allergic asthma', *The Journal of allergy and clinical immunology*, 133(1). Available at: <https://doi.org/10.1016/J.JACI.2013.09.049>.
- Vaisitti, T. *et al.* (2018) 'Novel Richter Syndrome Xenograft Models to Study Genetic Architecture, Biology, and Therapy Responses', *Cancer research*, 78(13), pp. 3413–3420. Available at: <https://doi.org/10.1158/0008-5472.CAN-17-4004>.
- Veldhoen, M. *et al.* (2008a) 'Transforming growth factor-beta "reprograms" the differentiation of T helper 2 cells and promotes an interleukin 9-producing subset', *Nature immunology*, 9(12), pp. 1341–1346. Available at: <https://doi.org/10.1038/NI.1659>.
- Weaver, C.T. *et al.* (2013) 'The Th17 Pathway and Inflammatory Diseases of the Intestines, Lungs and Skin', *Annual review of pathology*, 8, p. 477. Available at: <https://doi.org/10.1146/ANNUREV-PATHOL-011110-130318>.
- Wei, G. *et al.* (2009) 'Global mapping of H3K4me3 and H3K27me3 reveals specificity and plasticity in lineage fate determination of differentiating CD4+ T cells', *Immunity*, 30(1), pp. 155–167. Available at: <https://doi.org/10.1016/J.IMMUNI.2008.12.009>.
- Willis, S.N. *et al.* (2014) 'Transcription factor IRF4 regulates germinal center cell formation through a B cell-intrinsic mechanism', *Journal of immunology (Baltimore, Md. : 1950)*, 192(7), pp. 3200–3206. Available at: <https://doi.org/10.4049/JIMMUNOL.1303216>.
- Yamagata, T. *et al.* (1996) 'A novel interferon regulatory factor family transcription factor, ICSAT/Pip/LSIRF, that negatively regulates the activity of interferon-regulated genes.', *Molecular and Cellular Biology*, 16(4), p. 1283. Available at: <https://doi.org/10.1128/MCB.16.4.1283>.
- Yao, S. *et al.* (2013) 'Interferon regulatory factor 4 sustains CD8(+) T cell expansion and effector differentiation', *Immunity*, 39(5), pp. 833–845. Available at: <https://doi.org/10.1016/J.IMMUNI.2013.10.007>.
- Zambrano-Zaragoza, J.F. *et al.* (2014) 'Th17 Cells in Autoimmune and Infectious Diseases', *International Journal of Inflammation*, 2014. Available at: <https://doi.org/10.1155/2014/651503>.
- Zhou, Y. *et al.* (2011) 'IL-9 Promotes Th17 Cell Migration into the Central Nervous System via CC Chemokine Ligand-20 Produced by Astrocytes', *The Journal of Immunology*, 186(7), pp. 4415–4421. Available at: <https://doi.org/10.4049/JIMMUNOL.1003307>.

5 Appendix

5.1 Curriculum vitae

Persönliche Daten

Name: Daniel Staudenraus
Anschrift: Gerhart-Hauptmann-Straße 9
35039 Marburg
Geburtsdatum: 11.09.1990
Geburtsort: Saarbrücken
Staatsangehörigkeit: deutsch
E-Mail: Daniel@Staudenraus.com

Promotionsstudium

10.2016 – 10.2022
Phillipps Universität Marburg
Medizinische Mikrobiologie und Krankenhaushygiene
Wissenschaftlicher Mitarbeiter/Promotion mit dem Thema
„Identifizierung funktioneller Untereinheiten des
Transkriptionsfaktors IRF4“

Berufserfahrung

10.2015 – 02.2016
Uniklinik Frankfurt am Main
Institut für kardiovaskuläre Regeneration (AG Grote)
wissenschaftlicher Mitarbeiter

Studium

10.2013 – 09.2015
Goethe Universität, Frankfurt am Main
Masterstudium Molekulare Medizin
Abschluss: Master of Science (M. Sc.) Note: 1,3
Masterthesis:
“G-Protein coupled receptors in Multiple Sclerosis and
Experimental Autoimmune Encephalomyelitis”
durchgeführt am Max-Planck-Institut für Herz- und
Lungenforschung, Bad Nauheim (AG Offermanns)

10.2010 – 08.2013
Goethe Universität, Frankfurt am Main
Bachelorstudium Biochemie
Abschluss: Bachelor of Science (B. Sc.) Note: 1,4
Bachelorthesis:
“Einfluss der Hepatitis B Genotypen A und G auf die
Expression und Lokalisation von α -Taxilin“
durchgeführt am Bundesinstitut für Impfstoffe und
biomedizinische Arzneimittel, Langen (AG Hildt)

Schule und Zivildienst

09.2009 – 06.2010	Zivildienst im Hort Herrensohr, Saarbrücken
08.2001 – 07.2009	Gymnasium am Rotenbühl, Saarbrücken Abitur mit den Leistungsfächern: Biologie, Chemie, Englisch Notenschnitt: 1,8 Zertifizierter Abschluss des bilingualen Zweigs (Englisch)

5.2 Verzeichnis akademischer Lehrer

Meine Akademischen Lehrer in Frankfurt am Main:

Dimmeler, Dötsch, Ebersberger, Flemming, Glaubitz, Gottschalk, Güntert, Herrmann, Ludwig, Mühl, Niederberger, Pos, Schmidt, Schulte, Schwalbe, Steinle, Tampé, Ullrich und Wagenblast

5.3 Danksagung

Eine wissenschaftliche Arbeit ist nie das Werk eines Einzelnen und selbst die längsten Autorenlisten vermögen es nicht alle zu erfassen, die daran beteiligt waren. Für die erlebnisreiche Zeit im Institut für Medizinische Mikrobiologie und Krankenhaushygiene möchte ich mich bei allen Mitarbeitern bedanken.

Besonderer Dank gebührt hierbei Prof. Dr. Michael Lohoff, der es mir erst ermöglicht hat diese Arbeit zu schreiben und mir viel Freiraum zur Entfaltung lies, aber trotzdem immer unterstützend und leitend zur Stelle war. Innerhalb und außerhalb unseres Labors haben wir in den Jahren zusammen einige Dinge erlebt, die mir noch sehr lange im Gedächtnis bleiben werden. Spätabendliche Fahrten in die Notaufnahme, Steinpilze, tolle Reisetipps und immer ein aufmunterndes Wort in den frustreichen Zeiten. Danke, Michael!

Im Labor muss ich mich vor Allem bei Dr. Olaf Pinkenburg bedanken, der mir in meiner Anfangszeit mit viel Rat und seinem umfangreichen Wissen über molekularbiologische Methoden zur Seite stand. Danke an Hanna Leister, Dr. Dennis das Gupta, Manuel Gerlach, Dr. Hartmann Raifer, Dr. Felix Picard, Dr. Florence Fischer und Alekhya Porapu für die Diskussionen und Kooperationen zu euren und meinen Themen, die aus mir einen vielseitigeren Wissenschaftler gemacht haben.

Oft nicht auf der Publikation zu finden, aber trotzdem essenziell: Danke an die technische Assistenz der Medizinischen Mikrobiologie, die den Laden am Laufen hält und mir mit tausend Kleinigkeiten den Alltag so sehr erleichtert hat (Anne Hellhund, Claudia Trier, Nadine Buschmann, Anna Guralnik und Bärbel Camara).

All work and no play make Jack a dull boy. Danke an alle die, die mir in meiner Freizeit geholfen haben den Stress und Frust für ein paar Stunden hinter mir zu lassen und in den guten Zeiten immer für ein Bier (oder einen nerdigen Brettspielabend) zu haben waren: Felix Picard, Dane Kotas und Florence Fischer, Michael Klüver und Marina Nicolai, Hanna Leister, Dennis das Gupta und Manuel Gerlach.

Danke an meine Eltern, ohne die all dies nicht möglich gewesen wäre, an Denis und Kaja und den kleinen Nico für die schönen Tage abseits vom Labor, auch wenn sie seltener sind als mir lieb ist. Und schlussendlich für die wahrscheinlich größte Leistung überhaupt: Meine Stimmung in den dunklen Tagen nicht nur zu ertragen, sondern auch den Glauben an ein Projekt zu erhalten, den ich selbst schon aufgegeben hatte. Danke Hanna Leister.

5.4 Vollständiges Veröffentlichungsverzeichnis

Tischner, Denise, Myriam Grimm, Harmandeep Kaur, Daniel Staudenraus, Jorge Carvalho, Mario Looso, Stefan Günther, et al. **“Single-Cell Profiling Reveals GPCR Heterogeneity and Functional Patterning during Neuroinflammation.”** *JCI Insight* 2, no. 15 (August 3, 2017).

Kang, Chol Ho, Enno Hartmann, Lisa Menke, Daniel Staudenraus, El Fadil Abass, Hartmann Raifer, Alekya Porapu, et al. **“A Hyperactive Mutant of Interferon-Regulatory Factor 4.”** *European Journal of Immunology* 49, no. 5 (May 1, 2019): 812–15.

Carbó, José M., Theresa E. León, Joan Font-Díaz, Juan Vladimir de la Rosa, Antonio Castrillo, Felix R. Picard, Daniel Staudenraus, et al. **“Pharmacologic Activation of LXR Alters the Expression Profile of Tumor-Associated Macrophages and the Abundance of Regulatory T Cells in the Tumor Microenvironment.”** *Cancer Research* 81, no. 4 (February 15, 2021): 968–85.

Leister, Hanna, Maik Luu, Daniel Staudenraus, Aleksandra Krol Lopez, Hans Joachim Mollenkopf, Arjun Sharma, Nils Schmerer, et al. **“Pro- and Antitumorigenic Capacity of Immunoproteasomes in Shaping the Tumor Microenvironment.”** *Cancer Immunology Research* 9, no. 6 (June 1, 2021): 682–92.

Romero-Olmedo, Addi J., Axel Ronald Schulz, Svenja Hochstätter, Dennis Das Gupta, Iris Virta, Heike Hirseland, Daniel Staudenraus, et al. **“Induction of Robust Cellular and Humoral Immunity against SARS-CoV-2 after a Third Dose of BNT162b2 Vaccine in Previously Unresponsive Older Adults.”** *Nature Microbiology* 7, no. 2 (February 1, 2022): 195–99.

Romero-Olmedo, Addi J., Axel Ronald Schulz, Svenja Hochstätter, Dennis Das Gupta, Heike Hirseland, Daniel Staudenraus, Bärbel Camara, et al. **“Dynamics of Humoral and T-Cell Immunity after Three BNT162b2 Vaccinations in Adults Older than 80 Years.”** *The Lancet. Infectious Diseases* 22, no. 5 (May 1, 2022): 588–89.

Gupta, Dennis Das, Christoph Paul, Nadine Samel, Maria Bieringer, Daniel Staudenraus, Federico Marini, Hartmann Raifer, et al. **“IRF4 Deficiency Vulnerates B-Cell Progeny for Leukemogenesis via Somatically Acquired Jak3 Mutations Conferring IL-7 Hypersensitivity.”** *Cell Death & Differentiation* 2022, April 22, 2022, 1–14.

Staudenraus, Daniel, Alekhya Porapu, Hanna Leister, Dennis Das Gupta, and Michael Lohoff. **“Point Mutation L116R in Interferon-Regulatory Factor 4 Differentially Impacts Key Cytokine Production in Th2, Th9, and Th17 Cells.”** *European Journal of Immunology*, September 2022.

6 Publications

[DOI: 10.1002/eji.201847530]

A hyperactive mutant of interferon-regulatory factor 4

Interferon-regulatory factors (IRFs) are a family of transcription factors with pleiotropic functions in immune cells, including in generation of subsets of DCs and macrophages and B cell maturation [1]. IRF1 deficiency results in strongly diminished Th1 responses [2] and an inability to counteract pro-asthmatic Th9 responses [3].

IRF4 is thoroughly involved in T-cell subset differentiation. Work mainly from our group described decisive activities of IRF4 during generation of Th2, Th9, Th17, and Tfh cells [4, 5]. In addition, development of Tc17 and sustainment of effector CD8⁺ cells also depend on IRF4 [6]. These phenotypes have dramatic consequences in vivo: IRF4-deficient mice are resistant to models of multiple sclerosis, asthma, and inflammatory bowel disease [4, 5]; disease activity can be regained by adoptive transfer of WT CD4⁺ T cells. Vice versa, IRF4 deficiency leads to increased disease susceptibility after infection with the protozoan *Leishmania major* [5].

Amounts of IRF4 correlate with TCR signal strength [7] and varying amounts of IRF4 regulate distinct gene clusters in a complex with the transcription factor BATF [8]. These processes, which also include distinct binding affinities of IRF4 to its respective target sites, can determine T cell

fate, e.g., the generation of effector versus Tfh cells [9].

Theoretically, the possibility to alter IRF4's activity might not be restricted to varying its quantity, but also to change its structure: an autoinhibitory domain within IRF4 hinders DNA-binding unless interaction with the transcription factor PU.1 occurs [10]. However, no functional relevance of this domain for lymphocyte activity has been analyzed to our knowledge.

Therefore, two mutants of murine IRF4 were generated and integrated into a bicistronic retroviral vector also encoding for GFP. Mutant 1 (d421-450) lacks the final 30 C-terminal amino acids (AA), i.e., the autoinhibitory domain of IRF4, while the structurally important α -helix is conserved (Supporting Information Fig. S1). In mutant 2 (p411-450), the deletion extends into the α -helix, which should lead to a severely altered structure of the truncated molecule.

These mutants or WT IRF4 or an empty control vector (pGFP) were transduced into IRF4 deficient CD4⁺ Th cells to evaluate their functional qualities. Cells were then differentiated under Th1, Th2, Th9, or Th17 conditions, restimulated, and cytokine production was measured either by intracellular staining (Fig. 1A and B and Supporting Information Fig. S2) or by ELISA (Fig. 1C) from culture supernatants. Transduction by control retrovirus resulted in no cytokine production. Under Th17 conditions, d421-450 yielded a strikingly enhanced production of the marker cytokine IL-17A, by both staining and ELISA, compared to WT IRF4. In contrast, no cytokines were induced by d411-450, confirming its anticipated functional knock-out. Along with IL-17A, the production of the Th17 products IL-17F and IL-

21 was also doubled by d421-450 but not d411-450, as determined by ELISA.

In contrast to this clear effect of d421-450 on Th17 signature cytokines, the effect on Th2 products was less stringent (Fig. 1A–C). By ELISA, IL-4 production was also doubled, while IL-5 induction was slightly less pronounced and IL-13 production was almost untouched. Staining for IL-4 and IL-5 was too weak to enable validation of these results by flow cytometry. Staining for IL-13 confirmed almost no hyperactivity of d421-450 for this cytokine. By both cytometry and ELISA, the induction of the Th9 product IL-9 was also only slightly enhanced by d421-450. In all instances, d411-450 showed no cytokine-inducing activity. In Th1-differentiated cells, no positive effect of transfected IRF4 or d421-450 on IFN- γ production was noted. As reported before [4], substantial IFN- γ production occurred in nontransfected cells (Supporting Information Fig. S2), which, for unknown reasons and with all viruses, was even higher than in infected cells. As a control, the differences of IRF4 and d421-450 for IL-17 production were visible as before (Supporting Information Fig. S2).

Next, we tested whether the Th17-enhancing activity of d421-450 was extended to noncytokine products like the chemokine receptor CCR6 and the master transcription factor ROR γ T. CCR6 was also significantly more upregulated by d421-450 as compared to WT IRF4, as shown by flow cytometry (Fig. 1D). When measuring expression of *Rorc* by quantitative PCR (Supporting Information Fig. S3), we first confirmed equal infection with IRF4 and d421-450 expressing retroviruses by GFP expression (Supporting Information Fig. S3A) and enhanced IL-17A expression in the presence of d421-450 (Supporting

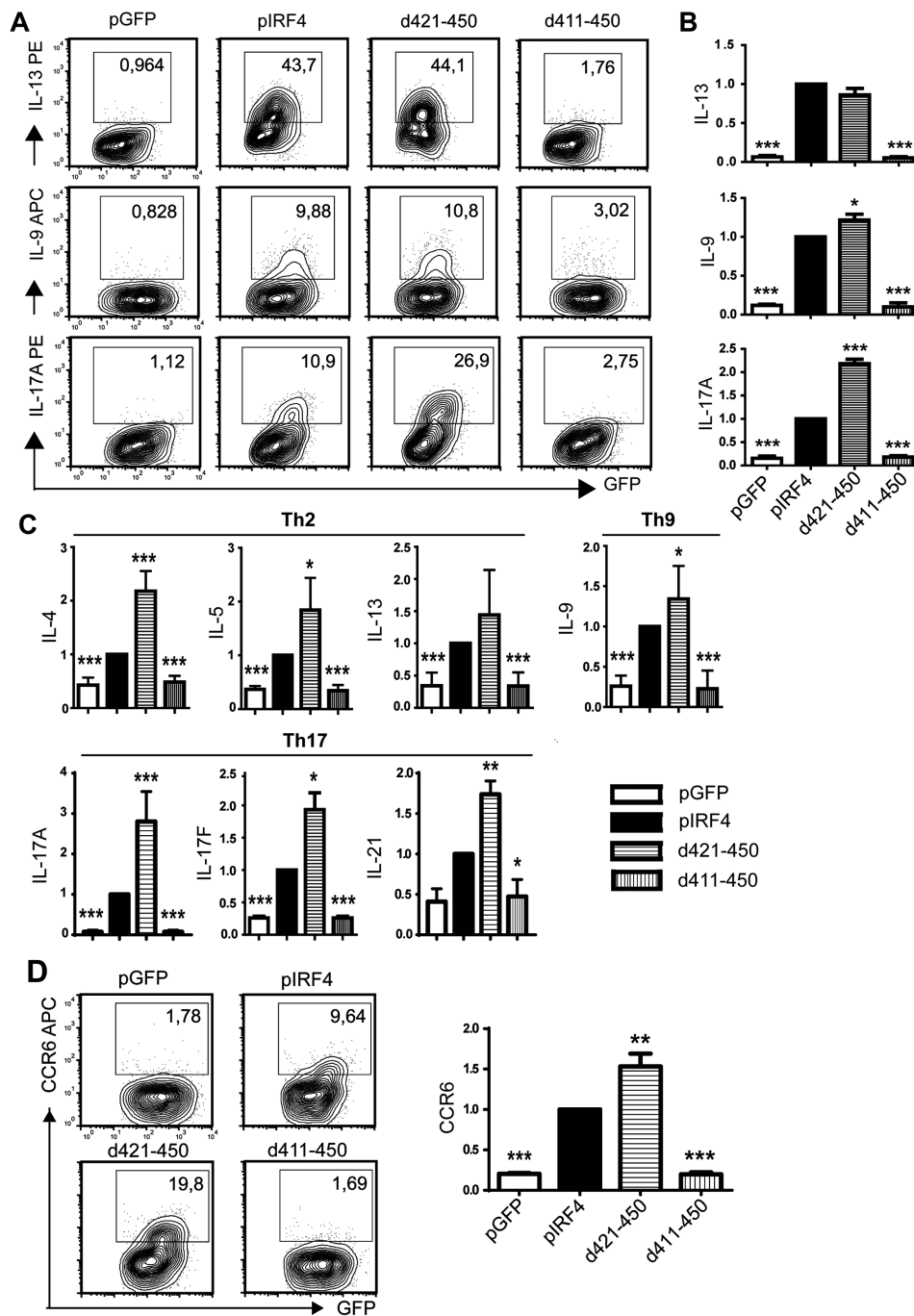


Figure 1. Activity of mutant d421-450 in Th cells. (A–D) Naive CD4⁺ Th cells were primed with anti-CD3, infected with the indicated retroviruses, differentiated into the indicated T cell subsets or Th17 cells, and were either left unstimulated (D) or restimulated with PMA/Ionomycin in the (A and B) presence or (C) absence of Brefeldin A. (A, B, and D) Cells were stained with antibodies against the indicated targets and analyzed by flow cytometry. Viable (forward/side scatter gating) GFP⁺ cells (as an example, see Supporting Information Fig. S3) reflecting infected cells are depicted. (A) Numbers in the quadrants show the percentage of positive (y-axis) cells among viable GFP⁺ cells. (D) Graphs are shown as mean ± SD and are pooled from more than six (B) or three (C and D) independent experiments. The value indicated was obtained by dividing the respective percentages (B and D) or cytokine concentrations (C) by the one measured for WT IRF4. **p* < 0.05, ***p* < 0.01, ****p* < 0.001; Student's *t*-test (two-tailed).

Information Fig. S3A). When *Rorc* expression was determined in aliquots of these cells, d421-450 again showed higher activity as WT IRF4, while the empty control vector was inactive.

To test whether the enhanced activity of d421-450 was restricted to CD4⁺ Th cells, several experiments were repeated in naive CD8⁺ T cells. Overall, cytokine expression was less than in CD4⁺ cells and we were unable to detect IL-9 by staining

in Tc cells cultured under Th9 conditions. Staining of IL-17A again demonstrated a clearly enhanced activity of d421-450 compared to WT IRF4 (Fig. 2A and B), while as in Th cells, the activity on IL-13 was much less pronounced. By ELISA, we were able to detect IL-9, IL-13, and IL-17A and confirmed strong upregulation of IL-17A by d421-450, while no effect was seen on IL-9 production and IL-13 secretion was only marginally increased (Fig. 2C). The

Tc17 enhancing activity was also reflected in upregulation of CCR6 (Fig. 2D and E). Mutant d411-450 always failed to show activity, confirming the results in Th cells.

It was important to ensure that the respective plasmids generated comparable protein amounts of IRF4 or d421-450. However, despite their similar transcription by quantitative PCR (not shown), Western Blotting with commercially available anti-IRF4 antibodies generated

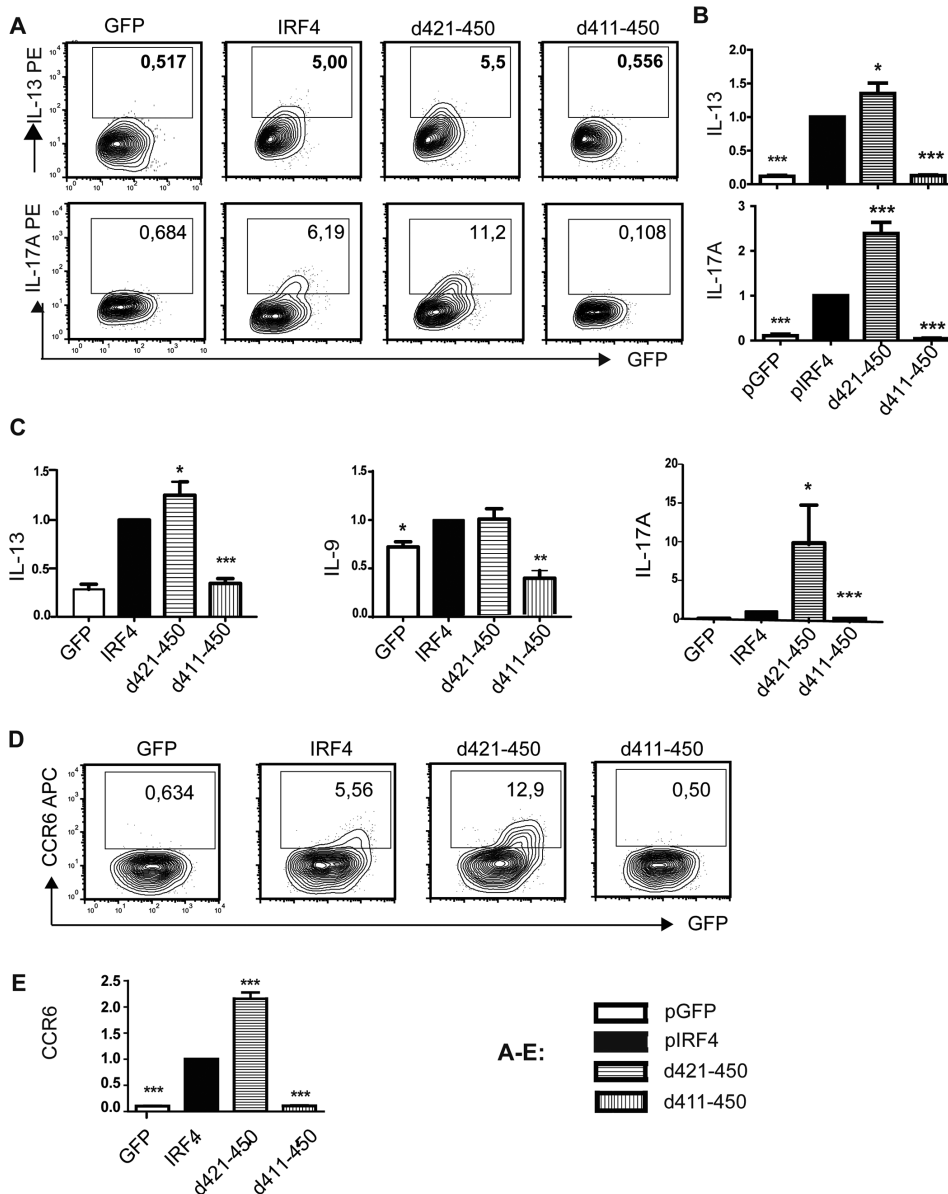


Figure 2. Activity of mutant d421-450 in Tc cells. (A–E) Naive CD8⁺ Tc cells were analyzed as described in Figure 1. (B–D) Graphs are shown as mean ± SD and are pooled from three independent experiments. **p* < 0.05, ***p* < 0.01, ****p* < 0.001; Student's *t*-test (two-tailed).


controversial results, probably due to structural alterations of d421-450 and therefore changing binding properties of the applied anti-IRF4 antibodies. Therefore, we generated His-tagged versions of IRF4 and d421-450 to allow detection by anti-His, not influenced by the IRF4 structure. Unfortunately, N-terminally added His yielded functionally inactive IRF4 (data not shown). In four experiments performed with a C-terminal His-tag and similar to those in Figure 1A, His-d421-450 increased IL-17A staining in type 17 differentiated CD4⁺ cells by a mean of 1.42-fold (*p* < 0.002) compared to His-IRF4. Although highly significant, this effect is

smaller than without His, likely because the C-terminal modification already partly neutralizes the autoinhibitory region. The amounts of His-IRF4 and His-d421-450 were similar when analyzed by Western Blotting (Supporting Information Fig. S4A), while comparable cell frequencies were transfected (Supporting Information Fig. S4B). Thus, increased d421-450 activity is not explained by higher protein quantities.

In conclusion, we here demonstrate a truncated version of IRF4 with considerably enhanced activity compared to WT IRF4. This increase is particularly obvious under Th17 conditions, less strin-

gent under Th2 or Th9 conditions, and not detectable under Th1 conditions. The increase can be recapitulated in Tc cells, suggesting a possible generalization of the results. The preferential activity in type 17 cells may hint to a modular structure of IRF4, whereby deletion of the autoinhibitory domain may unmask a type 17 inducing IRF4 subdomain different from type 2 or 9 promoting parts. If so, small chemicals targeting selective subdomains of IRF4 might turn out to be attractive therapeutic reagents.

Chol Ho Kang¹, Enno Hartmann¹,
Lisa Menke¹, Daniel Staudenraus¹,

El-Fadil Abass¹, Hartmann Raifer³,
Aleky Porapu¹, Bärbel Camara¹,
Anne Brüstle², Olaf Pinkenburg¹,
Maria Bieringer¹ and Michael Lohoff¹ 

¹ Institute for Medical Microbiology Hospital
Hygiene, Philipps University Marburg, Marburg,
Germany

² Department of Immunology and Infectious
Disease, John Curtin School of Medical Research,
Australian National University, Canberra,
Australia

³ Flow Cytometry Core Facility BMFZ, Philipps
University Marburg, Marburg, Germany

Acknowledgments: These studies were funded by the DFG (grant LO 396/8-1 to M.L.), the DZIF (M.L. and O.P.), Rhön-Klinikum A.G, and Kempkes Stiftung (to M.B.). We thank the flow cytometry core facility Marburg for their support.

References

- 1 Zhao, G. N. et al., *Biochim. Biophys. Acta* 2015. **1852**: 365–378.
- 2 Lohoff, M. et al., *Nat. Rev. Immunol.* 2005. **5**: 125–135.
- 3 Campos Carrascosa, L. et al., *Nat. Commun.* 2017. **8**: 15366.
- 4 Brüstle, A. et al., *Nat. Immunol.* 2007. **8**: 958–966.
- 5 Huber, M. et al., *Eur. J. Immunol.* 2014. **44**: 1886–1895.
- 6 Huber, M. et al., *Immunity* 2013. **39**: 797–799.
- 7 Man, K. et al., *Nat. Immunol.* 2013. **14**: 1155–1165.
- 8 Iwata, A. et al., *Nat. Immunol.* 2017. **18**: 563–572.
- 9 Krishnamoorthy, V. et al., *Immunity* 2017. **47**: 481–497.e7.
- 10 Brass, A. L. et al., *Genes Dev.* 1996. **10**: 2335–2347.

Abbreviation: AA: amino acid · IRF: interferon-regulatory factor

Keywords: IRF4 · Mutation · T cell differentiation · Th17 · Transcriptional activity

Full correspondence: Dr. Michael Lohoff,
Institute for Medical Microbiology Hospital
Hygiene, Philipps University Marburg,
Hans-Meerwein-Str. 2, 35043 Marburg,
Germany
e-mail: lohoff@med.uni-marburg.de

Received: 31/1/2018

Revised: 31/7/2018

Accepted: 13/9/2018

Accepted article online: 15/9/2018



The detailed *Materials and methods* for Technical comments are available online in the Supporting information

Point mutation L116R in interferon-regulatory factor 4 differentially impacts key cytokine production in Th2, Th9, and Th17 cells

Upon first activation, CD4⁺ T cells differentiate into specialized T helper subtypes, dependent on the key transcription factors (TFs) T-bet for Th1, GATA3 for Th2, PU.1 for Th9, and ROR γ t for Th17.

Our group established decisive roles for Interferon-Regulatory-Factor 4 (IRF4) in the differentiation of Th2 [1], Th9 [2], and Th17 [3] cells, while others showed an *in vivo* role for Th1 cells [4]. Thus, IRF4 may serve as an initiation factor for transcribing genes necessary for further differentiation [5, 6]. Our group hypothesizes that IRF4 has functional subunits, which preferably bind to one key TF and determine its activity. If so, IRF4 mutations might selectively affect T helper subtypes depending on which TF binds to that domain of IRF4. Accordingly, IRF4 lacking its autoinhibitory domain (AD) (Fig. 1A) specifically induces Th17 differentiation [7].

PU.1 and IRF4 direct Th9 differentiation. The description of the IRF4/PU.1/DNA crystal structure showed the tight interaction of IRF4 amino acids (AA) V111, L116, and D117, DNA, and the AA R222 and K223 of PU.1 [8]. Importantly, mutations of leucine 116 to arginine have been reported in patients with chronic lymphocytic leukemia (CLL), leading to increased levels of IRF4 and MYC [9] and a higher DNA binding capacity than wt IRF4 [10].

We thus asked if the L116R exchange affects IRF4 function in T cell subtypes, particularly during IL-9 production. Purified naive CD4⁺ T cells from IRF4^{-/-} mice were infected with retroviruses overexpressing GFP and variants of IRF4, followed by *in vitro* differentiation and evaluation of cytokine production. L116R mutations were introduced into either a wildtype (wt) IRF4 background or one lacking AD (dAD), i.e. L116R_{wt} or L116R_{dAD}. By flow cytometry, retroviral

overexpression into IRF4^{-/-} cells created slightly less IRF4 protein amounts than in control IRF4^{+/+} Th cells (Fig. S1A–C). An empty vector without IRF4 served as a control. Transfected cells express GFP to separate them from IRF4 negative cells within the same sample, as an internal control (Fig. S1C).

In a bead-based multiplex assay, we tested the effect of the mutants on cytokines in the supernatant of cells differentiated under Th2, Th9, and Th17 conditions restimulated with PMA/ionomycin. Importantly, we noted a strong IL-9-enhancing activity in Th2 cells expressing the L116R_{WT} mutant (Fig. 1B), also on the dAD background. While Th9 cells produced more IRF4-dependent IL-9 than Th2, there was no difference between mutants. Slight IL-9 induction was noted in Th17 cells, but at negligible amounts (Fig. S2A). Importantly, however, in Th17 cells IL-17A and IL-17F were strongly reduced by L116R_{WT} and L116R_{dAD} (Fig. S2A).

Enhancement in Th2 cells was limited to IL-9, but not seen in IL-5, IL-13, IL-2, IL-6, and IL-10. For IL-6 and IL-22, mutants even caused a drop in production. In Th9 cells, suppressive effects were seen for IL-13. IFN γ was already produced by empty vector control cells and IRF4 mutants had little impact, supporting no significant role for IRF4 during *in vitro* Th1 production [1, 3]. These screening experiments document an inducing effect of L116R mutants specifically on IL-9 production.

We then used ELISAs for IL-9 and IL-13 for supernatants from Th2 and Th9 cells (Fig. 2A), harvested after differentiation for 48h (Th9) or 72h (Th2) or after washing and restimulation for 8h. As before, the L116 mutants caused upregulation of IL-9 production, both on the IRF4 wt or dAD background and during primary culture as well as after restimulation. For IL-13, a

suppressive effect by the L116R mutants was observed in Th2 and Th9 cells.

These results were based on supernatants unable to separate transduced from untransduced cells in the same culture. Furthermore, transfection rates slightly differ between virus preparations encoding different mutations. Finally, these results made no statement on whether this increase was related to few individual or all transfected cells.

We therefore restimulated cells differentiated as described above and performed intracellular staining of cytokines followed by flow cytometry. The gating strategy is depicted in Fig. S2B and a representative experiment of Th2 and Th9 cells in Fig. S3. No cytokine production was observed in untransfected GFP⁻ cells (Fig. S2B) or in GFP⁺ cells transfected with empty control virus (Fig. S3). Transduction with IRF4 or dAD induced IL-9 or IL-13, (Fig. S3) as expected. The data raised in these experiments confirmed the above-described findings, namely significant inducing capacity of L116 mutants for IL-9 but not IL-13 production. This finding was related to a higher frequency of cytokine-producing cells rather than higher cytokine production per cell (Fig. S3A–D).

Quantification of flow cytometry for IL-9 and IL-13 producing cell frequencies in Th2 and Th9 differentiation cultures (Fig. 2B) confirmed effects of the mutants for IL-9 production particularly in Th2 cells, but also in Th9 cells, as compared to controls. A suppressive effect was again observed on IL-13 production in Th9 and less so in Th2 cells. The same mutants had again a strongly suppressive effect on IL-17 production in Th17 cells, in L116R_{wt} and L116R_{dAD} transduced cells.

The increase in IL-9 production of L116R transduced cells may be related to increased DNA binding capacity [10]. A

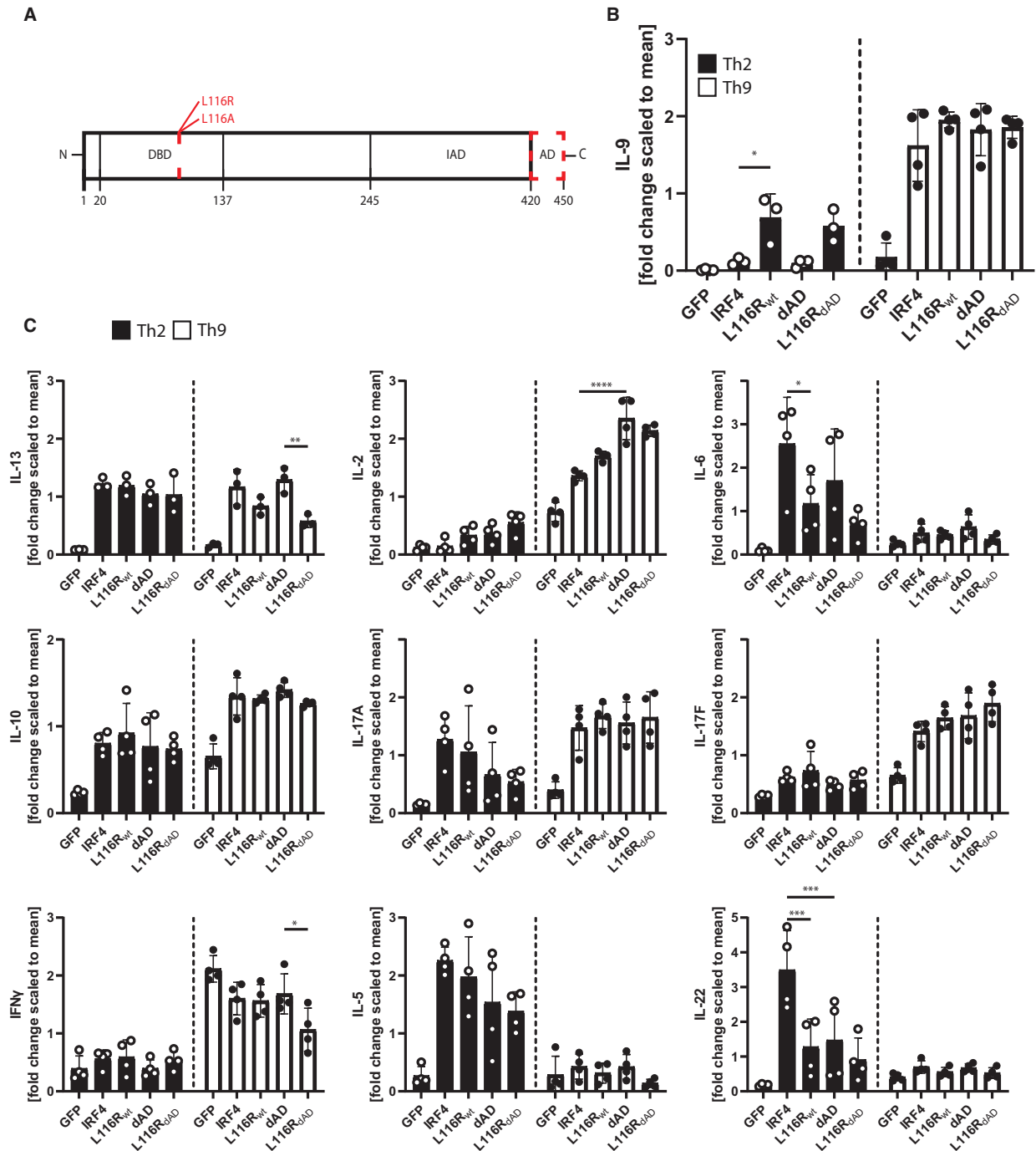


Figure 1. Schematic overview of IRF4 with DNA-binding domain (DBD), interferon association domain (IAD), and autoinhibitory domain (AD). Mutations marked in red (A). Multiplex assay for indicated cytokines from supernatants of IRF4^{-/-} T cells transduced with empty vector (GFP), wildtype IRF4 (WT), IRF4 with deleted AD (dAD), L116R mutation on IRF4wt and dAD background, in Th2 (72h) and Th9 (48h) differentiated cells (B,C). Data shown are standardized by generating fold changes to the mean of the respective cytokine per experiment \pm SD of 4 (for all cytokines but IL-13, which shows 3) biological replicates each from an independent experiment. p-values were calculated using two-way ANOVA with Tukey post hoc test.

smaller L116R-mediated effect in Th9 cells is likely due to an already more accessible IL-9 promoter and higher basal IL-9 production. In contrast, IL-13 production was

suppressed mainly in Th9 cells, but less so in Th2 cells, perhaps in turn reflecting a more accessible promoter and consecutive higher production of IL-13.

We could demonstrate for the first time that a single point mutation in IRF4 differentially affects T cell subtypes and selectively induces one cytokine while others

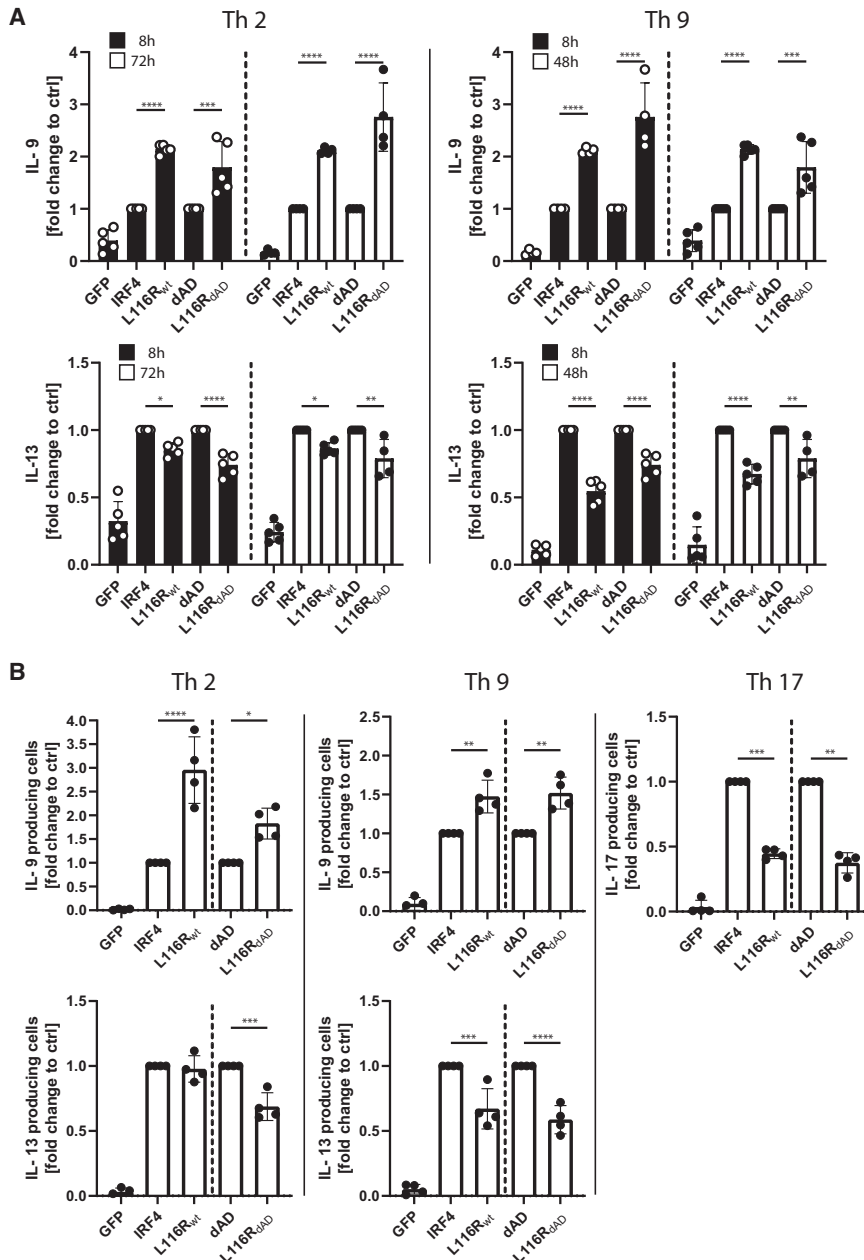


Figure 2. IL-9 and IL-13 ELISAs for Th2 and Th9 differentiated cells (A). IRF4^{-/-} T cells transduced with empty vector (GFP), IRF4wt, IRF4dAD, or respective L116R mutant, followed by 48h (Th9) or 72h (Th2) differentiation, before testing of supernatants (empty bars). Full bars show similarly treated cells but restimulated in fresh medium for 8h. Intracellular cytokine stainings for IL-9 and IL-13 in Th2 and Th9 cells and IL-17 in Th17 cells (B). IRF4^{-/-} T cells transduced with GFP, IRF4^{wt}, IRF4^{dAD} or their respective L116R mutants followed by Th2, Th9, and Th17 differentiation (48h for Th9, 72h for Th2 and Th17) and 3h restimulation, stained intracellularly (ICS) for IL-9 and IL-13 or IL-17. Data presented as fold change to the respective control \pm SD. For ELISA 4 (IL-9 Th2 72h and IL-9 Th9 48h) or 5 (all other conditions) and for ICS 4 biological replicates; each from an independent experiment. *p*-values were calculated using two-way ANOVA with Tukey post hoc test for ELISA and one-way ANOVA with Tukey post hoc test for ICS.

were unaltered or suppressed. L116R positively affects IL-9 production in both Th2 and Th9 cells, while at the same time decreasing IL-13 in Th9 and less in Th2 cells and leaving other cytokines unaltered. We find a prominent suppressive and thus divergent effect of L116R on IL-17 production in Th17 cells. Our data shows that for the same cytokine promoter, effects of IRF4 are affected by the skewing conditions, likely because the cytokine milieu dictates the differential availability of key TFs for complex formation.


Together, this work supports our hypothesis of functional subunits in IRF4, which regulate TF complex formation during differentiation of different T cell subtypes.

Acknowledgments: The authors thank the Deutsche Forschungsgemeinschaft (DFG) for funding LO 396/8-1 to M.L. Open access funding enabled and organized by Projekt DEAL.

Conflict of interest: The authors declare no commercial or financial conflicts of interest.

Data availability statement: The study results are available from the corresponding author upon request.

Peer review: The peer review history for this article is available at <https://publons.com/publon/10.1002/eji.202249869>

Daniel Staudenraus, Alekhya Porapu, Hanna Leister, Dennis Das Gupta and Michael Lohoff 

Institute of Medical Microbiology and Hospital Hygiene, Philipps-University Marburg, Marburg, Germany

References

- Lohoff, M. et al., *Proc. Natl. Acad. Sci. USA* 2002. 99: 11808–11812.
- Staudt, V. et al., *Immunity* 2010. 33: 192–202.
- Brüstle, A. et al., *Nat. Immunol.* 2007. 8: 958–966.
- Mahnke, J. et al., *Sci. Rep.* 2016. 6: 35521.
- Li, P. et al., *Nature* 2012. 490: 543–546.
- Ciofani, M. et al., *Cell* 2012. 151: 289–303.
- Kang, C. H. et al., *Eur. J. Immunol.* 2019. 49: 812–815.

- 8 Escalante, C. R. et al., *Mol. Cell* 2002. 10: 1097–1105.
- 9 Benatti, S. et al., *Hematol. Oncol.* 2021. 39: 707–711.
- 10 Sundararaj, S. et al., *Nucleic Acids Res.* 2021. 49: 2255–2265.

Full correspondence: Michael Lohoff
e-mail: lohoff@med.uni-marburg.de

Keywords: cytokine • interleukin • IRF4 • point mutation • T-cell-differentiation

Received: 22/2/2022

Revised: 5/8/2022

Accepted: 30/8/2022

Accepted article online: 1/9/2022



Additional supporting information may be found online in the Supporting Information section at the end of the article.

ARTICLE OPEN



IRF4 deficiency vulnerates B-cell progeny for leukemogenesis via somatically acquired *Jak3* mutations conferring IL-7 hypersensitivity

Dennis Das Gupta¹, Christoph Paul², Nadine Samel^{1,3}, Maria Bieringer¹, Daniel Staudenraus¹, Federico Marini⁴, Hartmann Raifer¹, Lisa Menke¹, Lea Hansal¹, Bärbel Camara¹, Edith Roth⁵, Patrick Daum⁵, Michael Wanzel⁶, Marco Mernberger^{6,7}, Andrea Nist⁶, Uta-Maria Bauer⁶, Frederik Helmprobst^{8,9}, Malte Buchholz¹⁰, Katrin Roth¹¹, Lorenz Bastian¹², Alina M. Hartmann¹², Claudia Baldus¹², Koichi Ikuta¹³, Andreas Neubauer¹⁴, Andreas Burchert¹⁴, Hans-Martin Jäck⁵, Matthias Klein¹⁵, Tobias Bopp^{15,16}, Thorsten Stiewe^{6,7}, Axel Pagenstecher^{8,9} and Michael Lohoff¹⁵✉

© The Author(s) 2022

The processes leading from disturbed B-cell development to adult B-cell progenitor acute lymphoblastic leukemia (BCP-ALL) remain poorly understood. Here, we describe *Irf4*^{-/-} mice as prone to developing BCP-ALL with age. *Irf4*^{-/-} preB-I cells exhibited impaired differentiation but enhanced proliferation in response to IL-7, along with reduced retention in the IL-7 providing bone marrow niche due to decreased CXCL12 responsiveness. Thus selected, preB-I cells acquired *Jak3* mutations, probably following irregular AID activity, resulting in malignant transformation. We demonstrate heightened IL-7 sensitivity due to *Jak3* mutants, devise a model to explain it, and describe structural and functional similarities to *Jak2* mutations often occurring in human Ph-like ALL. Finally, targeting JAK signaling with Ruxolitinib in vivo prolonged survival of mice bearing established *Irf4*^{-/-} leukemia. Intriguingly, organ infiltration including leukemic meningeosis was selectively reduced without affecting blood blast counts. In this work, we present spontaneous leukemogenesis following IRF4 deficiency with potential implications for high-risk BCP-ALL in adult humans.

Cell Death & Differentiation; <https://doi.org/10.1038/s41418-022-01005-z>

INTRODUCTION

Two signaling pathways via the Interleukin-7 receptor (IL-7R) and the preB cell receptor (preBCR) ensure an orderly progression of B lymphopoiesis [1–3]. ProB cells adhere to bone marrow (BM) stromal cells (SCs) expressing CXCL12 and VCAM-1 through CXCR4 and VLA-4 respectively, while SC-derived IL-7 induces their proliferation [4]. The formation of the preBCR composed of Igμ protein and the surrogate light chain (ψL), consisting of λ5 and VPRED, marks the entrance to the preB cell stage. Signaling via the preBCR in turn induces the transcription factor (TF) interferon regulatory factor 4 (IRF4) which is also critical during T-cell differentiation [5, 6]. In preB cells, IRF4 halts cycling and facilitates recombination of the light chain locus by RAG1/2 [1]. Despite its importance, *Irf4*^{-/-}

mice still develop, albeit less, surface (s)Igμ⁺ mature B cells [7], likely due to a partially redundant function of IRF8. Accordingly, *Irf4,8*^{-/-} B progenitors are completely arrested at the preB cell stage [8].

Disruption of this developmental track can provoke B-cell progenitor acute lymphoblastic leukemia (BCP-ALL). In humans, this disease preferentially affects children (age 0–19), while most deaths however occur in the adult population [9]. Cases affecting adolescents and young adults (AYA) display a different set of driver mutations compared to childhood BCP-ALL [10–13].

Herein, we report that adult *Irf4*^{-/-} mice spontaneously develop BCP-ALL with age and delineate the steps from disturbed *Irf4*^{-/-} B lymphopoiesis to overt leukemia.

¹Institute for med. Microbiology & Hospital Hygiene, Philipps University Marburg, Marburg, Germany. ²University Hospital Gießen and Marburg, Dept. of Ophthalmology, Philipps University Marburg, Marburg, Germany. ³MVZ for Laboratory Medicine and Microbiology, Koblenz-Mittelrhein, Germany. ⁴Institute of Medical Biostatistics, Epidemiology and Informatics (IMBEI), University Medical Center of the Johannes Gutenberg-University Mainz, Mainz, Germany. ⁵Division of Molecular Immunology, Nikolaus-Fiebiger Center, University of Erlangen-Nürnberg, Erlangen, Germany. ⁶Institute for Molecular Biology and Tumor Research (IMT), Center for Tumor- and Immunobiology (ZTI), Philipps University Marburg, Marburg, Germany. ⁷Genomics Core Facility, Philipps University Marburg, Marburg, Germany. ⁸Core Facility for Mouse Pathology and Electron Microscopy, Philipps University Marburg, Marburg, Germany. ⁹University Hospital Gießen and Marburg, and Philipps University, Institute of Neuropathology, Marburg, Germany. ¹⁰University Hospital Gießen and Marburg, and Philipps University, Clinic for Gastroenterology and Core Facility Small Animal Ultrasound, Marburg, Germany. ¹¹Core facility for Cellular Imaging, Philipps University Marburg, Marburg, Germany. ¹²Medical Department II, Hematology and Oncology, University Medical Center Schleswig-Holstein, Kiel, Germany. ¹³Institute for Frontier Life and Medical Sciences, Kyoto University, Kyoto, Japan. ¹⁴University Hospital Gießen and Marburg, and Philipps University, Dept. Hematology, Oncology and Immunology, Marburg, Germany. ¹⁵Institute for Immunology, Research Center for Immunotherapy (FZI), University Cancer Center, University Medical Center of the Johannes Gutenberg-University Mainz, Mainz, Germany. ¹⁶German Cancer Consortium (DKTK), Mainz, Germany. ✉email: lohoff@med.uni-marburg.de

Edited by T Mak

Received: 7 February 2022 Revised: 7 April 2022 Accepted: 8 April 2022

Published online: 22 April 2022

RESULTS

Irf4^{-/-} mice spontaneously develop preB cell leukemia

Following the serendipitous finding, that some aged *Irf4*^{-/-} mice developed tumors and died, we systematically observed 80 *Irf4*^{-/-} mice over time. We detected 14 tumors (incidence 17.5%), that spontaneously appeared in lymph node (LN) areas (mean age: 268d, median: 238d, Fig. 1a). Tumors were neither detected in mice younger than 150d nor in C57BL/6 wild-type (wt) mice housed in the same room.

All tumors (Fig. 1b shows a representative tumor in situ) were accompanied by lymphadenopathy (arrowheads) and increased spleen size (Fig. 1c). The suspected lymphomatous origin was corroborated microscopically (Fig. 1b, right panels), with infiltration of mononucleated cells into the BM, lung, and liver (Fig. 1d). Due to the known impaired maturation of *Irf4*^{-/-} preB cells [7], spontaneous eruption of preB-leukemia seemed plausible: In spleen sections (Fig. 1e), infiltrating cells stained positive for both B220 and Igμ (although less than untransformed “follicle” B cells) and Ki67. By flow cytometry, BM samples from tumor mice harbored an expanded pro/preB cell compartment (Hardy fraction (fr.)A-D [14], B220^{mid}sIgμ⁻) (Fig. 1f, g). Fr.A-D cells were detected also in peripheral lymphoid organs and blood of tumor mice (Fig. 1h). Following the Hardy classification (Fig. 1i), we determined tumor cells to be fr.C preB cells (B220^{mid}sIgμ⁻CD43⁺CD24⁺BP-1⁺) (Fig. 1j, k, sFig. 1a). In addition, Igμ, but not Igκ/λ was detected intracellularly (sFig. 1b). Lastly, tumors stained positive for surface λ5, part of the ψL (Fig. 1l). These attributes characterize the disease as preB-I cell BCP-ALL.

To prove clonality, we sequenced the VDJ junctions of the IgH region in three tumors (Supplementary Table 1). Almost all sequences per tumor were identical, demonstrating clonality. The tumors (three examples) further displayed copy number variations (CNV) (sFig. 1h), targeting differing genomic regions. Finally, transfer of tumor cells robustly elicited leukemia in wt acceptor mice (sFig. 1d–g) with as little as 500 transferred cells (sFig. 1f, g), indicating bona fide malignancy.

B lymphopoiesis in *Irf4*^{-/-} mice harbors a hyperproliferative preB-I cell compartment

The uniform appearance of BCP-ALL in *Irf4*^{-/-} mice suggested a defined preleukemic pro/preB cell state vulnerable to immortalization. Dimensional reduction of BM samples stained for B-cell differentiation markers, identified an enlarged fr.C preB cell compartment already in healthy *Irf4*^{-/-} mice (Fig. 2a–c, sFig. 2a). This disturbed, but productive B-cell maturation confirms and extends previous reports [7]. Expression analysis of IL-7Rα and of CD2 (sFig. 2b, c), which accompanies cytosolic Igμ expression [15] further showed an increased frequency of CD2^{-dim}IL-7Rα⁺B220⁺sIgμ⁻ preB cells in *Irf4*^{-/-} mice.

Purified BM B220⁺ cells from *Irf4*^{-/-} and wt mice were cultured with IL-7 (Fig. 2d–g) to compare proliferative capacities. After 6d, *Irf4*^{-/-} cells had expanded roughly three-fold, whereas wt cell numbers decreased. Phenotypically, *Irf4*^{-/-} cells accumulated at the fr.C stage (Fig. 2e, f) and expressed surface λ5 (Fig. 2g, h); exactly like *Irf4*^{-/-} leukemia. In contrast, wt cells differentiated further, losing surface CD43 (making them fr.D) (Fig. 2e, f) with some cells expressing sIgμ (fr.E). Thus, IL-7 unmasked the leukemic potential of the fr.C compartment in *Irf4*^{-/-} mice with both unchecked proliferation and a reinforced differentiation block. Notably, IL-7 dependent *Irf4*^{-/-} preB-I cell proliferation was blocked by NIBR3049 and Ruxolitinib, inhibitors of the IL-7R downstream actors JAK3 and JAK1 respectively (sFig. 2d).

Irf4^{-/-} B-cell progenitors exhibit reduced retention to the BM niche

As overt leukemia is characterized by systemic presence, we tested whether already preleukemic *Irf4*^{-/-} B-cell progenitors would leak from the BM. To reduce the complex Hardy

classification, we identified early B-cell progenitors, approximately until the preB-I stage, by B220⁺CD2^{-dim} expression (sFig. 2b). We detected higher frequencies of splenic B220⁺CD2^{-dim} cells in *Irf4*^{-/-} than in wt mice (Fig. 2h), which accumulated with age. Thus, premature BM evasion adds to the impaired differentiation and hyperproliferation that characterize *Irf4*^{-/-} preleukemia.

Potentially, this finding represented a systemic consequence of reduced vicinity to BM niche cells. We, therefore, analyzed the proximity of *Irf4*^{-/-} and wt B220⁺CD2^{-dim} cells to IL-7⁺ BMSCs in situ using *Il-7*^{eGFP} reporter mice (Fig. 2j–m, sFig. 2e, f, Supplementary Movie 1) [16]. In femur cryosections, the B220⁺CD2^{-dim} subset (Fig. 2j, arrowheads) but not the whole *Irf4*^{-/-} B220⁺ cell compartment was on average located further away from IL-7⁺ BMSCs, compared to wt control (Fig. 2l, m). We excluded differences in IL-7⁺ BMSC abundance between genotypes (sFig. 2g).

B progenitor retention to BM is secured via the interaction of CXCR4 on pro/preB cells with the IL-7⁺ BMSC-derived chemokine CXCL12 [17, 18]. Notably, *Irf4*^{-/-} pro/preB cells expressed markedly lower levels of CXCR4 compared to wt cells (Fig. 2n). Chemokine migration assays with Hardy fr.A-D cells showed that *Irf4*^{-/-} cells indeed migrated significantly less towards CXCL12 (Fig. 2o). Thus, reduced CXCR4-CXCL12 interaction likely induces the systemic seeding of *Irf4*^{-/-} B progeny. Inversely, direct cell interactions are likely not responsible, because *Irf4*^{-/-} and wt fr.A-D cells adhered equally to monolayers of OP-9 cells in vitro (sFig. 2h).

The IL-7-JAK-STAT-axis is recurrently altered in *Irf4*^{-/-} leukemia

Most likely, a second, acquired genetic alteration was necessary for bona fide leukemia development and arose with low frequency per time, explaining the affected age and relatively low penetrance. Importantly, IL-7 deprivation of BM-evaded pro/preB cells should create strong survival stress and potential selection pressure for bona fide leukemogenesis. To identify somatically acquired mutations, we performed whole-exome sequencing (WES) of three independent tumors (T8, T10, T11) compared to sorted B220⁺sIgμ⁻ cells from *Irf4*^{-/-} BM. Comparisons of the single nucleotide variants (SNVs) between the three samples identified nine genes affected in all three tumor samples (Fig. 3a). Out of these, SNVs in four genes (*Rrs1*, *Jak3*, *AW82073*, and *Duxf3*) showed alternate base frequencies close to 0.5 or 1 (Fig. 3b), suggesting that they could be present on one or both alleles of all leukemic cells. Although we did not exclude the oncogenic potential of the other three genes, we focused on *Jak3*, because it is associated with IL-7R signaling. We detected *Jak3* mutations also in other tumors TD1, TD2, TD3, and T14 by Sanger- and RNA-sequencing (Fig. 3c, Supplementary Table 2). Thus, seven out of seven tested tumors carried *Jak3* mutations (“JAK3_{mut}”). All mutations targeted either the active kinase domain or the pseudokinase domain regulating JAK3 activity. Some of these SNVs have been described before [19]. Further, using two different classifiers, no gene fusions could be detected (see methods). Analysis of typical BCP-ALL genes [20] identified some respective mutations at low frequencies, indicative of subclonal events (Fig. 3d). Among these, mutations in *Jak1*, the partner to JAK3 in IL-7R signaling, were detected in both T8 and T11.

To analyze the role of the JAK3_{mut}, we transduced *Irf4*^{-/-} preB-I cell cultures with retroviruses (RVs) encoding no or wt JAK3 or the JAK3_{mut} R653H and T844M. Culturing transduced cells in the presence of aIL-7 to test for IL-7 independency unexpectedly resulted in cell death after a few days with no benefit for cells expressing JAK3_{mut} (sFig. 3a, b). To test if JAK3_{mut} would confer advantages with limited IL-7, RV-infected *Irf4*^{-/-} preB-I cell cultures were exposed to decreasing IL-7 concentrations (Fig. 3e–g). At 0.1 and 0.01 ng/ml IL-7, both JAK3_{mut}, but not

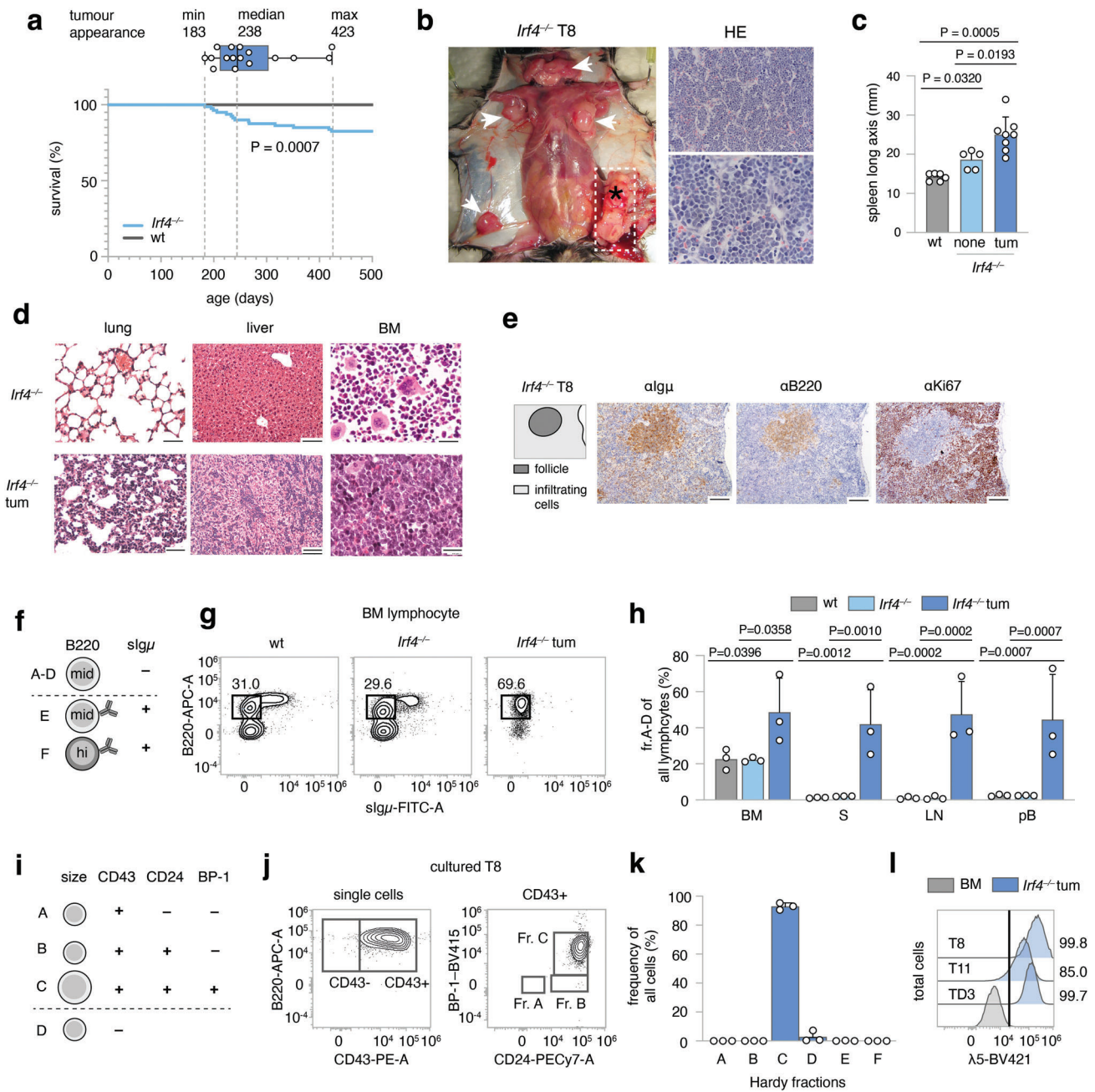


Fig. 1 Spontaneous emergence of preB-I cell BCP-ALL in adult $lrf4^{-/-}$ mice. **a** A cohort of 80 $lrf4^{-/-}$ and wt mice was observed over 500 days for tumor development. Kaplan–Meier plot of survival. Box and whisker plot indicates minimum, maximum and median age at tumor appearance of the 14 affected mice. **b** Macroscopic appearance of an exemplary tumor (asterisk) and LNs (arrowheads) in an $lrf4^{-/-}$ mouse. Right: Hematoxylin-Eosin (HE) staining from the tumor. Scale bars: top: 50 μ m, bottom: 20 μ m. **c** Longitudinal spleen (S) axis (mm) of $lrf4^{-/-}$ mice with ($n = 8$) or without ($n = 5$) tumor and control wt mice ($n = 6$). tum = tumor. **d** HE stainings of lung, liver, and BM of tumor mouse T8 and a healthy $lrf4^{-/-}$ mouse. Scale Bars: 50 μ m (lung and liver), 20 μ m (BM). **e** IHC-stainings of T8 mouse spleen for $Ig\mu$, B220, and Ki67. Scale bars: 100 μ m. **f** Schematic representation of gross Hardy fractioning by surface B220 and $Ig\mu$ expression. **g** Whole BM cells from wt, $lrf4^{-/-}$, and tumor mice were stained for B220 and $slg\mu$ expression and analyzed by flow cytometry. **h** Quantification of cell frequencies gated as in (**g**) for BM, S, LN, and pB (peripheral blood) of $n = 3$ mice per group. **i** Tabular representation of Hardy fr. A–D by size, CD43-, CD24-, and BP-1-surface expression. **j** Surface expression of markers as in (**i**) of in vitro cultured T8 tumor cells **k** quantification of cell frequencies gated as in (**j**) for three tumors (T8, T11, TD3) **l** surface $\lambda 5$ expression on T8, T11, and TD3 by flow cytometry in comparison to whole BM cells from $lrf4^{-/-}$ mice (BM) as a negative control. Statistical significance testing was performed with (**c**) one-way Welch-ANOVA followed by Dunnett’s T3 multiple comparison test and (**h**) with two-way ANOVA followed by pair-wise Tukey corrected comparisons within each organ. Bars depict mean \pm SD, dots indicate mice (**h**) or distinct $lrf4^{-/-}$ tumors (**k**).

JAK3_{wt}-RV led to the outgrowth of transduced over untransduced cells after 6d of culture (Fig. 3f, g). Thus, JAK3_{mut} confer IL-7-hypersensitivity, but not -independency. Accordingly, ex vivo cultured Jak3-mutated T8 and T11 cells also still depended on IL-7

(sFig. 3c, d). However, the tumor cells exhibited increased proliferation (sFig. 3e) and $\lambda 5$ surface retention (sFig. f, g) in decreased IL-7 concentrations when compared to wt or $lrf4^{-/-}$ preB cell culture.

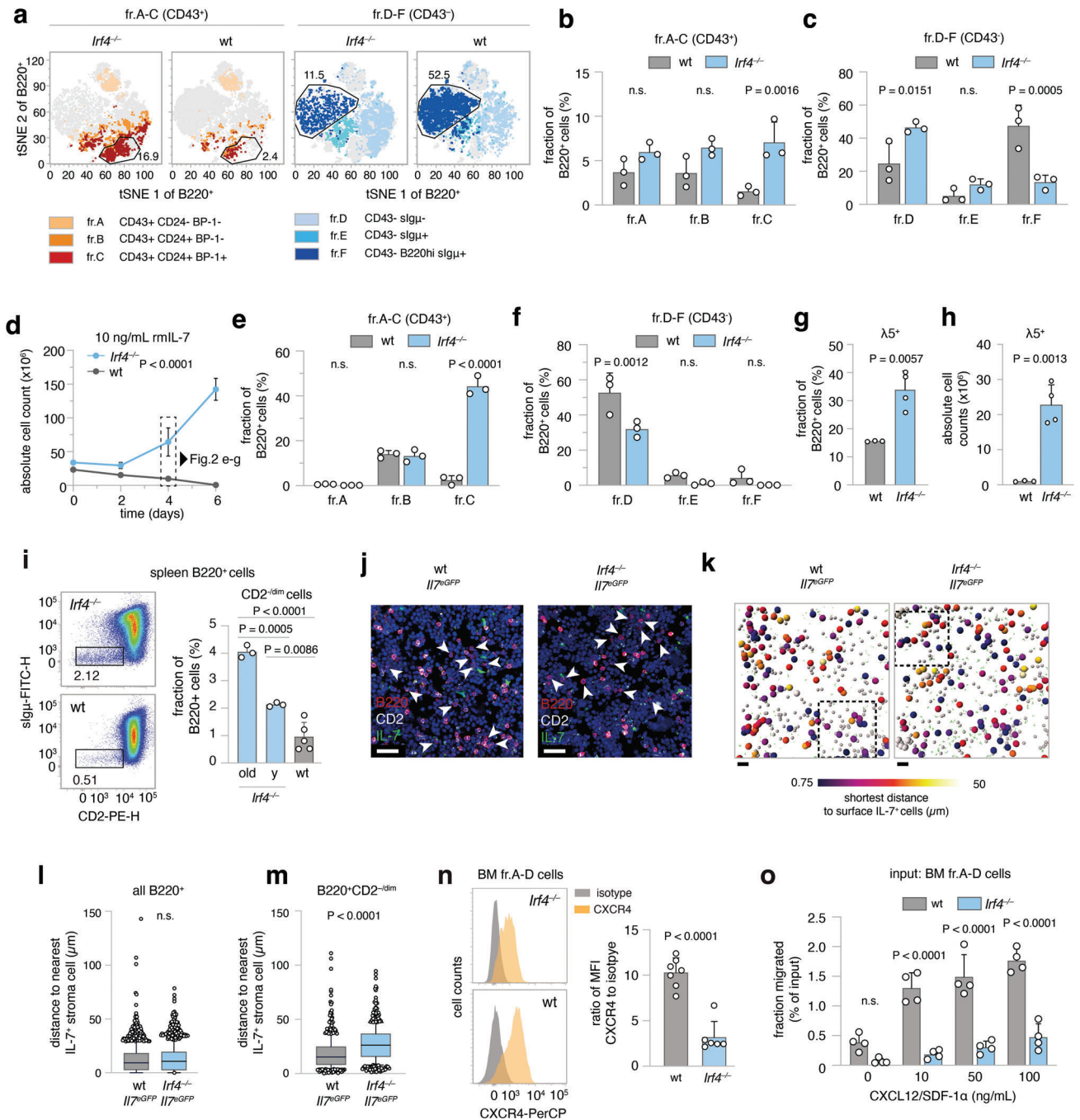


Fig. 2 *Irf4*^{-/-} B lymphopoiesis is preleukemically altered. **a–c** flow cytometric analysis of BM cells for Hardy markers as in Fig. 1j. **a** tSNE of BM cells gated on B220⁺ cells. Colors correspond to Hardy fractions identified by the markers detailed in the legend. **b** and **c** quantification of Hardy fraction frequencies for *n* = 3 mice per genotype. **d–h** BM cells from *Irf4*^{-/-} and wt mice were cultured in the presence of 10 ng/mL rmlL-7 for 6 days and **d** counted every two days. **e, f** After 4 days, cells were stained as in **a–c** and Hardy fractions quantified. **g** frequency and **h** absolute cell counts of $\lambda 5^+$ cells on day 4. **i** spleen cells from *Irf4*^{-/-} (“y” = young: 6–10 weeks and old: >6 months) and wt mice were analyzed for the presence of CD2^{-dim}slg μ ⁺ cells within the B220⁺ gate. one-way ANOVA, Tukey post hoc. **j–m** 7 μ m cryosections from *Irf4*^{-/-} *Il-7^{CreGFP}* and wt *Il-7^{CreGFP}* mice were stained for B220, CD2, GFP, and DAPI. **j** exemplary regions of BM cryosections. Arrowheads indicate B220⁺CD2^{-dim} cells. Scale bars = 15 μ m. **k** automated B220⁺ cell detection; gray spheres indicate B220⁺ cells, larger spheres B220⁺CD2^{-dim} cells, color-coded for their distance to GFP⁺ cells. Rectangles indicate magnified areas in **j**. Scale bars = 40 μ m. **l, m** quantification of distances to IL-7⁺ cells for **l** all B220⁺ and **m** B220⁺CD2^{-dim} cells. (*n* = 4 mice per genotype, one cryosection from femur metaphysis per mouse analyzed). Box and whiskers indicate mean and 95-IQR, dots indicate cells outside 95-IQR. **n** BM cells from *Irf4*^{-/-} and wt mice were gated on B220⁺slg μ ⁺ fr.A–D cells and analyzed for CXCR4 expression (left panels as representative staining). Data is presented for *n* = 7 (wt) and *n* = 6 (*Irf4*^{-/-}) mice as the ratio of geometric mean for CXCR4 to isotype staining. **o** MACS-purified fr.A–D cells from BM were placed in the top insert of a Boyden chamber and left to migrate towards differing concentrations of CXCL12 for 16 h. Dots represent *n* = 4 biologically independent experiments, presented as migrated percentage of input cells. Two-Way ANOVA, Sidak post hoc for (**b, c, e, f, o**), Two-tailed unpaired *t* test for (**g, h, l–n**).

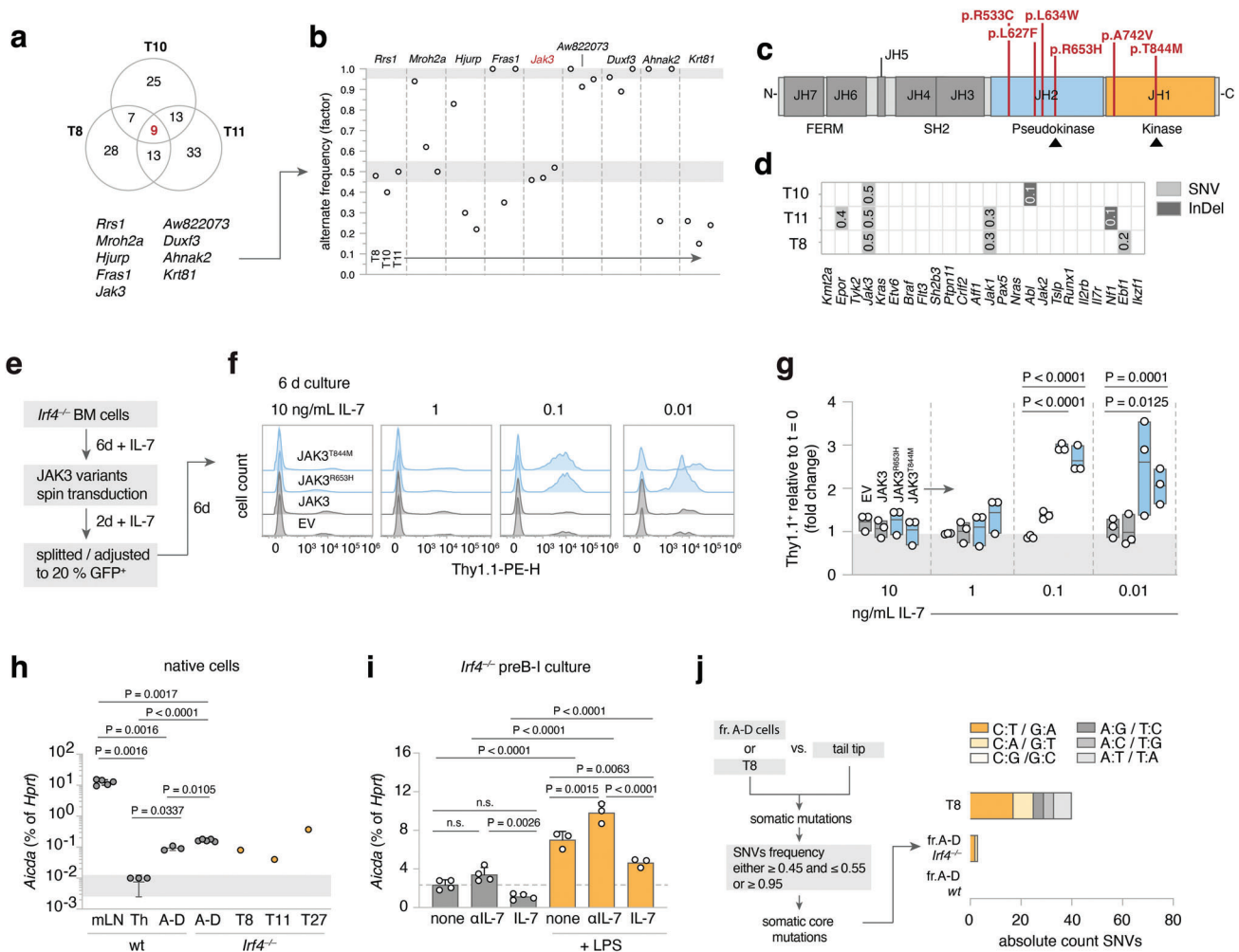


Fig. 3 leukemia-derived *Jak3* mutations heighten IL-7 sensitivity of *Irf4*^{-/-} preB-I cells. **a** Venn diagram of shared mutated SNV genes among WES from three *Irf4*^{-/-} leukemia samples (T8, T10, T11) **b** the nine shared genes were filtered for SNV frequency. gray areas: >0.95 and 0.45–0.55 margins as core mutation filters. **c** the five detected distinct *Jak3* SNVs were mapped onto JAK3 primary structure (JH = Jak homology domain). **d** *Irf4*^{-/-} leukemia WES were analyzed for mutations (SNV or InDel = insertions/deletions) in genes commonly altered in human BCP-ALL. Numbers indicate rounded frequencies of alteration. **e–g** *Irf4*^{-/-} BM cells were cultured for 6d with 10 ng/mL rmlL-7, transduced with control or *JAK3*_{mut} coding RVs, rested for 2 days, and then split into decreasing IL-7 concentrations. **f** Histograms for the Thy1.1 RV infection marker 6 days after splitting. **g** Quantification of Thy1.1⁺ cells after 6 days relative to start of culture ($t = 0$). Dots indicate $n = 3$ independent experiments, plotted as floating bars. EV = empty vector. **h** qRT-PCR from wt and *Irf4*^{-/-} cells for *Aicda* mRNA expression, relative to *Hprt* expression for $n = 3$ (Th (= T helper) and sorted fr.A-D wt BM cells), $n = 5$ (mLN (= mesenteric lymph node) and sorted fr.A-D *Irf4*^{-/-} BM cells), $n = 1$ per tumor T8, T11, T27. **i** *Irf4*^{-/-} preB-I cell cultures from whole BM cells were cultured in combinations of IL-7, α L-7, and LPS for 24 h, as indicated, and analyzed for *Aicda* levels by qRT-PCR for $n = 4$ (no LPS) and $n = 3$ (LPS) samples. **j** WES from fr.A-D cells and T8 were compared to tail-tip samples to identify SNVs. Filtering on SNV frequency “0.45–0.55 or ≥ 0.95 ” yielded putative “core mutations”. Absolute numbers of nucleotide exchanges are presented as stacked bars, colors give the type of nucleotide exchange. Two-way ANOVA, Sidak post hoc for **g–i**.

Aicda is upregulated in *Irf4*^{-/-} preB cells by LPS and deprivation of IL-7

Because six out of seven *Jak3* mutations were C to T base exchanges (Table 2), we suspected a specific mutagenic agent. DNA-editing enzymes including the APOBEC family member AID can deaminate cytosines, e.g., during somatic hypermutation [21, 22]. Repair mechanisms most often ultimately cause C to T conversions [23, 24]. Notably, AID is induced in wt preB cells by IL-7 withdrawal and LPS stimulation and acts as a facilitator of human BCP-ALL [25]. Therefore, we compared *Aicda* expression in sorted *Irf4*^{-/-} and wt fr.A-D cells to that of wt mesenteric (m)LN- and CD4⁺ T_H1-cells as controls and to individual leukemia samples. While mLN cells highly expressed *Aicda*, fr.A-D preB- and leukemia cells, but not T_H1-cells, also expressed readily detectable amounts (Fig. 3h).

Furthermore, like their wt counterpart [25], in vitro expanded *Irf4*^{-/-} preB-I cells upregulated *Aicda* further under LPS treatment

and during IL-7 withdrawal (Fig. 3i). This finding can explain how BM evasion and exposure to pathogens might cooperatively initiate mutagenic processes via AID in vulnerable *Irf4*^{-/-} preB-I cells.

To test if T8 exhibited signs of previous AID activity on a global level, we analyzed C:T/G:A-transition frequencies in WES of T8, as well as BM-sorted *Irf4*^{-/-} and wt fr.A-D cells compared with matched tail-tip samples. Indeed, we found a marked preponderance of C:T/G:A-transitions in T8, when filtering on putative somatic core SNVs (Fig. 3j).

Jak3 mutations in mice mirror *Jak2* mutations in human Ph-like ALL

Next, we compared *Irf4*^{-/-} leukemia to the complex landscape of human BCP-ALL subtypes (reviewed in refs. [11, 26, 27]), using a published human BCP-ALL cohort for which a random forest classifier had been established (Methods for details) [28]. Only

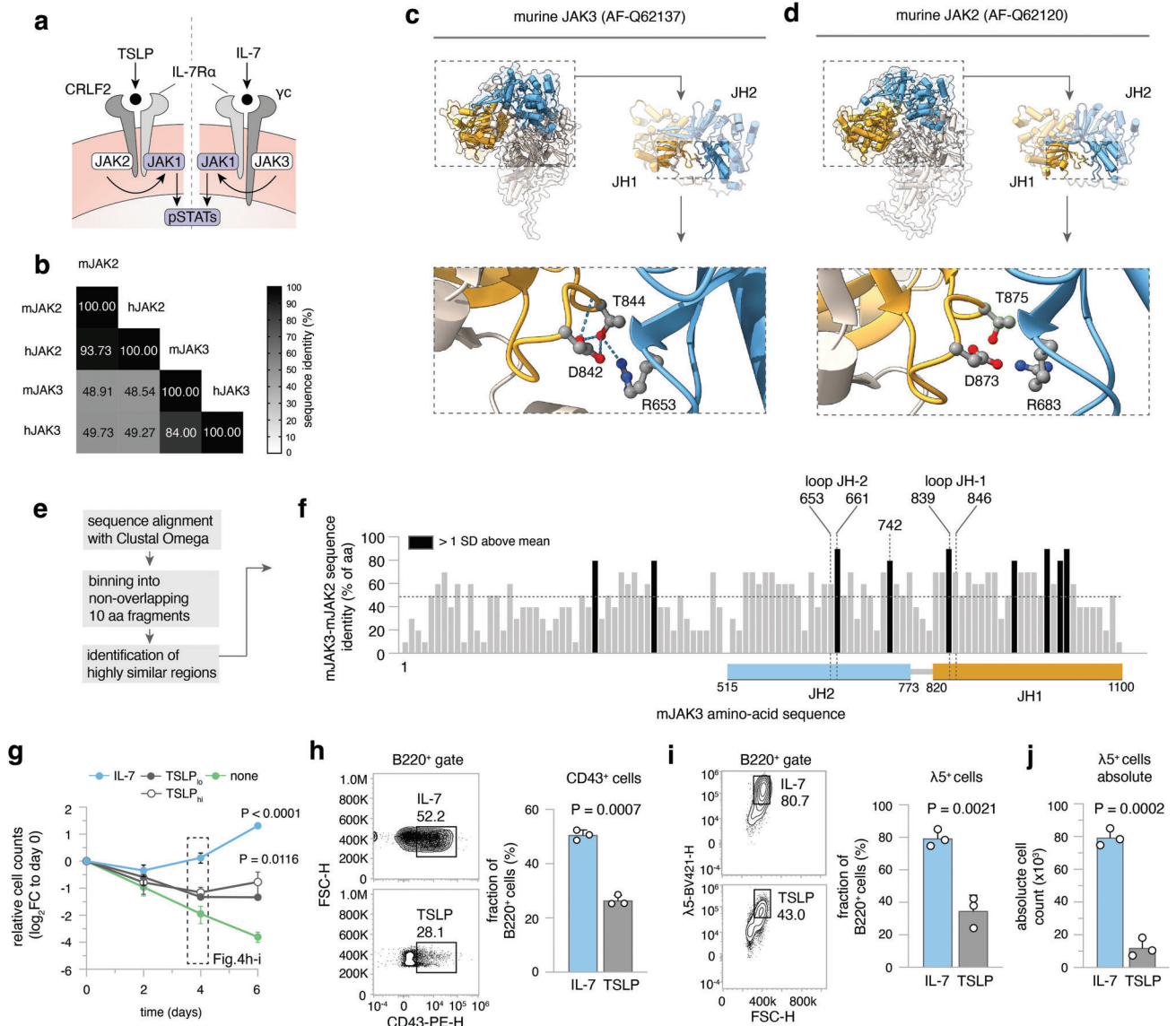


Fig. 4 Ph-like ALL in humans harbors *Jak2* mutation corresponding to *Jak3* mutations in *Irf4*^{-/-} BCP-ALL. **a** Cartoon depicting IL-7 and TSLP receptor components. **b** Multiple sequence alignment results (using Clustal Omega) of mouse (m) and human (h) JAK3 and JAK2 amino-acid sequences are presented as a matrix. Numbers and shade indicate sequence identity as percentage of amino acids. **c-d** Alpha-fold structure predictions of murine **c** JAK3 and **d** JAK2 are presented. Colors indicate domains: orange = JH1, blue = JH2. JH1-JH2 interface is magnified and T844/T875, R653/R683, D842/D873 amino acids are highlighted as ball-and-sticks representations. Dotted lines = hydrogen bonds. **e** Overview of analysis for **f**: Sequences of mJAK2 and mJAK3 were aligned using Clustal Omega. The sequence of mJAK3 was binned into 10 non-overlapping amino-acid fragments and the sequence identity to mJAK2 plotted along the mJAK3 sequence. Dotted line = mean protein-wide sequence identity, black bars = areas with sequence identity greater than 1 SD above mean. JH1 and JH2 domain regions are mapped onto the sequence, JH1 and JH2 domain regions are indicated by colored rectangles below. **g-j** *Irf4*^{-/-} BM cells were cultured for 6 days in the presence of 10 ng/mL rIL-7, 10, or 100 ng/mL rTSLP_(lo/hi) or no cytokine (none). **g** log₂ of cell counts relative to day 0 for *n* = 3 independent experiments plotted as means \pm SD. One-way ANOVA, Sidak post hoc comparing cytokine effect. **h-i** On day 4, **h** CD43⁺ and **i** λ 5⁺ cells within B220⁺ cells were recorded for IL-7 and TSLP treated cultures. Numbers indicate percentages within the depicted gates of B220⁺ cells. **j** Absolute counts of λ 5⁺ cells at day 4. Dots in **h-j** indicate *n* = 3 independent experiments, presented as bars (mean \pm SD). Unpaired two-tailed *t* test for **h-j**.

mildly (potentially due to the interspecies comparison) elevated prediction scores were generated for Ph⁺, Ph-like, KMT2a- and DUX4-rearranged human BCP-ALL (sFig. 4a, b). Since all of these except Ph-like are defined by specific gene rearrangements, that we had not detected in *Irf4*^{-/-} mouse leukemia, we excluded them as comparable candidates.

Ph-like ALL harbors recurrent genetic alterations in signaling molecules, especially in CRLF2 and JAK2 [20]. While BCP-ALL overall preferentially affects children, the incidence of the Ph-like subtype increases from 10% in children to above 25% in AYA and

adults [20, 29], reminiscent of the older age of *Irf4*^{-/-} leukemic mice. Furthermore, a published dataset of 154 Ph-like BCP-ALL cases exhibited 10-fold reduced *IRF4* transcripts, when compared to other BCP-ALL subtypes [20].

While in human Ph-like ALL, *Jak2* is commonly mutated, we report recurrent *Jak3* mutations in *Irf4*^{-/-} mice. As both proteins are part of distinct but similar signaling complexes in B-cell progenitors (Fig. 4a), we investigated structural and functional similarities between the specific *Jak3* and *Jak2* mutations. Comparisons of amino-acid sequences revealed high protein-

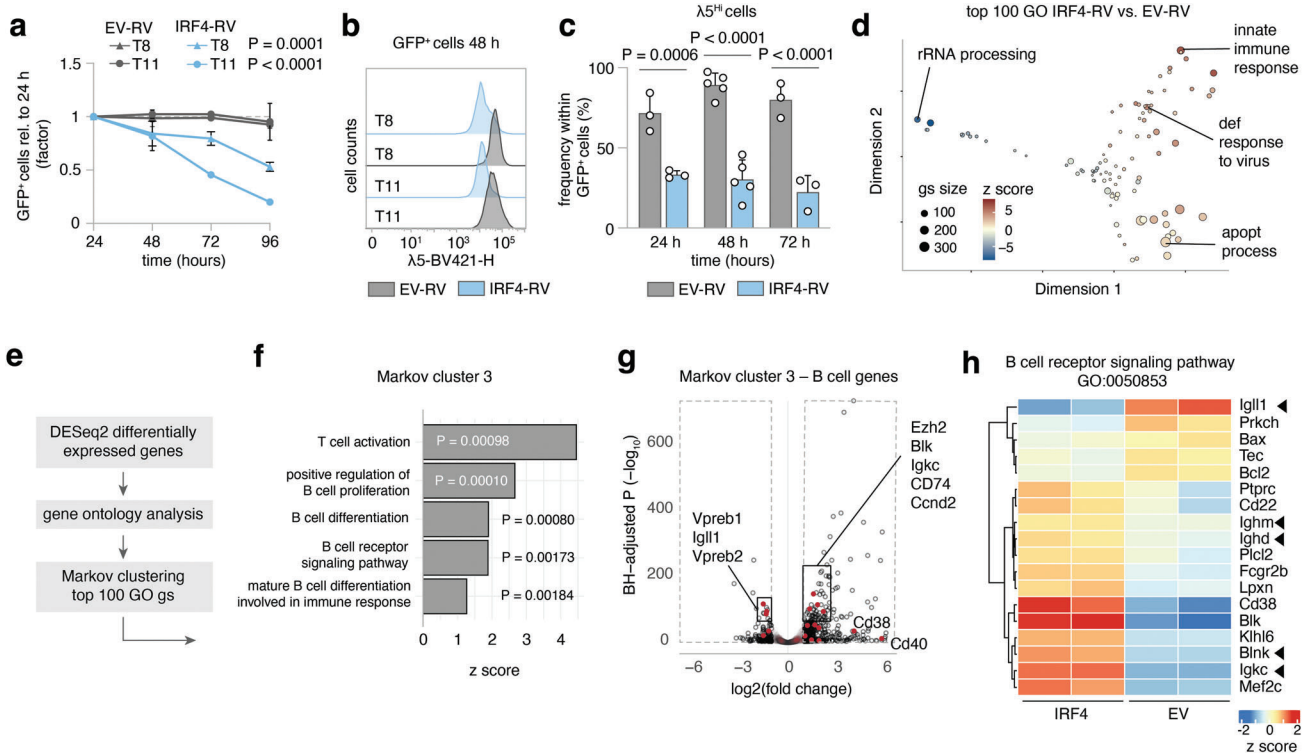


Fig. 5 IRF4 re-expression results in apoptosis and differentiation of leukemia cells. **a–c** T8 and T11 cells were transduced with IRF4-RV or control empty vector (EV)-RV. **a** GFP⁺ cell frequency normalized to 24 h after transduction was recorded. One-Way ANOVA, Sidak post hoc for RV effect per tumor. Mean \pm SD of $n = 3$ independent experiments. **b** Representative histogram of $\lambda 5$ surface expression of GFP⁺ cells at 48 h. **c** Pooled Quantification of $\lambda 5^{\text{Hi}}$ cells for three (24, 72 h) to five (48 h) independent experiments for T8 and T11. **d–h** T8 cells were collected in duplicates at 24 h after EV-RV and IRF4-RV transduction and subjected to bulk RNAseq. **d** MDS plot of top 100 gene ontology (GO) gene-sets varying between EV and IRF4 transduced T8. Representative gene sets annotated. Size of circles = number of genes, color = z score. **e** Analysis strategy for GO gene-set clustering using Markov clustering. **f** Gene-sets from Markov cluster 3 and corresponding P values and z scores. **g** Volcano plot of B-cell genes from Markov cluster 3 (red) highlighted within all differentially regulated genes (black). **h** Heat map of B-cell receptor signaling GO gene-set. Immunoglobulin genes and the tumor suppressor *Blnk* are marked. Color = z score.

wide interspecies and intermolecular similarities for both proteins (Fig. 4b). Mapping the two amino acids R653 and T844 (mutated in *Irf4*^{-/-} mice) onto JAK3 structure predictions, generated by the alpha-fold algorithm [30], revealed that the two amino acids are in direct contact at an interface of JH1-JH2 domains (Fig. 4c). This interface specifically is highly conserved in JAK2 compared to JAK3 (Fig. 4d, f, sFig. 4c, d). Intriguingly, R683 (corresponding to R653 in JAK3) is by far the most commonly mutated amino acid in JAK2 in Ph-like ALL, while mutations targeting T875 (corresponding to T844) also have been described [31]. These findings suggest that mutations in human JAK2 and mouse JAK3 affect a highly similar functional hotspot.

As mentioned above, JAK2 and JAK3 are part of distinct, but similar receptors: JAK3 binds the common γ -chain involved in IL-7 signaling, while JAK2 associates with CRLF2 involved in TSLP signaling. Both signals involve the IL-7R α chain and the same downstream pathways (STATs, PI3K) [32]. Therefore, the alternative presence of JAK3/JAK2 mutations between mouse and human BCP-ALL might reflect different cytokine preferences. Human proB/preB cells proliferate in response to both TSLP and IL-7 [33]. However, in *Irf4*^{-/-} BM cells IL-7, but not TSLP induced robust proliferation (Fig. 4g) as well as high frequencies and absolute counts of CD43⁺ (Fig. 4h) and $\lambda 5^+$ preB cells (Fig. 4i, j).

IRF4 re-expression leads to cell death and differentiation

As *Irf4* deletion was a prerequisite for leukemia in our model, we examined the effect of forced IRF4 re-expression, using RVs coding for GFP alone (EV-RV) or plus IRF4 (IRF4-RV). When re-introducing IRF4 into T8 or T11, GFP⁺ IRF4-expressing-, but not

GFP⁺ control cells gradually disappeared over time (Fig. 5a). AnnexinV/PI stainings confirmed apoptosis (not shown). Further, we noted the loss of surface $\lambda 5$ -expression induced by IRF4-RV (Fig. 5b, c). Comparing the transcriptomes of still viable cells 24 h after transduction revealed strong induction of “apoptotic process” and “innate immune response” gene ontology (GO) gene-sets (gs) (Fig. 5d). Markov clustering of GO gs affected by IRF4 re-expression (Fig. 5e, f) further identified several coregulated B-cell differentiation gs (Fig. 5f), with downregulated ψ L components *Igll1*, *Vpreb1*, and *Vpreb2*, but upregulated differentiation genes including *Igm*, *Igk*, and *Blnk* (Fig. 5g, h, sFig. 5a, b). Similar results were obtained for T11 (sFig. 5c, d). Therefore, fully transformed leukemia remained targetable by IRF4 re-expression.

Small compound agents affecting *Irf4*^{-/-} leukemia cells in vitro

Next, we screened a collection of kinase inhibitors for their capacity to kill *Irf4*^{-/-} leukemia cells in vitro. We included NIBR3049 targeting JAK3, Ruxolitinib, an inhibitor of JAK1/2 (downstream of JAK3), and Dexamethasone, a cornerstone for treating lymphomatous malignancies. Furthermore, we included inhibitors of NF κ B (IKK, TAK1), JNK, MEK, ERK, PP2A, GFI1, FAK, and the Bruton tyrosine kinase (BTK) acting downstream of the BCR.

A variety of these substances potentially killed tumor cells (sFig. 6a), implying the involvement of multiple pathways in leukemia cell survival. The efficacy of Ruxolitinib and NIBR3049 corroborated our results concerning *Jak3* driver mutations. Furthermore, inhibitors of GFI1 and PP2A, as well as NF κ B and

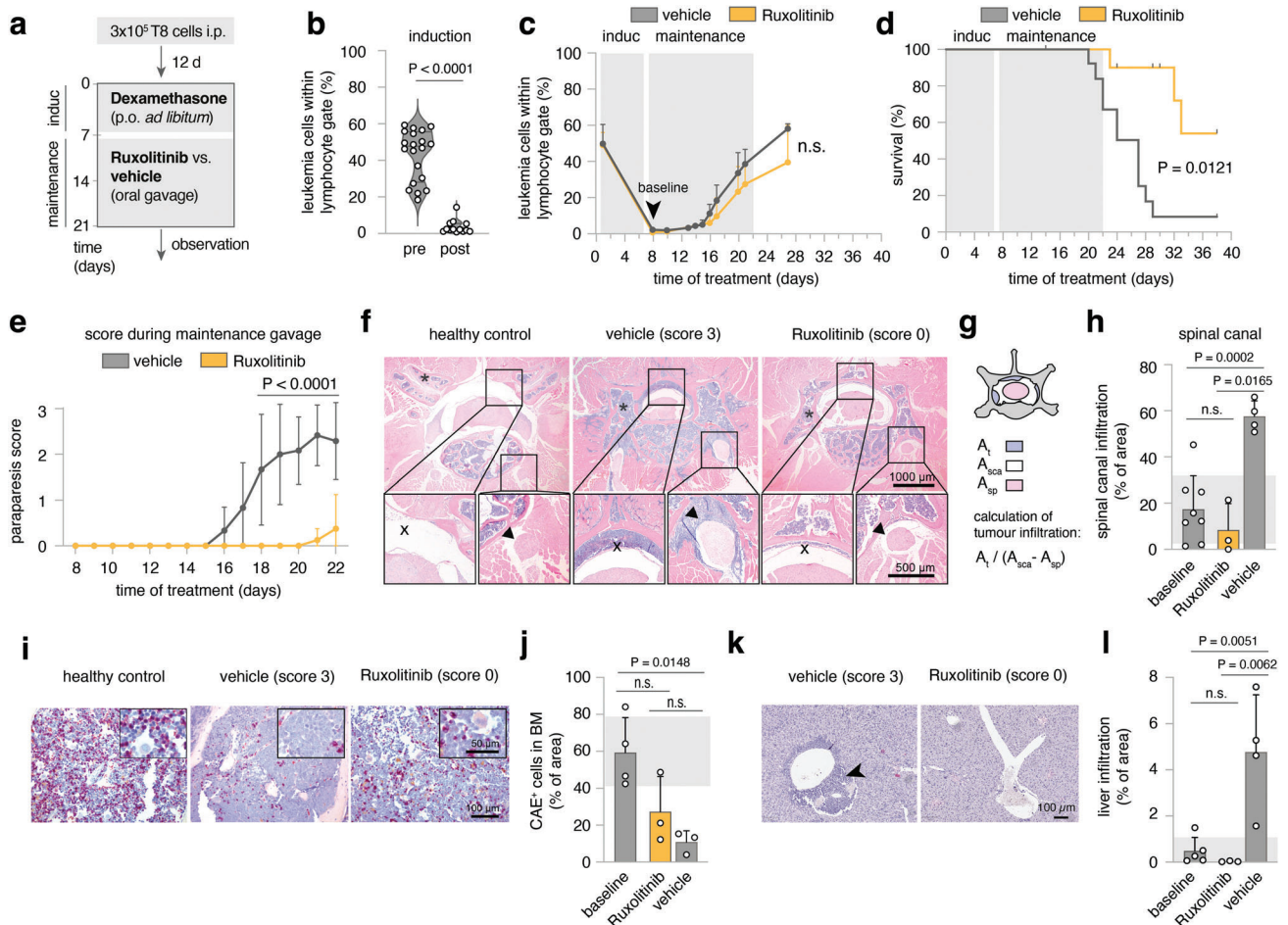


Fig. 6 Ruxolitinib reduces leukemic meningeosis and organ infiltration in vivo. **a** Schematic overview of experimental design. Day 0: injection of mice with 2×10^5 T8 cells. After 12 days initiation of Dexamethasone induction therapy supplied in drinking water for seven days. Maintenance therapy comprised either Ruxolitinib-phosphate (11 mice) or vehicle control gavage (13 mice) twice daily for 14 days. Mice were scored daily and blood sampling was performed regularly. **b** Leukemia cell frequency ($B220^+slg\mu$) within lymphocyte gate before and after induction with Dexamethasone. Two-tailed unpaired *t* test $P < 0.0001$. **c** time-course of leukemia cell frequencies in peripheral blood for Ruxolitinib and vehicle-treated mice. **d** Survival as Kaplan–Meier plot analyzed with Log-rank test. In the Ruxolitinib group, four mice were excluded and censored due to intervention-related adverse reactions or due to their use in the analysis described in **f–l**. **e** Disease scores, determined as described in methods. Mean \pm SD of the scores per indicated treatment group analyzed by two-way ANOVA, Sidak post hoc. $n = 2$ replicate experiments for **b–e** with similar outcome. **f** Exemplary histopathology (HE) of healthy or leukemia bearing mice (score 3, vehicle-treated or score 0, Ruxolitinib-treated). One representative mouse per condition. Bar size in the bottom right corners. Top panels: an overview of cross-sectioned lumbar vertebra, bottom inserts from spinal canal (left) and spinal nerve root (right). **g** Schematic representation of the calculation of tumor infiltration into the spinal canal. (A_t : area of tumor infiltration, A_{sca} : area of total spinal canal, A_{sp} : area of the spinal cord). **h** Quantification of spinal canal infiltration according to **g** for $n = 8$ after induction (baseline), $n = 3$ score 0 (Ruxolitinib) and $n = 4$ score 3 (vehicle) mice. **i** Representative CAE stainings from vertebral BM for score 0 and score 3 mice. **j** Quantification of area occupied by CAE⁺ cells relative to total BM area for $n = 4$ (baseline), $n = 3$ (score 0, Ruxolitinib) and $n = 4$ (score 3, vehicle) mice. **k** Representative HE stainings from liver tissue for score 0 and score 3 mice, Scale bar bottom right. **l** Quantification of tumor infiltrated area relative to whole liver area for $n = 5$ (baseline), $n = 3$ (score 0, Ruxolitinib) and $n = 4$ (score 3, vehicle) mice. Each dot represents measurements of three complete liver cross-sections per mouse.

JNK, were potent. In contrast, inhibiting BTK, MEK and ERK had no impact.

In vivo therapy of established *Irf4*^{-/-} B-ALL

Next, we implemented JAK inhibition as in vivo treatment for *Irf4*^{-/-} leukemia. We began induction therapy with Dexamethasone around day 12 after adoptively transferring 3×10^5 T8.1 cells i.p. into wt mice (Fig. 6a), when overt leukemia was noted in peripheral blood (pB) (Fig. 6b “pre”). After 7d of treatment, leukemic cell numbers in pB were robustly reduced (Fig. 6b “post”), although few cells reproducibly remained detectable (Fig. 6c). Maintenance therapy was continued with Ruxolitinib or vehicle control by oral gavage twice daily for the following 12 days (Fig. 6a, c). Importantly, the half-life of Ruxolitinib in mice is only 0.8 h (“Australian Public

Assessment Report for Ruxolitinib”, Australian Government), implying that any observed in vivo effectiveness might be underestimated.

Despite maintenance therapy, leukemic cells in pB reappeared, with no significant difference between treatment groups (Fig. 6c). However, treatment with Ruxolitinib resulted in a clear survival benefit (Fig. 6d) and marked improvement of a prominent neurological symptom: in sham-treated animals, temporary limpness of the tail and hind legs occurred seconds after gavage, which we quantified using a newly established scoring system (ranging from 0 to 3, see Methods).

Mechanistically, ultrasound imaging revealed an echogenic paravertebral mass (sFig. 7a, b) in score 3, but not score 0 mice. By histology, score 3 correlated with severe infiltration of blasts into

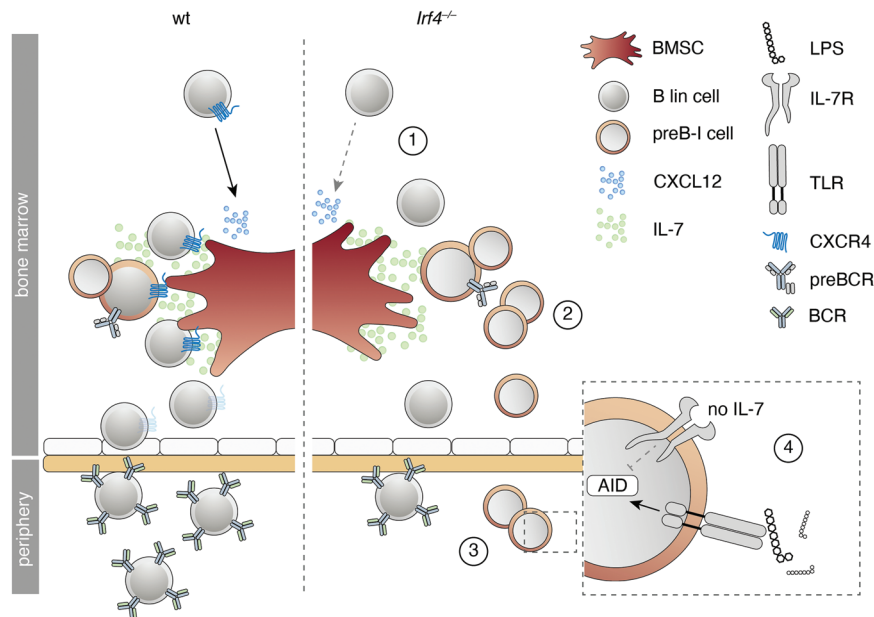


Fig. 7 Summary of the preB-I preleukemic state induced by IRF4 deficiency. Cartoon summarizing the findings for IRF4 deficient compared to wt B lymphopoiesis. B lineage (lin) cells are less responsive to BMSC-derived CXCL12 due to reduced surface CXCR4 expression (1). *lrf4*^{-/-} preB-I cells exhibit impaired differentiation and IL-7 dependent hyperproliferation (2). *lrf4*^{-/-} preB cells escape into the periphery (3), where a combination of IL-7 deprivation and danger-associated molecular patterns (such as LPS) might induce AID expression (4), fueling mutagenesis.

the spinal canal (X in Fig. 6f), extending into spinal nerve roots (arrowhead in Fig. 6f). Therefore, paraparesis likely represented a manifestation of mouse leukemic meningeosis, exacerbated by gavage-induced increases in intraabdominal pressure.

Paraparesis was reproducibly relieved during Ruxolitinib treatment (Fig. 6e), correlating with the suppression of perimyeloid infiltration that ensued in vehicle-treated mice after the end of induction therapy (Fig. 6f, h). In contrast, the severely impaired hematopoiesis in sham-treated mice, indicated by low CAE⁺ cell frequencies, was not significantly ameliorated by Ruxolitinib (Fig. 6i, j).

These findings raised the possibility that Ruxolitinib preferentially targets infiltration of solid organs rather than BM or pB. Accordingly, Ruxolitinib fully blocked the liver infiltration as observed in sham-treated mice (Fig. 6k, l). As tissue infiltration is regulated by homing receptors, we treated T8.1 and T8.2 cells with Ruxolitinib in vitro and recorded the expression of CD29 (integrin β 1), which pairs with various integrin alpha chains involved in cell- and tissue adhesion [34, 35]. Notably, on T8.1 and T8.2, Ruxolitinib reduced CD29 expression dose-dependently (sFig. 6c–e) while it even slightly increased expression of MHC I molecules (H2D^b, H2K^b), stained as a specificity control.

DISCUSSION

The herein described spontaneous leukemogenesis in *lrf4*^{-/-} mouse stresses the particular vulnerability of preB-I cells. Our data provide insights for (a) conditions promoting leukemogenesis, (b) functional consequences of *Jak* mutations, (c) parallels of mouse and human BCP-ALL and (d) potential in vivo treatment:

(a) We provide evidence for a two-hit leukemogenesis model: The first hit (*lrf4* loss) resulted in reduced differentiation, IL-7-dependent hyperproliferation, and impaired retention at the BM niche (Fig. 7). A second hit (targeting *Jak3* in our model) created a dominant survival signal, probably founding overt preB-I leukemia.

The induction of BCP-ALL in *lrf4*^{-/-} mice are similar to *Ikzf1* and *Pax5* mutated mouse models [36–38], implying similarities between these TF-alterations. Probably, one shared mechanism

is the differentiative impairment. Importantly, for *lrf4*^{-/-} fr.A-D cells we even detect slightly higher levels of *Pax5* compared to wt fr.A-D cells (sFig. 8), ruling out that the findings in *lrf4*^{-/-} mice merely mirror those of *Pax5* deficiency. The reverse remains conceivable; that *Ikzf1* and *Pax5* mutations converge in lowering IRF4 expression.

In addition to mice mutated in *Pax5* or *Ikzf1*, *lrf4/lrf8*^{-/-}, and *lrf4/spi1*^{-/-} mice have been shown to develop leukemia early in life at a high incidence [39, 40]. Contrasting these studies, we report that a single deficiency for IRF4 fully suffices for leukemogenesis. We excluded secondary alterations in *lrf8*, *Spi1* in our model: we found unchanged expression and gene sequence of IRF8 (not shown) and normal amounts of *Spi1* transcripts (sFig. 8a) in *lrf4*^{-/-} fr.A-D cells. The single IRF4 deficiency models potential clonal initiating events better than *lrf4/lrf8*^{-/-} or *lrf4/spi1*^{-/-} mice, because *lrf4*^{-/-} mice harbor productive B-cell development.

We newly describe that a preleukemic alteration can lead to reduced BM retention, presenting a tentative explanation for the induction of mutagenic signals, as deprivation from IL-7 and exposure to bacterial compounds can cooperatively induce the mutagenic agent AID [25].

(b) Why do *Jak3* mutations only lead to enhanced sensitivity to, but not complete independence of IL-7? Analysis of JAK3 and JAK2 structure implied that mutations of R683/R653 and T875/T844 might decrease JH1-JH2 interaction strength. This would imply reduced auto-inhibition as the GOF mechanism—in line with findings for the JAK family member TYK2 [41]. This alone cannot explain cytokine independency, owing to the receptor biology: The two preassembled receptor chains keep JAKs intracellularly separated [42]. Ligand binding is needed for a conformational change that brings JAKs into the proximity needed for cross-phosphorylation.

To explain our observations, we propose an oncogene model with two equilibria (Fig. 8a, b): the first is determined by cytokine concentration and dictates the probability of receptor conformation change (Fig. 8a). The second, independent equilibrium (Fig. 8b), is determined by the interaction strength at the JH1-

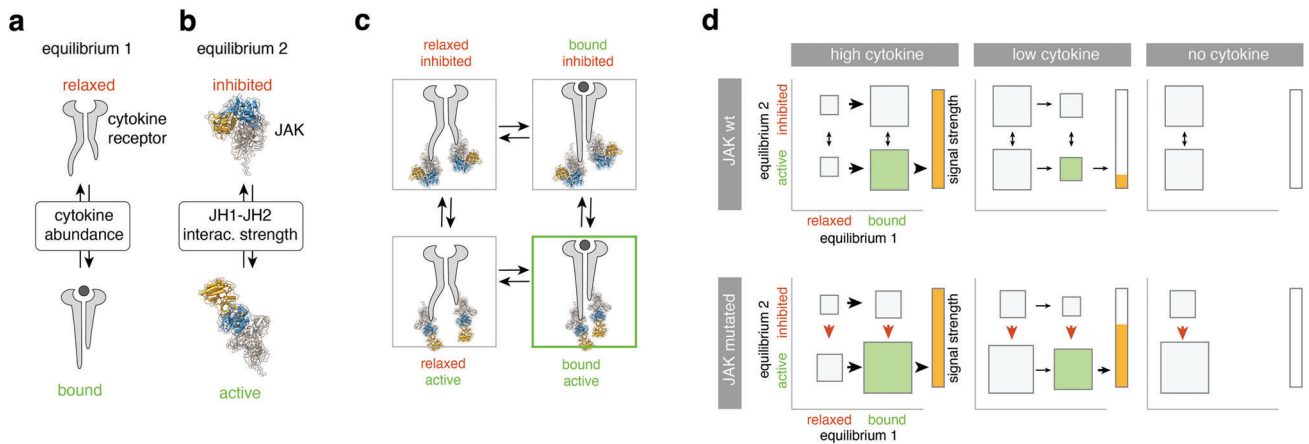


Fig. 8 **A “two-equilibrium model” explains JAK mutant effects in primary pre-B1 cells.** **a** Equilibrium 1 is determined by cytokine abundance and dictates the cytokine receptor state (bound vs. relaxed). **b** Equilibrium 2 is determined by the interaction strength between JH1 and JH2 domains in JAKs and dictates the JAK state (inhibited vs. active). **c** Equilibria 1 and 2 interact to create four possible states. Green lettering indicates signaling favoring state. Green frame indicates the actively signaling state. **d** For high (left), low (middle), and no (right) cytokine in the presence or absence of JAK3 mutations, hypothetical probabilities of equilibria states as in **c** are presented. Size of rectangles signifies likelihood of state relative to others. Arrows indicate shifts of equilibria, red arrows indicate the effect of JAK mutations. Green rectangle = active signaling state (bound and active). Bars to the right of each panel indicate signal strength as a direct result of the two equilibria adjacent to it.

JH2 interface and dictates the probability of JH1 and JH2 dissociation. Only the combination of the “bound” and “active” state (Fig. 8c) would result in the elicitation of a signal (Fig. 8c, green frame).

In this model, JAK mutations would only affect the second equilibrium (Fig. 8d, red arrows). Sporadic ligand binding would still be needed for elicitation of signaling. The model stringently predicts the better exploitation of low cytokine concentrations for JAK_{mut} that we observed in vitro. Figure 8d depicts theoretical probabilities of receptor states in the presence (top row) or absence (bottom row) of JAK mutations.

Our findings that JAK3_{mut} confer heightened cytokine sensitivity, but not -independence, is in contrast to what has been found for JAK2-R683G mutants expressed in the commonly used BaF3 cell line [43]. However, BaF3 cells depend on IL-3 and not IL-7R α cytokines (i.e., IL-7 or TSLP). Therefore, it remains conceivable, that the IL-3 receptor provides a different physiology, which may deviate from the IL-7R physiology in primary B progenitors.

(c) The finding that *lrf4*^{-/-} pre-B1 cells respond preferentially to IL-7 over TSLP presents a possible explanation, why mouse models of BCP-ALL acquire *Jak3* mutations, and human Ph-like ALL typically harbors *Jak2* mutations. Our comparison of JAK structure predictions yielded corresponding mutations likely to elicit similar downstream effects.

(d) Lastly, our in vivo experiments reinforce Ruxolitinib as a potential treatment for JAK-driven BCP-ALL. The compound represents an important therapeutic agent in myeloproliferative disease and is already studied for the treatment of Ph-like-ALL [44, 45]. We describe a preferential effect of Ruxolitinib on CNS- and organ infiltration, potentially due to reductions in integrin expression on leukemia cells. These effects are of potential translational importance because current CNS-targeted therapies for ALL remain toxic.

METHODS

Mice

C57Bl/6 mice were purchased from Charles River, Sulzfeld, Germany. *lrf4*^{-/-} mice [7] and *Il-7*^{eGFP} mice [46] (provided by Koji Tokoyoda, DRFZ Berlin) were bred on the C57Bl/6 background and housed in the animal facility of the Biomedical Research Center at the University of Marburg, Germany. If not stated otherwise, all mice used in the presented experiments were 8–12 weeks old and sex-matched.

Tumor cell lines and cell culture

Stable tumor cell lines T8.1, T8.2, and T11 were established from primary *lrf4*^{-/-} leukemia cells (derived from primary tumor 8, i.e., T8, or tumor 11 (T11)) by culturing them on a monolayer of irradiated (30 Gy) ST2 stromal cells [47] grown to confluency in Opti-MEM medium (31985070, ThermoFisher Scientific) supplied with 1% cell culture supernatant from JIL-7.6 J558 cells [48] (a gift from Fritz Melchers, Berlin) as a source of IL-7. After several passages, T8 and T11 cells grew independently of ST2 cells. For in vitro inhibitor experiments, 2.5×10^5 T8.1 or T8.2 cells (or T11 cells) were cultured in 500 μ L RPMI medium in 48 well plates in the presence of the indicated concentrations of inhibitors. To determine the percentage of viable cells, samples were stained using Annexin V and propidium iodide (PI) (see below) after 48 h. Substances used include Dexamethasone (S7654, Selleckchem), Oxacaenol (O9890, Sigma), GANT61 (Sigma, G9048), SP203580 (EI-286-0001, Enzo), SP600125 (EI-305-0010, Enzo), PD98059, Promega), Ibrutinib (S2680, Selleckchem), BAY11-7082 (ALX-270-219, Alexis), Dexamethasone (PZN 08704491, mibe GmbH) and Ocaidaic acid (O4511, Sigma).

Murine pro/preB cell cultures

Femur and tibia bones from 8 to 12 weeks old mice were explanted and cleaned from adherent tissues. Cells were extracted via centrifugation at 11×10^3 RPM for 10 s. Total BM cells were enriched for B220⁺ (slgM⁺) B lineage cells using an in-house magnetic-activated cell sorting protocol. Briefly, whole bone marrow cells were stained with a mix of FITC-conjugated antibodies to (IgM), CD11b, B220, Ter119, CD49b, CD4, and CD8 (all from eBioscience), followed by incubation with an anti FITC/streptavidin/biotin/magnetic bead complex (Miltenyi Biotec) and magnetic sorting using a microcentrifugation tube stand (Miltenyi Biotec) [49]. Sorting efficiency, as confirmed by flow cytometry, routinely exceeded 90%. Cells were seeded at a density of 1×10^5 cells per well in 200 μ L RPMI complete (96-well plates, Greiner). Pro/preB cell cultures were propagated with 10 ng/mL rmlL-7 (217-17, Peprotech) in RPMI-1640 medium complete (R8758, Sigma-Aldrich, supplemented with: 10% FCS (Sigma-Aldrich), 2 mM L-glutamine (Biochrom), 50 μ M β -mercaptoethanol (Sigma-Aldrich), 0.03/0.05 g per 500 mL Penicillin G/Streptomycin Sulfate, 1% non-essential amino acids (PAA Laboratories)). In some experiments, pro/preB cells (1.25×10^6 /mL medium) were treated for 24 h with LPS (Sigma, 1 μ g/ml), anti-IL-7 (BioXCell, 10 μ g/ml), rmlL-7, or respective combinations, before generating mRNA for qRT-PCR.

Transwell migration assay and OP-9 adhesion assay

For the transwell migration assays, Hardy fr.A-D cells were magnetically sorted from BM of wt and *lrf4*^{-/-} mice as described above (with addition of FITC-conjugated anti-IgM antibody), and 2×10^5 cells in RPMI (without additives, FCS-free) containing 10 ng/mL rmlL-7 seeded in 50 μ L in the top

chamber of 96-well 5 µm pore uncoated 96-well transwell plates (HTS transwell® Corning). The bottom chamber was flooded with 200 µL RPMI containing indicated concentrations of rmCXCL12 (PeproTech). After 16 h, inserts were removed, cells in the bottom chamber were collected, counted, and analyzed for B220 surface expression using flow cytometry. The fraction of migrated cells was calculated as $n(\text{migrated}) \times \text{freq}_{\text{B220}}(\text{migrated})/n(\text{input}) \times \text{freq}_{\text{B220}}(\text{input})$. Normalization to B220⁺ cells reduced interexperimental differences due to differences in cell purity after magnetic selection. For OP-9 adhesion assays, 5×10^3 OP-9 cells (a gift from Hyun-Dong Chang, DRZF Berlin) were seeded in 96-well microtiter plates 24 h before the assay. On the day of the assay, fr.A-D cells were purified as above and 2×10^5 fr.A-D cells were seeded on top of OP-9 monolayers in RPMI complete + 10 ng/mL rmlL-7. Plates were centrifuged briefly to accelerate cell descension. After 1 h, suspended cells were collected in the supernatant and by washing OP-9 monolayers two times with PBS.

Flow cytometry and cell sorting

For surface staining of B lineage markers, cells were harvested, resuspended in PBS/1% FCS and stained with anti-B220 (RA3-6B2, Biolegend), anti-Igµ (II/41, BD Bioscience), anti-CD43 (RM2-5, Biolegend), anti-CD24 (M1/69, invitrogen), anti-BP-1 (BP-1, BD Bioscience), anti-CD2 (RM2-5, Biolegend), anti-CXCR4 (L276F12, Biolegend), anti-CD127 (=IL-7Ra) (A7R34, BD Bioscience), anti-CD179b (=λ5) (LM34, BD Bioscience) as indicated (20 min at room temperature in the dark). All antibodies were employed at a dilution of 1:500. Fluorescence was recorded using either a FACS Aria III (BD) or an Attune NxT (Thermo-Fisher) analyzer. Data analysis was performed using the FlowJo V10 software (BD). For dimensional reduction, we used the t-Distributed Stochastic Neighbor Embedding (tSNE) [50] algorithm built into FlowJo V10. Epitopes on BM cells from *Irf4*^{-/-} and wt control mice used for dimensional reduction analysis comprised B220, slgµ, CD43, CD24, BP-1. For RNA and WES analyses, BM cells were surface labeled for B220 and slgµ expression, and B220⁺slgµ⁻ cells were sorted using a FACS Aria III (BD Bioscience). Sorting efficiency was routinely above 95%. To determine cell viability, AnnexinV/PI staining was performed using 5 µL AnnexinV (640905, Biolegend) per 500 µL HBSS. After 20 min of incubation at room temperature in the dark, 1 µL PI (421301, Biolegend) was added, and cells were immediately measured.

CNVs analysis

CNVs were analyzed in tumor samples 8, 10, and 14 and compared to *Irf4*^{-/-} normal tail tissue. Whole DNA was extracted from 5×10^6 cells per sample using the Macherey-Nagel NucleoSpin Tissue kit (REF 740952.50) according to the manufacturer's protocol. Library preparation was performed using the Illumina Nextera DNA kit according to the manufacturer's instructions. Sequencing was performed on an Illumina-HiSeq-1500 platform in rapid-run mode at the Genomics Core Facility of Philipps-University Marburg. Fastq quality control was performed using custom scripts. Raw sequenced reads were aligned to the Ensembl Mus musculus reference (revision 79) using Bowtie2 (version 2.0.0) [51] with standard parameterization. Analysis of CNVs was performed using the cn.mops (Copy Number estimation by a Mixture Of PoissonS) package (version 1.18.1) [52] with the following parameterization: prior impact = 1, lower threshold = 0.9, upper threshold = 0.5, minimum width = 4. Window length was set to 10000 and the algorithm was run in unpaired mode.

BM cryosections and analysis of B progenitor vicinity to IL-7⁺ BMSCs

Mouse femora from *Irf4*^{-/-} or wt *il-7^{eGFP}* reporter mice were explanted, cleaned from soft tissues, and fixated overnight in 4% PFA PBS (Alfa Aesar). Samples were then dehydrated by incubation in 30% sucrose in PBS for 24 h. Dried and dehydrated femora were snap-frozen in cryomolds® (Tissue-Tek) using O.C.T freezing medium (Tissue-Tek) by being placed in a beaker of Hexan, surrounded by a beaker of Acetone and dry ice. Samples were stored at -20 °C until processing. Cryosections of 7 µm were generated with a Leica cryostat (DB80 LX microtome blades, Leica) using Kawamoto tape [53] (Section-lab) as described before [54]. Cryosections were stained with antibodies against B220 (RA3-6B2, Biolegend), CD2 (14-0021-85, eBioscience), conjugated to AF555 using lightning-Link kit, Abcam), GFP (Rockland goat polyclonal anti-GFP, 600-101-215) with secondary rabbit anti-goat F(ab')₂ AF488 (thermo-scientific A21222). Samples were then mounted in DAPI ProLong Gold Antifade (ThermoFisher Scientific). Images

were recorded using a Leica confocal (SP8i) microscope. Image analysis was performed in IMARIS (version 9.7.2).

Histological analyses

Tissue samples were immediately fixed in 4% PFA PBS solution. Histological analysis was performed on 3 µm thick sections from paraffin-embedded tissue as described previously [55]. Briefly, rehydrated paraffin sections were first blocked with 0.3% H₂O₂ and goat normal serum. For immunohistochemical (IHC) stainings, rat antibodies against CD45R/B220 (clone RA3-6B2, BD) and Ki67 (clone TEC-3, Dako) were then incubated on the tissue slices and the bound antibody was detected with biotinylated goat anti-rat IgG (Southern Biotechnology). Bound antibody was visualized with the Vectastain-kit (Vector Laboratories) according to the manufacturer's protocol. Hematoxylin-Eosin (HE) stainings were performed according to standard procedures. Cells of the granulocytic lineage were stained on paraffin-embedded tissues with the Naphthol AS-D Chloracetate (Specific Esterase, CAE) Kit (Ref: 91C-1KT, Sigma-Aldrich) according to the manufacturer's protocol.

In the in vivo therapeutic experiments, we calculated the narrowing of the spinal cord using the equation $A_T/(A_{sca}-A_{sp})$, where A_{sca} is the area of the spinal canal, A_T that of the tumor, and A_{sp} that of the spinal cord area. Two different cross-sections per animal were examined. The infiltration of the liver was calculated by dividing the tumor area in the liver by the whole area of the liver section. Three whole liver sections were analyzed per animal. All measurements were performed using Fiji [56].

Whole-exome sequencing and biostatistical analysis

To determine SNV within leukemia samples, genomic (g)DNA was extracted both from primary *Irf4*^{-/-} tumors as well as FACS-sorted control B220⁺slgµ⁻ BM fr.A-D cells using the High Pure PCR Template Preparation kit from Roche (11796828001). The integrity of the resultant gDNA was confirmed in a 2% Agarose gel. MacroGen in Seoul performed SureSelect All Exon V6 library preparation and sequenced exons on a NovaSeq platform producing 2×150 bp reads at a coverage of 100× (50× on-target coverage). Fastq quality control was performed using FASTQC (version 0.11.9). Raw sequenced reads were aligned to the Ensembl Mus musculus reference (revision 96) using STAR (version 2.6.1d) using default parametrization. Soft-clipped aligned reads were then subjected to variant calling analysis. Position-wise pile-up files were generated using samtools (version 1.9) with the mpileup option and a pile-up quality threshold of 15, both for single sample and matched variant calling. Subsequently, variant calling was performed for SNP and InDel detection using VarScan2 (version 2.3.9) on single samples with the following parametrization: sampling depth = 100,000, minimum variant frequency = 0.05, minimum coverage = 8, minimum variant reads = 2, minimum average read quality = 15 and a *p* value threshold was set to 0.05. Only primary alignments were considered, the strand filter was enabled, and duplicates were removed. As a comparison, matched tumor-normal variant calling was performed with VarScan as well using an identical parameter setting with the somatic *p* value threshold set to 0.05.

For Fig. 3n raw sequenced reads were aligned to the Ensembl Mus musculus reference (revision 96) using Burrows-Wheeler Aligner (BWA version 0.7.17) using default parametrization [57]. Prior to variant calling, aligned reads were filtered using a custom filter that excludes reads with more than three mismatches, more than two indels, or a mapping quality below 20 using pysam (version 0.16.0.1). Duplicates were marked and removed using Picard (GATK version 4.1.6.0) [58]. Filtered aligned reads were then subjected to variant calling analysis. Position-wise pile-up files were generated using samtools (version 1.9) with the mpileup option and a minimal base quality threshold of 20. Subsequently, variant calling performed for SNP detection using VarScan2 (version 2.4.4) using matched tumor-normal (somatic) mode with the following parametrization: sampling depth = 100,000, minimum variant frequency = 0.2, minimum coverage = 8, minimum variant supporting reads = 5, minimum average read quality = 20 and a somatic *p* value threshold was set to 0.05. Only primary alignments were considered, and the strand filter was enabled. SNP calls were filtered to high confidence somatic mutations using VarScan's somaticFilter method, SNPs with a variant allele frequency above 0 in the matched reference sample were excluded.

Sanger sequencing and polymerase chain reaction

SNVs in the JAK3 gene were confirmed by Sanger sequencing of PCR fragments spanning the *Jak3* pseudokinase and kinase region (primers

used for PCR amplification and Sanger Sequencing: mJAK3 for, mJAK3 vs s. Supplemental Data). Sequencing services were provided by Microsynth Seqlab. To determine the clonality of tumor cells, the V_H region was amplified by PCR. Amplicons were run on an agarose gel and extracted using the QIAquick Gel Extraction Kit (Qiagen). DNA fragments were then cloned into the vector pJet1.2 (Thermo Scientific) and transformed into DH10B *E. coli*. The indicated numbers of clones (Fig. 1g) for each PCR amplicon were sequenced and aligned with software from IMGT/V-quest [59].

Retroviral transduction of *Jak3*-mutants and IL-7 independency assay

The coding sequence of murine *Jak3* was amplified from pCineo-Jak3 (a gift from Olli Silvennoinen from Tampere-university in Finland) and cloned into the pMSCV-Thy1.1 expression plasmid using *Bam*HI and *Sall* restriction digestion. Site-directed mutagenesis was performed following the manufacturer's protocol using the Quick-Change II site-directed mutagenesis kit (Agilent Technologies; primers employed are listed in the Supplemental Materials). Viral supernatant from mutated pMSCV-Thy1.1-*Jak3* constructs was produced as described previously [49]. For viral transduction, 5×10^5 IL-7 dependent primary *Irf4*^{-/-} pre-B1 cell cultures were resuspended in 400 μ L RPMI medium (D5030, Sigma-Aldrich) with 600 μ L viral supernatant and 1.5 μ L polybrene and spun in culture plates at 2700 rpm for 90 min at 37 °C. Cells were then replenished with a conditioned medium and rested for 24 h. Transduction efficiency was measured by flow cytometry using surface staining for Thy1.1 (OX-70, Biolegend). For the IL-7 independency assay (Fig. 3b), transduced cells were split and cultured with either recombinant murine (rm)IL-7 or 10 μ g/ml neutralizing anti-IL-7 antibody (BE0048, Bio X Cell).

RNA-sequencing and biostatistical analysis

RNA extraction from primary tumor samples and FACS-sorted B220⁺ slg μ ⁻ pro/preB cells was performed using Trizol extraction. Quality control was performed using the Bioanalyzer RNA 6000 NanoChip (Agilent Technologies). Library preparation was performed at the Institute for Immunology, University Medical Center of the Johannes Gutenberg-University Mainz using the NEBNext Ultra Library Prep kit (New England Biolabs). For deep sequencing, the Illumina-HiSeq-4000 platform was used (Beijing Genomic Institute). Quality control on the sequencing data were performed with the FastQC tool (version 0.11.2, <https://www.bioinformatics.babraham.ac.uk/projects/fastqc/>). RNA-sequencing reads were aligned to the ENSEMBL *Mus_musculus.GRCm38* reference genome. The corresponding annotation (ENSEMBL v76) was also retrieved from ENSEMBL FTP website. The STAR aligner (version 2.4.0) was used to perform mapping to the reference genome. Alignments were processed with the featureCounts function [60] of the Rsubread package, using the annotation file also used for supporting the alignment. Exploratory Data Analysis was performed with the pcaExplorer package [61]. Differential expression analysis was performed with DESeq2 package [62], setting the false discovery rate (FDR) cutoff to 0.1. DESeq2 datasets were analyzed using the GeneTonic [63] and pcaExplorer packages. To assess the possible occurrence of gene fusions, we applied two different methods, Star-Fusion (version 1.10.1) and Arriba (version 2.1.0). For STAR-Fusion, required meta reference files were created from the Ensembl *Mus_musculus* reference (revision 100) as recommended in the STAR-Fusion manual. In case of Arriba, we used the mm10 + GENCODEM25 assembly. In each case, we used the dockerized versions of the tools. Raw fastq files were used as an input for both tools. Subsequently, raw reads were mapped using the recommended alternative STAR settings recommended in the tools manual to leverage chimeric reads from the alignments. Default filters as recommended by the STAR-Fusion and Arriba manuals were applied to limit the false-positive rate. For the same reason, known blacklisted regions as provided by the Arriba release were excluded from the analysis.

BCP-ALL subtype predictions using random forest classifier

Human genes (GRCh38.p13, v104) with annotated orthologous genes in mice were extracted from ensembl database using the BiomaRt online tool. Gene counts from RNA-sequencing of a previously published human BCP-ALL cohort [28] and of murine tumor samples were subsetted to include only human-mouse orthologous genes. The resulting gene counts were normalized by variant stabilization transformation using the R package DESeq2 version 1.32.0. Allocation of the murine tumor samples to human BCP-ALL molecular subtypes was performed based on gene

expression using a random forest machine learning algorithm (R package caret version 6.0-88) trained on the human cohort. Predictions were plotted using R package pheatmap version 1.0.12. Differential gene expression was analyzed in R package DESeq2 and resulting gene lists ranked by log₂-fold-change were analyzed in GSEA version 4.1.0.

JAK structure and sequence analysis

Mouse JAK2 (AF-Q62120) and JAK3 (AF-Q62137) structure predictions were acquired from the AlphaFold protein structure database [64] and visualized in UCSF ChimeraX (version 1.2.5) [65]. Multiple sequence alignments were performed using the EMBL-EBI Clustal Omega tool.

Quantitative real-time (qRT)-PCR

Total RNA was extracted both from primary *Irf4*^{-/-} tumors as well as FACS-sorted control B220⁺ slg μ ⁻ BM fr.A-D cells of either *Irf4*^{-/-} or wt animals using the Gdansk extractme kit (EM09.1) according to the manufacturer's protocol. cDNA was prepared from whole RNA samples using the RevertAid cDNA kit from Thermo Fisher (K1621). qRT-PCR for *Aicda*, *Spi1*, and *Pax5* was performed using the SybrGreen MasterMix reagent (4385612, AppliedBiosystems) in a StepOnePlus cyclor (AppliedBiosystems). Data presented as percentage of HPRT using the formula $x = 1 / 2^{(\text{cycles}_{Aicda} - \text{cycles}_{HPRT})} \times 100$.

In vivo therapeutic studies and ultrasound imaging

Mice were injected with 3×10^5 T8.1 cells intraperitoneally and monitored daily for clinical symptoms. When mice began showing signs of general morbidity, leukemia was confirmed by FACS analysis of tail vein blood for B220⁺ slg μ ⁻ blast cells. When blast cells in pB reached 25 (mean 50)%, therapy was initiated with oral Dexamethasone (Jenapharm) at 6 mg/L supplied ad libitum in the drinking water for seven days. Maintenance therapy comprised either Ruxolitinib-phosphate (S5243, Sellekchem) 1 mg (in 2% DMSO, 30% PEG300 in H₂O, as proposed by the manufacturer), Defactinib (S7654, Sellekchem) 1.2 mg (in 5% DMSO, 50% PEG300, 5% Tween 80 in H₂O, as proposed by the manufacturer) or vehicle control (5% DMSO, 50% PEG300, 5% Tween 80 in H₂O) administered twice daily via oral gavage. During the course of the disease, this treatment led to paraparesis of the hind legs and tail. A clinical scoring system was established according to the extent of paraparesis and mice were scored daily accordingly: Scores 0–3: (0) no paraparesis, (1) paraparesis induced by treatment intervention, resolves within 30 s, (2) paraparesis induced by treatment intervention, does not resolve within 30 s, (3) persistent paraparesis, independent of treatment intervention. Score 3 prompted sacrifice of affected mice. High-resolution ultrasound imaging was performed using a Visual Sonics Vevo 2100 System (FUJIFILM VisualSonics, Toronto, Canada) with microscan transducer MS-550-D, 22–55 MHz (FUJIFILM VisualSonics, Toronto, Canada) as described previously [66].

Statistical analysis

Statistical analysis was performed using the GraphPad 9.0 software. Data are commonly presented as mean \pm SD. Prior to significance testing, normal distribution and homogeneity of variances were confirmed by Shapiro–Wilk test and Brown–Forsythe testing. Statistical significance when comparing two normally distributed groups was evaluated using two-tailed unpaired *t* tests. In case of significant differences in variances between groups, Welch's correction was applied to account for non-normal distribution of data. When comparing multiple groups, a one-way or two-way analysis of variance was performed, depending on the number of variables that differed between compared groups. This was followed by a Tukey's Sidak, or Dunnett's *post hoc* test, as indicated in figure legends. An alpha level of $P < 0.05$ was employed for significance testing. In the in vivo experiment, all animals were included in the analyses.

Reporting summary

Further information on research design is available in the Nature Research Reporting Summary linked to this article.

DATA AVAILABILITY

The RNAseq datasets generated during the current study have been deposited in the Gene Expression Omnibus (GEO) archive and are available under the accession number GSE192424. The WES datasets can be accessed under PRJNA706650 in the sequencing read archive (SRA).

REFERENCES

- Johnson K, Hashimshony T, Sawai CM, Pongubala JMR, Skok JA, Aifantis I, et al. Regulation of immunoglobulin light-chain recombination by the transcription factor IRF-4 and the attenuation of interleukin-7 signaling. *Immunity* 2008;28:335–45.
- Geier JK, Schlissel MS. Pre-BCR signals and the control of Ig gene rearrangements. *Semin Immunol* 2006;18:31–9.
- Herzog S, Reth M, Jumaa H. Regulation of B-cell proliferation and differentiation by pre-B-cell receptor signalling. *Nat Rev Immunol* 2009;9:195–205.
- Fistonich C, Zehentmeier S, Bednarski JJ, Miao R, Schjervén H, Sleckman BP, et al. Cell circuits between B cell progenitors and IL-7+ mesenchymal progenitor cells control B cell development cell circuits control B cell development. *J Exp Med* 2018;215:2586–99.
- Huber M, Lohoff M. IRF4 at the crossroads of effector T-cell fate decision. *Eur J Immunol* 2014;44:1886–95.
- Lohoff M, Mak TW. Roles of interferon-regulatory factors in T-helper-cell differentiation. *Nat Rev Immunol* 2005;5:125–35.
- Mittrücker H-W, Matsuyama T, Grossman A, Kündig TM, Potter J, Shahinian A, et al. Requirement for the transcription factor LSIRF/IRF4 for mature B and T lymphocyte function. *Science* 1997;275:540–3.
- Lu R, Medina KL, Lancki DW, Singh H. IRF-4.8 orchestrate the pre-B-to-B transition in lymphocyte development. *Gene Dev* 2003;17:1703–8.
- Katz AJ, Chia VM, Schoonen WM, Kelsh MA. Acute lymphoblastic leukemia: an assessment of international incidence, survival, and disease burden. *Cancer Cause Control* 2015;26:1627–42.
- Tasian SK, Hurtz C, Wertheim GB, Bailey NG, Lim MS, Harvey RC, et al. High incidence of Philadelphia chromosome-like acute lymphoblastic leukemia in older adults with B-ALL. *Leukemia* 2016;31:981–4.
- Roberts KG. Genetics and prognosis of ALL in children vs adults. *Hematol Am Soc Hematol Educ Program* 2018;2018:137–45.
- Mullighan CG. Genomic characterization of childhood acute lymphoblastic leukemia. *Semin Hematol* 2013;50:314–24.
- Liu Y-F, Wang B-Y, Zhang W-N, Huang J-Y, Li B-S, Zhang M, et al. Genomic profiling of adult and pediatric b-cell acute lymphoblastic leukemia. *Ebiomedicine* 2016;8:173–83.
- Hardy RR, Carmack CE, Shinton SA, Kemp JD, Hayakawa K. Resolution and characterization of pro-B and pre-pro-B cell stages in normal mouse bone marrow. *J Exp Med* 1991;173:1213–25.
- Sen J, Arceci RJ, Jones W, Burakoff SJ. Expression and ontogeny of murine CD2. *Eur J Immunol* 1989;19:1297–302.
- Zehentmeier S, Pereira JP. Cell circuits and niches controlling B cell development. *Immunol Rev* 2019;289:142–57.
- Tokoyoda K, Egawa T, Sugiyama T, Choi B-I, Nagasawa T. Cellular niches controlling B lymphocyte behavior within bone marrow during development. *Immunity* 2004;20:707–18.
- Ma Q, Jones D, Springer TA. The chemokine receptor CXCR4 is required for the retention of B lineage and granulocytic precursors within the bone marrow microenvironment. *Immunity* 1999;10:463–71.
- Batista CR, Lim M, Laramée A-S, Abu-Sardanah F, Xu LS, Hossain R, et al. Driver mutations in Janus kinases in a mouse model of B-cell leukemia induced by deletion of PU.1 and Spi-B. *Blood Adv* 2018;2:2798–810.
- Roberts KG, Li Y, Payne-Turner D, Harvey RC, Yang Y-L, Pei D, et al. Targetable kinase-activating lesions in Ph-like acute lymphoblastic leukemia. *N. Engl J Med* 2014;371:1005–15.
- Refsland EW, Harris RS. The APOBEC3 family of retroelement restriction factors. *Curr Top Microbiol* 2013;371:1–27.
- Petersen-Mahrt SK, Harris RS, Neuberger MS. AID mutates E. coli suggesting a DNA deamination mechanism for antibody diversification. *Nature* 2002;418:99–104.
- Noia JD, Neuberger MS. Altering the pathway of immunoglobulin hypermutation by inhibiting uracil-DNA glycosylase. *Nature* 2002;419:43–8.
- Wilson TM, Vaisman A, Martomo SA, Sullivan P, Lan L, Hanaoka F, et al. MSH2–MSH6 stimulates DNA polymerase η , suggesting a role for A:T mutations in antibody genes. *J Exp Med* 2005;201:637–45.
- Swaminathan S, Klemm L, Park E, Papaemmanuil E, Ford A, Kweon S-M, et al. Mechanisms of clonal evolution in childhood acute lymphoblastic leukemia. *Nat Immunol* 2015;16:766–74.
- Malard F, Mohty M. Acute lymphoblastic leukaemia. *Lancet* 2020;395:1146–62.
- Mullighan CG. How advanced are we in targeting novel subtypes of ALL? *Best Pract Res Clin Haematol* 2019;32:101095.
- Bastian L, Schroeder MP, Eckert C, Schlee C, Tanchez JO, Kämpf S, et al. PAX5 biallelic genomic alterations define a novel subgroup of B-cell precursor acute lymphoblastic leukemia. *Leukemia* 2019;33:1895–909.
- Jain N, Roberts KG, Jabbour E, Patel K, Eterovic AK, Chen K, et al. Ph-like acute lymphoblastic leukemia: a high-risk subtype in adults. *Blood* 2017;129:572–81.
- Jumper J, Evans R, Pritzel A, Green T, Figurnov M, Ronneberger O, et al. Highly accurate protein structure prediction with AlphaFold. *Nature* 2021;596:583–9.
- Herold T, Schneider S, Metzeler K, Neumann K, Hartmann L, Roberts KG, et al. Philadelphia chromosome-like acute lymphoblastic leukemia in adults have frequent IGH-CRLF2 and JAK2 mutations, persistence of minimal residual disease and poor prognosis. *Haematologica*. 2016;102:130–8.
- Corfe SA, Paige CJ. The many roles of IL-7 in B cell development; mediator of survival, proliferation and differentiation. *Semin Immunol* 2012;24:198–208.
- Milford TM, Su RJ, Francis OL, Baez I, Martinez SR, Coats JS, et al. TSLP or IL-7 provide an IL-7R α signal that is critical for human B lymphopoiesis. *Eur J Immunol* 2016;46:2155–61.
- Härzschel A, Zucchetto A, Gattei V, Hartmann TN. VLA-4 expression and activation in B cell malignancies: functional and clinical aspects. *Int J Mol Sci* 2020;21:2206.
- Springer TA. Adhesion receptors of the immune system. *Nature* 1990;346:425–34.
- Tijchon E, Havinga J, Leeuwen FNvan, Scheijen B. B-lineage transcription factors and cooperating gene lesions required for leukemia development. *Leukemia* 2013;27:541–52.
- Martin-Lorenzo A, Hauer J, Vicente-Duenas C, Auer F, Gonzalez-Herrero I, Garcia-Ramirez I, et al. Infection exposure is a causal factor in B-cell precursor acute lymphoblastic leukemia as a result of Pax5-inherited susceptibility. *Cancer Discov* 2015;5:1328–43.
- Schjervén H, Ayongaba EF, Aghajani-farah A, McLaughlin J, Cheng D, Geng H, et al. Genetic analysis of Ikaros target genes and tumor suppressor function in BCR-ABL1+ pre-B ALL. *Leukemia* 2017;214:793–814.
- Pang SHM, Minnich M, Gangatirak P, Zheng Z, Ebert A, Song G, et al. PU.1 cooperates with IRF4 and IRF8 to suppress pre-B-cell leukemia. *Leukemia* 2016;30:1375–87.
- Jo S-H, Schatz JH, Acquaviva J, Singh H, Ren R. Cooperation between deficiencies of IRF-4 and IRF-8 promotes both myeloid and lymphoid tumorigenesis. *Blood* 2010;116:2759–67.
- Lupardus PJ, Ultsch M, Wallweber H, Kohli PB, Johnson AR, Eigenbrot C. Structure of the pseudokinase–kinase domains from protein kinase TYK2 reveals a mechanism for Janus kinase (JAK) autoinhibition. *Proc Natl Acad Sci* 2014;111:8025–30.
- McElroy CA, Holland PJ, Zhao P, Lim J-M, Wells L, Eisenstein E, et al. Structural reorganization of the interleukin-7 signaling complex. *Proc Natl Acad Sci* 2012;109:2503–8.
- Hertzberg L, Vendramini E, Ganmore I, Cazzaniga G, Schmitz M, Chalker J, et al. Down syndrome acute lymphoblastic leukemia, a highly heterogeneous disease in which aberrant expression of CRLF2 is associated with mutated JAK2: a report from the International BFM Study Group. *Blood* 2010;115:1006–17.
- Tasian SK, Assad A, Hunter DS, Du Y, Loh ML. A Phase 2 study of ruxolitinib with chemotherapy in children with Philadelphia chromosome-like acute lymphoblastic leukemia (INCB18424-269/AALL1521): dose-finding results from the part 1 safety phase. *Blood* 2018;132:555–555.
- Verstovsek S, Mesa RA, Gotlib J, Levy RS, Gupta V, DiPersio JF, et al. A double-blind, placebo-controlled trial of ruxolitinib for myelofibrosis. *N. Engl J Med* 2012;366:799–807.
- Hara T, Shitara S, Imai K, Miyachi H, Kitano S, Yao H, et al. Identification of IL-7–producing cells in primary and secondary lymphoid organs using IL-7–GFP knock-in mice. *J Immunol* 2012;189:1577–84.
- Ogawa M, Nishikawa S, Ikuta K, Yamamura F, Naito M, Takahashi K, et al. B cell ontogeny in murine embryo studied by a culture system with the monolayer of a stromal cell clone, ST2: B cell progenitor develops first in the embryonal body rather than in the yolk sac. *Embo J* 1988;7:1337–43.
- Ceredig R, Boekel Eten, Rolink A, Melchers F, Andersson J. Fetal liver organ cultures allow the proliferative expansion of pre-B receptor-expressing pre-B-II cells and the differentiation of immature and mature B cells in vitro. *Int Immunol* 1998;10:49–59.
- Kang CH, Hartmann E, Menke L, Staudenraus D, Abass E-F, Raifer H, et al. A hyperactive mutant of interferon-regulatory factor 4. *Eur J Immunol* 2018;49:812–5.
- Maaten LVD, Hinton G. Visualizing data using t-SNE. *J Mach Learn Res* 2008;9:2579–625.
- Langmead B, Salzberg SL. Fast gapped-read alignment with Bowtie 2. *Nat Methods* 2012;9:357–9.
- Klambauer G, Schwarzbauer K, Mayr A, Clevert D-A, Mitterecker A, Bodenhofer U, et al. cnMOPS: mixture of Poissons for discovering copy number variations in next-generation sequencing data with a low false discovery rate. *Nucleic Acids Res* 2012;40:e69.
- Kawamoto T. Use of a new adhesive film for the preparation of multi-purpose fresh-frozen sections from hard tissues, whole-animals, insects and plants. *Arch Histol Cytol* 2003;66:123–43.
- Zehentmeier S, Roth K, Cseresnyes Z, Sercan Ö, Horn K, Niesner RA, et al. Static and dynamic components synergize to form a stable survival niche for bone marrow plasma cells. *Eur J Immunol* 2014;44:2306–17.

55. Canene-Adams K. Preparation of formalin-fixed paraffin-embedded tissue for immunohistochemistry. *Methods Enzymol* 2013;533:225–33.
56. Schindelin J, Arganda-Carreras I, Frise E, Kaynig V, Longair M, Pietzsch T, et al. Fiji: an open-source platform for biological-image analysis. *Nat Methods* 2012;9:676–82.
57. Li H, Durbin R. Fast and accurate short read alignment with Burrows–Wheeler transform. *Bioinformatics* 2009;25:1754–60.
58. McKenna A, Hanna M, Banks E, Sivachenko A, Cibulskis K, Kernysky A, et al. The genome analysis toolkit: a MapReduce framework for analyzing next-generation DNA sequencing data. *Genome Res* 2010;20:1297–303.
59. Brochet X, Lefranc M-P, Giudicelli V. IMG/TV-QUEST: the highly customized and integrated system for IG and TR standardized V-J and V-D-J sequence analysis. *Nucleic Acids Res* 2008;36:W503–8.
60. Liao Y, Smyth GK, Shi W. featureCounts: an efficient general purpose program for assigning sequence reads to genomic features. *Bioinformatics* 2014;30:923–30.
61. Marini F, Binder H. pcaExplorer: an R/Bioconductor package for interacting with RNA-seq principal components. *BMC Bioinformatics* 2019;20:331.
62. Love MI, Huber W, Anders S. Moderated estimation of fold change and dispersion for RNA-seq data with DESeq2. *Genome Biol* 2014;15:550.
63. Marini F, Ludt A, Linke J, Strauch K. GeneTonic: an R/Bioconductor package for streamlining the interpretation of RNA-seq data. *Biorxiv*. 2021; <https://www.biorxiv.org/content/10.1101/2021.05.19.444862v1>.
64. Varadi M, Anyango S, Deshpande M, Nair S, Natassia C, Yordanova G, et al. AlphaFold Protein Structure Database: massively expanding the structural coverage of protein-sequence space with high-accuracy models. *Nucleic Acids Res*. 2021;50:D439–D444.
65. Pettersen EF, Goddard TD, Huang CC, Meng EC, Couch GS, Croll TI, et al. UCSF ChimeraX: structure visualization for researchers, educators, and developers. *Protein Sci* 2021;30:70–82.
66. Buchholz SM, Goetze RG, Singh SK, Ammer-Herrenau C, Richards FM, Jodrell DJ, et al. Depletion of macrophages improves therapeutic response to gemcitabine in murine pancreas cancer. *Cancers* 2020;12:1978.

ACKNOWLEDGEMENTS

The authors want to thank Koji Tokoyoda (DRFZ, Berlin) for supplying *Il-7^{eGFP}* mice for breeding, Olli Silvennoinen (Tampere-university, Finland) for supplying us with the JAK3 construct, and Fritz Melchers (DRFZ Berlin) for the JIL-7.6 J558 and ST2 cells. Further, Hyun-Dong Chang and Anja Hauser (both DRFZ, Berlin) for supplying OP-9 cells and Kawamoto materials, respectively.

AUTHOR CONTRIBUTIONS

DDG, CP, NS, MB, FH, ML designed experiments; DDG, CP, NS, MB, DS, LM, BC, FH, LH performed experiments; DDG, CP, MB, HR, ER, PD, MW, MM, AN, UMB, FM, FH, MB, HMJ, AN, AB, MK, TB, TS, AP, LB, AH, CB, ML analyzed data; DDG and ML prepared the manuscript.

FUNDING

D.D.G. received personal funding through the German Cancer Aid, Mildred-Scheel doctoral scholarship (70112922). M.L. was funded by the Deutsche Forschungsgemeinschaft (DFG) (LO 396/8-1) and the Else Kröner-Fresenius-Stiftung. Open Access funding enabled and organized by Projekt DEAL.

COMPETING INTERESTS

The authors declare no competing interests.

STUDY APPROVAL

All animal experiments were approved by the local government (Regierungspräsidium Gießen, G49/2018, G34/2021) and conducted according to the German animal protection law.

ADDITIONAL INFORMATION

Supplementary information The online version contains supplementary material available at <https://doi.org/10.1038/s41418-022-01005-z>.

Correspondence and requests for materials should be addressed to Michael Lohoff.

Reprints and permission information is available at <http://www.nature.com/reprints>

Publisher's note Springer Nature remains neutral with regard to jurisdictional claims in published maps and institutional affiliations.



This article is licensed under a Creative Commons Attribution 4.0 International License, which permits use, sharing, adaptation, distribution and reproduction in any medium or format, as long as you give appropriate credit to the original author(s) and the source, provide a link to the Creative Commons licence, and indicate if changes were made. The images or other third party material in this article are included in the article's Creative Commons licence, unless indicated otherwise in a credit line to the material. If material is not included in the article's Creative Commons licence and your intended use is not permitted by statutory regulation or exceeds the permitted use, you will need to obtain permission directly from the copyright holder. To view a copy of this licence, visit <http://creativecommons.org/licenses/by/4.0/>.

© The Author(s) 2022